DOE/ID/12839--T1

DOE/ID/12839--T1

DE92 017960

CHARACTERIZATION OF OIL AND GAS RESERVOIR HETEROGENEITY

Annual Report
For the Period
November 1, 1990 - October 31, 1991
Work Performed Under the Grant #DE-FG07-90ID12839

Prepared for

U.S. Department of Energy
Idaho Operations Office
785 DOE Place
Idaho Falls, ID 83402

Prepared by

Petroleum Development Laboratory
University of Alaska Fairbanks
425 Duckering Building
Fairbanks, AK 99775-1260

MASTER

DISTRIBUTION OF THIS DOCUMENT IS UNLIMITED

other aspects of this project--geological, petrophysical, engineering data--to further a synergistic appreciation of the characteristics of these potentially important reservoirs, located on the Alaskan North Slope.

A generalized thermodynamic model is presented in this report for predicting asphaltene equilibria and precipitation of asphaltenes from a crude under influence of a miscible solvent. In this model the asphaltenes in crude are represented by a discretized normal distribution function which characterizes the various pseudo-component asphaltene fractions. The properties of each asphaltene fraction are determined from average molecular weight of each fraction. The model is coupled with the Peng-Robinson equation of state model to compute vapor-liquid equilibria, and with the Peng-Robinson departure function model to calculate molar volume and solubility parameter for the equilibrium liquid phase of the oil-solvent mixtures. The experimental asphaltene precipitation data can be used to determine the model parameters using a nonlinear multi-parameter regression technique and to determine molar distribution of asphaltenes in crude oil or in equilibrium solid and liquid phases after mixing the crude oil and solvent. Scott and Magat theory is used for this purpose. The model can be used to predict the amount of asphaltene precipitation, the solid-liquid equilibrium constants for each asphaltene fraction at different pressures, temperatures, and compositions of the injection fluid.

A preliminary geologic description of the Milne Point Unit is also presented in this report. The Milne Point Unit is located adjacent to the West Sak Field. Resources are estimated at 100 million barrels of oil and the production is from the Kuparuk River Formation.

Results obtained to date show the Kuparuk River Formation at the Milne Point Unit is composed of two high-quality, consolidated, oil-bearing sandstone members. Future work will include additional well log data analyses and evaluation of the depositional environment.

DISCLAIMER

This report was prepared as an account of work sponsored by an agency of the United States Government. Neither the United States Government nor any agency thereof, nor any of their employees, makes any warranty, express or implied, or assumes any legal liability or responsibility for the accuracy, completeness, or usefulness of any information, apparatus, product, or process disclosed, or represents that its use would not infringe privately owned rights. Reference herein to any specific commercial product, process, or service by trade name, trademark, manufacturer, or otherwise does not necessarily constitute or imply its endorsement, recommendation, or favoring by the United States Government or any agency thereof. The views and opinions of authors expressed herein do not necessarily state or reflect those of the United States Government or any agency thereof.

ACKNOWLEDGEMENTS

This report was prepared for the U.S. Department of Energy under the Cooperative Agreement No. DE-FG07-90ID12839. The financial support of the U.S. Department of Energy, Idaho Operations Office, is gratefully acknowledged. The matching support was provided by the Petroleum Development Laboratory, University of Alaska Fairbanks. The research work described herein was made possible by the cooperation and assistance of North Slope Operators, and the Alaska Oil and Gas Conservation Commission who provided the well log and core data. This report is a result of the work performed by the following co-investigators: Dr. Vidyadhar A. Kamath, Dr. David Ogbe, Dr. Tom Mowatt, Mr. Walt Munly and Mr. Shirish Patil. This manuscript was prepared by Dr. Vidyadhar A. Kamath, Dr. David Ogbe, Dr. Tom Mowatt, Mr. Walt Munly and was typed by Ms. Vickie Ivester.

Dr. G. D. Sharma, Director
Petroleum Development Laboratory

TABLE OF CONTENTS

Chapter #	Chapter Title	Page
	ABSTRACT	ii
	ACKNOWLEDGEMENTS	iv
	LIST OF FIGURES	vi
	LIST OF TABLES	ix
	EXECUTIVE SUMMARY	x
1.0	RESERVOIR DESCRIPTION OF ENDICOTT FIELD	1
	1.1 Overview and Geology of Endicott Field	1
	1.2 Endicott Reservoir Description Procedure	6
	1.3 Endicott Reservoir Description	8
	1.3.1 Structural Analysis	8
	1.3.2 Log-Derived Petrophysical Properties	13
	1.4 Future Endicott Reservoir Characterization	48
	1.5 Nomenclature	51
	1.6 References	51
2.0	PETROGRAPHIC CHARACTERISTICS OF SELECTED STRATIGRAPHIC HORIZONS: UGNU SWPT #1 AND WEST SAK SWPT #1	52
	2.1 Introduction	52
	2.2 Petrographic Analyses	52
	2.3 Sample Descriptions	54
	2.3.1 Ugnu SWPT #1 Samples	55
	2.3.2 West Sak SWPT #1 Samples	75
3.0	MODELING OF ASPHALTENE EQUILIBRIA: A POLYDISPERSED MOLECULAR THERMODYNAMIC MODEL	86
	3.1 Introduction	86
	3.2 Nature of Asphaltenes and Resins	88
	3.3 Asphaltene Precipitation Modeling: Review	91
	3.3.1 Molecular-Thermodynamic Approach	92
	3.3.2 Thermodynamic-Colloidal Approach	93
	3.4 Description of a Generalized Polydispersed Molecular Thermodynamic Model for Asphaltene Equilibria Predictions	93
	3.4.1 Discretization of the Normal Distribution Function	96
	3.4.2 Asphaltene Pseudocomponent Property Estimation	98
	3.4.3 Solid-Liquid Equilibria Calculations	100
	3.4.4 Estimation of Molar Volume and Solubility Parameter for the Oil or Oil-Solvent Mixture	102
	3.4.5 Stepwise Procedure for Prediction of Asphaltene Precipitation Upon Addition of a Solvent to Oil	103
	3.4.6 Future Work	112
	3.5 Nomenclature	113
	3.6 References	115
4.0	MILNE POINT UNIT	118
	4.1 Introduction	118
	4.2 Results to Date	120
	4.3 Preliminary Geological Analysis	122
	4.4 Future Plans	125
	4.5 References	125
	APPENDIX: Published AAPG Abstract from Tom Mowatt et al.	126

LIST OF FIGURES

Figure #	Figure Title	Page
1.1	Alaska North Slope Fields (Source: Curtis and Huxley, 1985)	2
1.2	Location Map of Endicott Field (Source: Curtis and Huxley, 1985)	2
1.3	Generalized North Slope Stratigraphic Column (Adapted from Bird ,1987)	3
1.4	Endicott Group Stratigraphic Position and Lithologic Description (Woidneck, et al, 1987)	7
1.5	Endicott Field Well Location Map (Woidneck, et. al, 1987)	10
1.6	Endicott Wells Analyzed in this Study with Cross Sections A-A' and B-B' Plotted	10
1.7	Endicott East-West Cross Section A-A'	11
1.8	Endicott North-South Cross Section B-B'	12
1.9	Top Zone 2A Structure Contour Map C.I. 50'	19
1.10	Zone 2A Porosity Contour Map C.I. 2%	20
1.11	Zone 2A Water Saturation Contour Map C.I. 10%	20
1.12	Zone 2A 3-D Porosity Isopach	21
1.13	Zone 2A 3-D Water Saturation Isopach	22
1.14	Zone 2B Structure Contour Map C.I. 50'	23
1.15	Zone 2B Porosity Contour Map C.I.2%	24
1.16	Zone 2B Water Saturation Contour Map C.I. 20%	25
1.17	Zone 2B 3-D Porosity Isopach	26
1.18	Zone 2B 3-D Water Saturation Isopach	27
1.19	Porosity - Sw: Zone 2B	28
1.20	Porosity - Sw: Zone 2A	28
1.21	Top Zone 3A Structure Contour Map C.I. 50'	29
1.22	Zone 3A Porosity Contour Map C.I. 2%	36
1.23	Zone 3A Water Saturation Contour Map C.I. 10%	37
1.24	Zone 3A 3-D Porosity Isopach	38

LIST OF FIGURES

Figure #	Figure Title	Page
1.25	Zone 3A 3-D Water Saturation Isopach	39
1.26	Top Zone 3B Structure Contour Map C.I. 50'	40
1.27	Zone 3B Porosity Contour Map C.I. 2%	41
1.28	Zone 3B Water Saturation Contour Map C.I. 10%	42
1.29	Top Zone 3C Structure Contour Map C.I. 50'	43
1.30	Zone 3C Porosity Contour Map C.I. 2%	44
1.31	Zone 3C Water Saturation Contour Map C.I. 2%	45
1.32	Zone 2A 3-D Net Pay Isopach	46
1.33	Zone 2B 3-D Net Pay Isopach	47
1.34	Zone 3A 3-D Net Pay Isopach	49
1.35	Zone 3B 3-D Net Pay Isopach	50
2.1	Ugnu SWPT #1, 3532' (50 x PL)	55
2.2	Ugnu SWPT #1, 3526' (50 x PL)	56
2.3	Ugnu SWPT #1, 3507' (50 x PL)	57
2.4	Ugnu SWPT #1, 3497' (50 x PL)	58
2.5	Ugnu SWPT #1, 3493' (50 x PL)	59
2.6	Ugnu SWPT #1, 3457' (50 x PL)	60
2.7	Ugnu SWPT #1, 3452' (50 x PL)	61
2.8	Ugnu SWPT #1, 3425' (50 x PL)	62
2.9	Ugnu SWPT #1, 3422' (50 x PL)	63
2.10	Ugnu SWPT #1, 3412' (50 x PL)	64
2.11	Ugnu SWPT #1, 3264' (50 x PL)	65
2.12	Ugnu SWPT #1, 3241' (50 x PL)	66
2.13	Ugnu SWPT #1, 3235' (50 x PL)	68
2.14	Ugnu SWPT #1, 3174' (50 x PL)	69

LIST OF FIGURES

Figure #	Figure Title	Page
2.15	Ugnu SWPT #1, 3235' (50 x PL)	70
2.16	Ugnu SWPT #1, 3112' (50 x PL)	71
2.17	Ugnu SWPT #1, 3059' (50 x PL)	72
2.18	Ugnu SWPT #1, 3996' (50 x PL)	74
2.19	West Sak SWPT #1, 3960' (50 x PL)	75
2.20	West Sak SWPT #1, 3923' (50 x PL)	76
2.21	West Sak SWPT #1, 3917' (50 x PL)	77
2.22	West Sak SWPT #1, 3953' (50 x PL)	78
2.23	West Sak SWPT #1, 3812' (50 x PL)	79
2.24	West Sak SWPT #1, 3804' (50 x PL)	80
2.25	West Sak SWPT #1, 3780' (50 x PL)	81
2.26	West Sak SWPT #1, 3769' (50 x PL)	82
2.27	West Sak SWPT #1, 3761' (50 x PL)	83
2.28	West Sak SWPT #1, 3723' A (50 X PL) B (50 X xsPL)	84
2.29	West Sak SWPT #1, 3715' (50 x PL)	85
3.1	Schematic Representation of Various Fractions and Phases of Oil and Oil-Solvent Mixtures	95
3.2	Discretization of a Continuous Normal Distribution Function of Asphaltene Fractions	99
4.1	Base Map of Milne Point Wells with Analyzed Wells Indicated by Larger Circles	119
4.2	TVD Log Plot of Milne Point Well B-3	121
4.3	Middle Kuparuk Porosity & Sw, Milne Point Unit	124

LIST OF TABLES

Table #	Table Title	Page
1.1	Endicott Lithostratigraphic Zones and Subzones (Woidneck, et al, 1987)	5
1.2	Endicott Wells Utilized in Well Log Analysis to Date	9
1.3	Zone 1 Tops at Endicott Field	15
1.4	Petrophysical Properties of Endicott Zone 2A	16
1.5	Petrophysical Properties of Endicott Zone 2B	17
1.6	Petrophysical Properties of Endicott Zone 3A	32
1.7	Petrophysical Properties of Endicott Zone 3B	33
1.8	Petrophysical Properties of Endicott Zone 3C	34
1.9	Weighted Zone Averages of Porosity and Water Saturation at Endicott Field	35
4.1	Milne Point Wells Utilized in Well Log Analysis to Date	120
4.2	Petrophysical Properties of the Middle Kuparuk, Milne Point Unit, as Determined to Date	122
4.3	Petrophysical Properties of the Lower Kuparuk, Milne Point Unit	123

EXECUTIVE SUMMARY

This report summarizes the work conducted during the period: November 1, 1990, to October 31, 1991, by the Petroleum Development Laboratory (PDL) as part of the project "Characterization of Oil and Gas Reservoir Heterogeneity in Alaska." This research project (Grant No. DE-FG07-90ID12839) is jointly funded by the U.S. Department of Energy (Idaho National Engineering Laboratory) and the University of Alaska Fairbanks (Petroleum Development Laboratory).

The State of Alaska is the largest oil producing state in the nation. Alaska currently provides nearly 25% of the nation's domestic oil production, and contains about 20% of the total U.S. proven reserves. More important, there is the potential to add to the known reserves on the Alaskan North Slope when the additional exploration for oil begins in the Arctic National Wildlife Refuge. The key to sustaining long-term oil production in Alaska is to improve the recovery efficiencies from the giant producing fields such as Prudhoe Bay, Kuparuk River, and Endicott, and to develop other marginally economic fields (contain heavy oil) such as the super-giant West Sak and Ugnu. The objective of this cooperative research program is to characterize Alaskan reservoirs in terms of their reserves, physical and chemical properties, geologic configuration and structure, and the development potential.

The report presents the work performed in four areas:

- Reservoir description of the Endicott field using well logs.
- Petrographic characteristics of selected stratigraphic horizons from the Ugnu and West Sak fields.
- Modeling of asphaltene equilibria using a polydispersed thermodynamic model.
- Preliminary description of the Milne Point Unit using well logs.

The Endicott field is located in the Beaufort sea, about eight miles east of Prudhoe Bay. It is the first arctic offshore field to be developed on the North Slope of Alaska. The reserves estimates include one billion stock tank barrels of oil-in-place and three-quarters of a trillion cubic feet of gas. It is being produced from artificial gravel islands, and production is from the Mississippian Kekiktuk Formation.

The reservoir description of the Endicott field includes a detailed well log data analysis. Using well logs from 15 Endicott wells, the various producing subzones were delineated, and well-to-well correlations are presented. Petrophysical properties such as net pay, porosity, water saturation, and net-to-gross ratios were calculated. Three dimensional plots and subsurface contour maps are presented to illustrate the spatial distribution of the petrophysical properties. Stratigraphic cross sections were generated to better define the spatial distributions of the petrophysical properties. The description of the depositional environment is considered an important aspect of this project, and will be discussed in future reports.

The results of petrographic analyses of core samples taken from selected stratigraphic horizons representing the West Sak and Ugnu intervals in Ugnu SWPT #1 and West Sak SWPT #1 are presented in the second chapter of this report. The purpose of the petrographic analysis is to provide direct, substantive characterization of the mineralogy and textural relationships of the rocks in the Ugnu and West Sak intervals. Furthermore, the integration of the petrographic study with the other geological, petrophysical, and engineering information will enhance our understanding of the characteristics of these potentially important reservoirs.

The third chapter of this report describes the modeling of asphaltene equilibria by treating asphaltenes as heterogeneous mixture of pseudocomponents. Results from both field and laboratory studies have shown that asphaltenes can be deposited during the recovery of asphaltic crudes by immiscible or miscible gas flooding. Other field conditions where asphaltene precipitation have been reported include natural depletion, gas-lift operations, caustic flooding and acidization. Asphaltene precipitation is an important problem especially in miscible gas flooding processes because it can reduce formation absolute permeability, affect well productivities and injectivities, alter rock wettability characteristics, and even cause plugging of producing wells. The need to study the problem of asphaltene deposition is particularly important to Alaska because of the types of enhanced oil recovery projects planned or currently underway on the Alaska North Slope. For example, part of the Prudhoe Bay field is produced by an enriched gas miscible flood project where asphaltene deposition has been observed. Similar floods are also planned for the Kuparuk River and Endicott fields. Miscible flooding is also considered as one of the technically feasible processes for the recovery of heavy oil from the West Sak field. The oil industry is looking for economically viable methods to control organic deposition

and to remedy the problem of asphaltene precipitation. The development of models to predict asphaltene precipitation is an important step in solving this problem, and this is the objective of the work described in this report.

The proposed model treats the asphaltenes in crude as a polydispersed heterogeneous mixture. The model is coupled with the Peng-Robinson equation of state to determine the vapor-liquid equilibria. The Peng-Robinson departure function is used to compute the molar volume and solubility parameter for the equilibrium liquid phase of the oil-solvent mixtures. The new model can be used to predict asphaltene equilibria and the precipitation of asphaltenes from a mixture of crude oil and miscible solvent.

The data collected from experimental work on asphaltene precipitation will be used in a nonlinear multi-parameter regression model to determine the optimum model parameters and to determine molar distribution of asphaltenes in crude oil or in equilibrium solid and liquid phases in crude oil-solvent mixture.

A preliminary reservoir description of the Milne Point Unit is presented in Chapter 4 of this report. The Milne Point Unit is located adjacent to the West Sak Field. The field is operated by Conoco, Inc., and it is estimated to contain 100 Million barrels of oil-in-place. Production is from the Cretaceous Kuparuk River Formation at depths ranging from 6950 ft to 7000 ft subsea.

Results from drilling and formation evaluation show that the Kuparuk River Formation at Milne Point is composed of two high-quality, consolidated, oil-bearing sandstone members. These sand members are found within the Middle and Lower Kuparuk River Formation. Stratigraphically, the Middle Kuparuk generally thickens toward the southeast; the Lower Kuparuk, in contrast, shows no general trend of sand thickening toward the south.

Data calculated from well log analyses show that average porosities in the producing zones range from 16% to 29%, and the average water saturation is about 33%. Several normal faults have also been identified within the Milne Point Unit. Additional well log analysis will be performed in the future, and the results will be integrated with a study of the depositional environment to provide a more detailed reservoir description of the Milne Point Unit.

CHAPTER 1.0

RESERVOIR DESCRIPTION OF ENDICOTT FIELD

1.1 OVERVIEW AND GEOLOGY OF ENDICOTT FIELD

Endicott field is located in the Beaufort Sea, approximately eight miles east of Prudhoe Bay and one to four miles offshore from the Sagavanirktok River delta (Figures 1.1 and 1.2). It is the first arctic offshore field to be developed, and is being produced from artificial gravel islands. Original oil-in-place was estimated at one billion stock tank barrels and original gas reserves were estimated to be three-quarters of a trillion cubic feet (Woidneck, et al, 1987).

Production is from Mississippian Kekiktuk Formation, within the Endicott Group (Figure 1.3), where it is positioned on a major North Slope structural feature aligned from northwest to southeast beneath Alaska's arctic shoreline. The northern most extent of the Endicott Group (including Kekiktuk) reaches to the Barrow Arch along only its most southeastern extent. It is in this area that Endicott field is found.

Woidneck, et al, (1987) have described the Kekiktuk Formation at Endicott in terms of three fluvial lithostratigraphic units, labeled from bottom to top as Zones 1, 2, and 3. Zone 1, early Visean in time, is shaly but includes interbedded coal and sandstone layers. It was depositionally located within a slowly-subsiding intermontaine basin that was being buried by fine-grained terrigeneous and coal-forming deposits. As such, it is comprised primarily of swampy, low energy deposits. Sediment influx was from low-lying source areas surrounding the basin. As expected from this depositional environment, Zone 1 is not the predominant hydrocarbon bearing zone at Endicott.

Relative uplift of a sedimentary source area northeast of Endicott field during mid-Visean time allowed for development of a braided-stream system proximal to the source area and a distal meandering stream system. It was this environment that resulted in Zone 2 braided stream deposition. The major area of braided stream sand deposition formed southeast of Endicott field, but a secondary axis of deposition developed concurrently near the Endicott field. Down-to-the-southwest syndeposi-

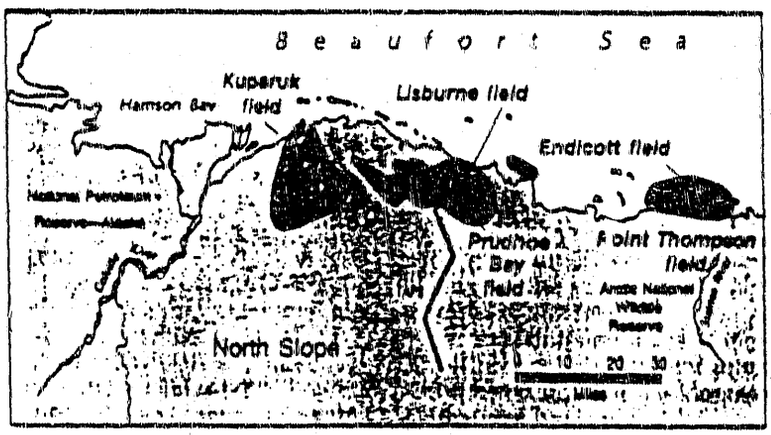

Figure 1.1: Alaska North Slope Fields
(Source: Curtis and Huxley, 1985)

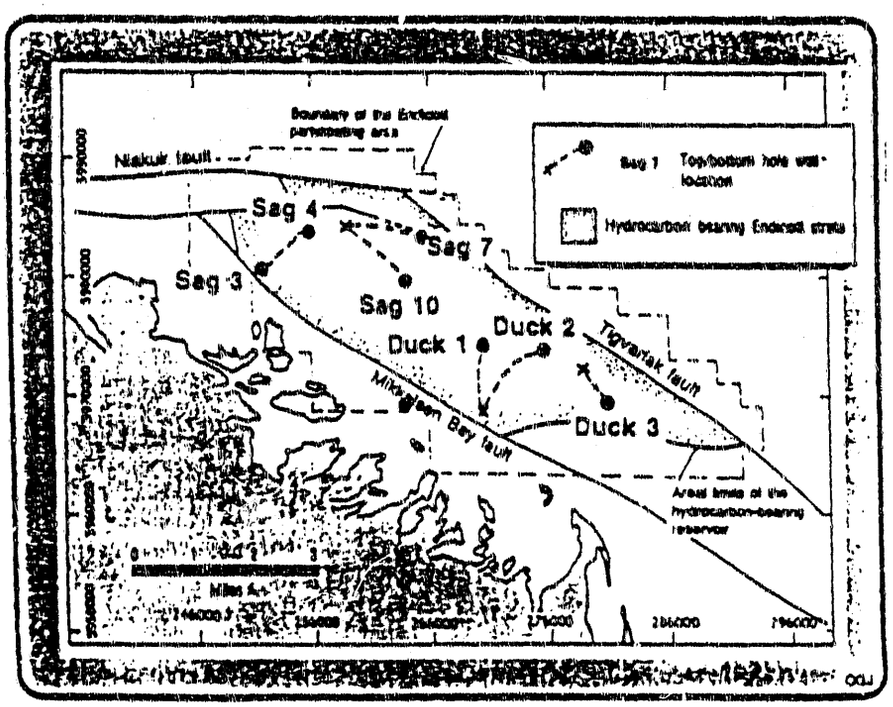

Figure 1.2: Location Map of Endicott Field
(Source: Curtis and Huxley, 1985)

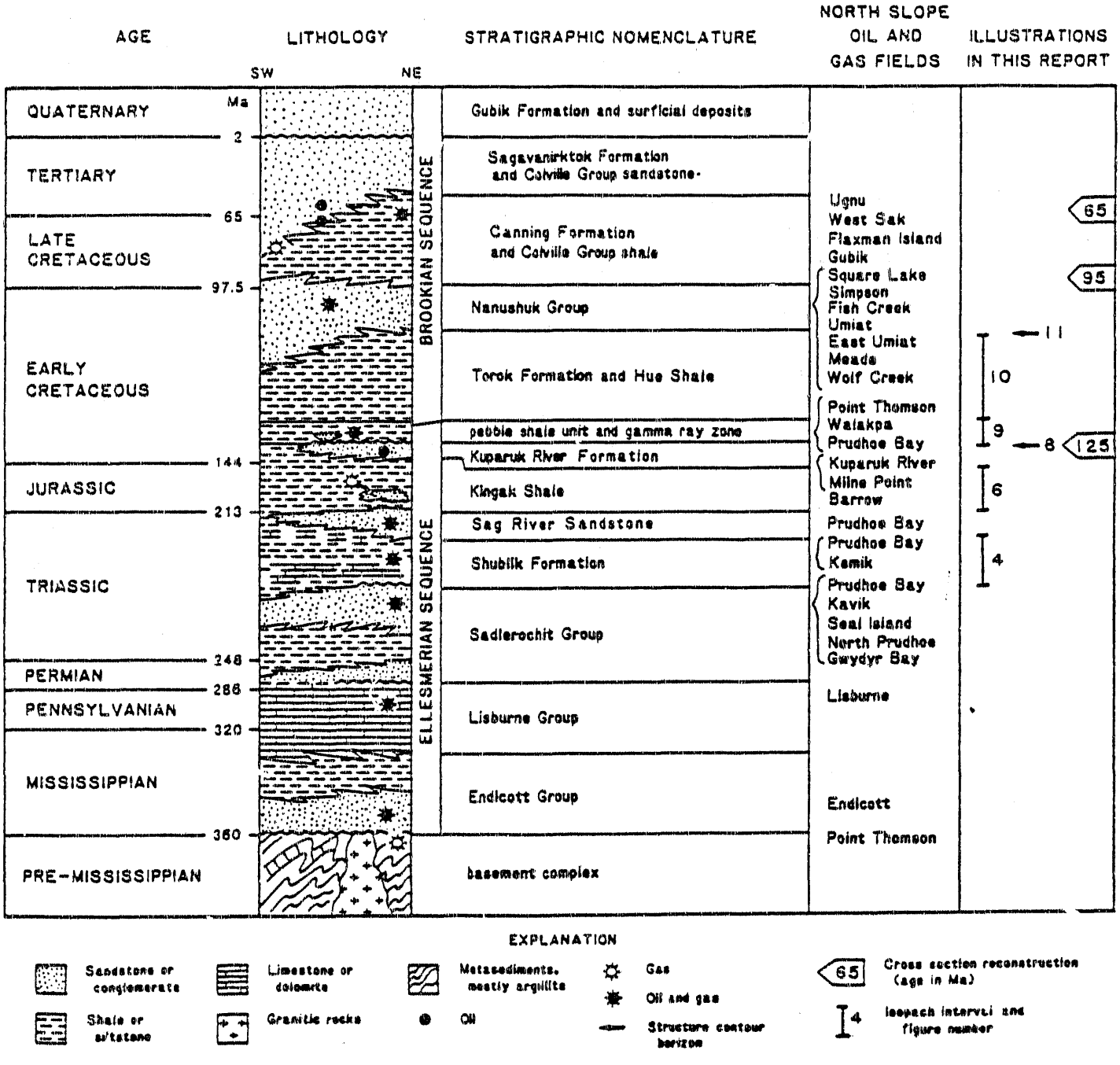

Figure 1.3: Generalized North Slope Stratigraphic Column (Adapted from Bird ,1987)

tional faulting during Zone 2 time is evidenced by local Zone 2 thickening adjacent to the downthrown side of northwest striking faults.

Although generally composed of nigh-energy, unconsolidated braided river deposits, Zone 2 also includes both permanent and ephemeral lake deposits. The braided streams led to medium-to-coarse grained multi-layered sandstone bedsets while lake deposition resulted in shales. Minor conglomerate and coal zones also occur in Zone 2. Commonly occurring upward-fining sand bodies near the top of this zone are interpreted as amalgamated point bar deposits and probably represent an increase in stream sinuosity. Woidneck, et al (1987) have determined overall sand proportions in Zone 2 to be greater than 60%. Such a high proportion of sand is believed to be a result of overlapping sand bodies coalescing to form sheet-like deposits.

The top of Zone 2 is frequently indicated by a barrel or blockly shaped gamma ray profile, and is often 50 to 100 feet beneath a major correlatable coal bed in Zone 3.

However, in contrast to the identifiable boundary separating Zone 2 from Zone 1, the transition from Zone 2 to Zone 3 is gradual, resulting in some degree of uncertainty in pinpointing the top of Zone 2. This zone is subdivided into Zones 2A and 2B by a shale interval near its center. Zones 2 and 3 are the major Endicott producing intervals.

Zone 3 is interpreted by Melvin (1987) as consisting of point bar deposits within the meandering stream system. This is consistent with a changing late-Visean depositional environment at Endicott. Although syndepositional faulting continued, the energy of the fluvial system diminished due to lowered source terrain relief (in response to erosion), or displacement of tectonic activity and associated high energy activity northwestward. Sandstones with lesser amounts of conglomerate and coal make up this zone. Evidence of point bar deposition is found in the abundance of stacked, upward-fining sequences with basal conglomerates. Interbedded floodplain mudstones and fine-grained sandstones deposited within interchannels of the floodplain also occur. Zone 3 is subdivided into three subzones (A, B, and C from bottom to top). Zones 3A and 3C are sand prone and separated by a major shaly interval (Zone 3B). The top of Zone 3 is gradational and difficult to determine exactly.

Table 1.1 summarizes Kekiktuk lithostratigraphic zones as defined above for the Endicott locality. To the west and south, Zone 3 grades laterally into the overlying Kayak shale, and Zone 2 pinches out. Zone 1 onlaps basement just west of the Prudhoe Bay State No. 1 (Woidneck, et al, 1987). As such, the zonal definitions in Table 1.1 are limited primarily to the Endicott area.

Table 1.1
Endicott Lithostratigraphic Zones and Subzones (Woidneck, et al, 1987)

Kekiktuk Interval	Zone	Subzone
Upper	3	3C 3B 3A
Middle	2	2B 2A
Lower	1	--

The Kekiktuk Formation at Endicott makes up a northwest trending elongate depocenter which thickens southeastward beyond the field limits. Net sandstone thickness also follows this trend. Despite thinner Kekiktuk isopachs within Endicott, high primary porosity combined with porosity enhancement by dissolution of framework grains and cement led to better reservoir conditions here. Low primary porosity south and west of Endicott is partly due to decreased grain size. In addition, Woidneck, et al (1987) believe that lower permeability associated with smaller grain size may have led to greater cementation and suppressed development of secondary porosity in these areas.

A combination of structure and stratigraphy form the trap in which Endicott hydrocarbon accumulations occur. Woidneck, et al (1987) have determined that this trap formed partly in response to tilting of an antiformal fault block which dips four to six degrees southwest. The crestal portion of the trap is truncated by a major unconformity (the Lower Cretaceous Unconformity or LCU) which dips gently to the south-

east. Seal-forming marine shales of the Lower Cretaceous "Highly Radioactive Zone" (HRZ) overlie the LCU.

Major normal faults define three sides of the field (Figure 1.2). The northwest striking Mikkelsen Bay and Tigvariak faults enclose the western and eastern sides, respectively. Both faults have a down-to-the-west sense of movement. The northern limit of the field occurs along the west striking, down-to-the-north Niakuk fault zone. Shales of the Itkilyariak Formation form a barrier to upward hydrocarbon migration over the untruncated portion of the structure. Figure 1.4 describes the stratigraphic relationship of these formations.

Seismic data indicate that Endicott faults can be categorized into one group which was active synchronous with and after LCU time, and into another group which was not. The Niakuk fault zone falls in the former category. The Mikkelsen Bay and Tigvariak faults fall in the latter, as the LCU is unbroken by these faults. They were active during Late Mississippian time, having affected Kekiktuk and Kayak deposition. Seismic and geologic analysis of offsets of several Kekiktuk coal markers across the Mikkelsen Bay fault indicate this fault to be a growth fault during Kekiktuk time with greatest sediment accumulation on the downthrown side. Because growth does not occur in the shallower Itkilyariak formation, syndepositional fault movement within the Endicott Group is constrained to pre-Itkilyariak time. The Niakuk fault zone offsets the LCU, indicating post-Lower Cretaceous movement on this fault. Greater amounts of offset associated with pre-LCU horizons indicate pre-LCU movement also occurred across the Niakuk Fault.

1.2 ENDICOTT RESERVOIR DESCRIPTION PROCEDURE

Following a review of the literature discussing Endicott Field, the Endicott zones were identified at key wells and were correlated throughout the wells in the field. Correlation entailed visual inspection and comparison of well log traces from neighboring wells. Occasionally, the correlation process was aided by listings of zone tops in well completion reports obtained from AOGCC. The computer programs developed by Scientific-Software Intercomp, LOGCALC, were then used in the conversion of data from measured well depths (MWD) to true vertical depths (TVD), generation of cross sections, and in the detailed well log analysis. Surf II, a contouring program written by the Kansas Geological Survey, was utilized in generation of contour plots.

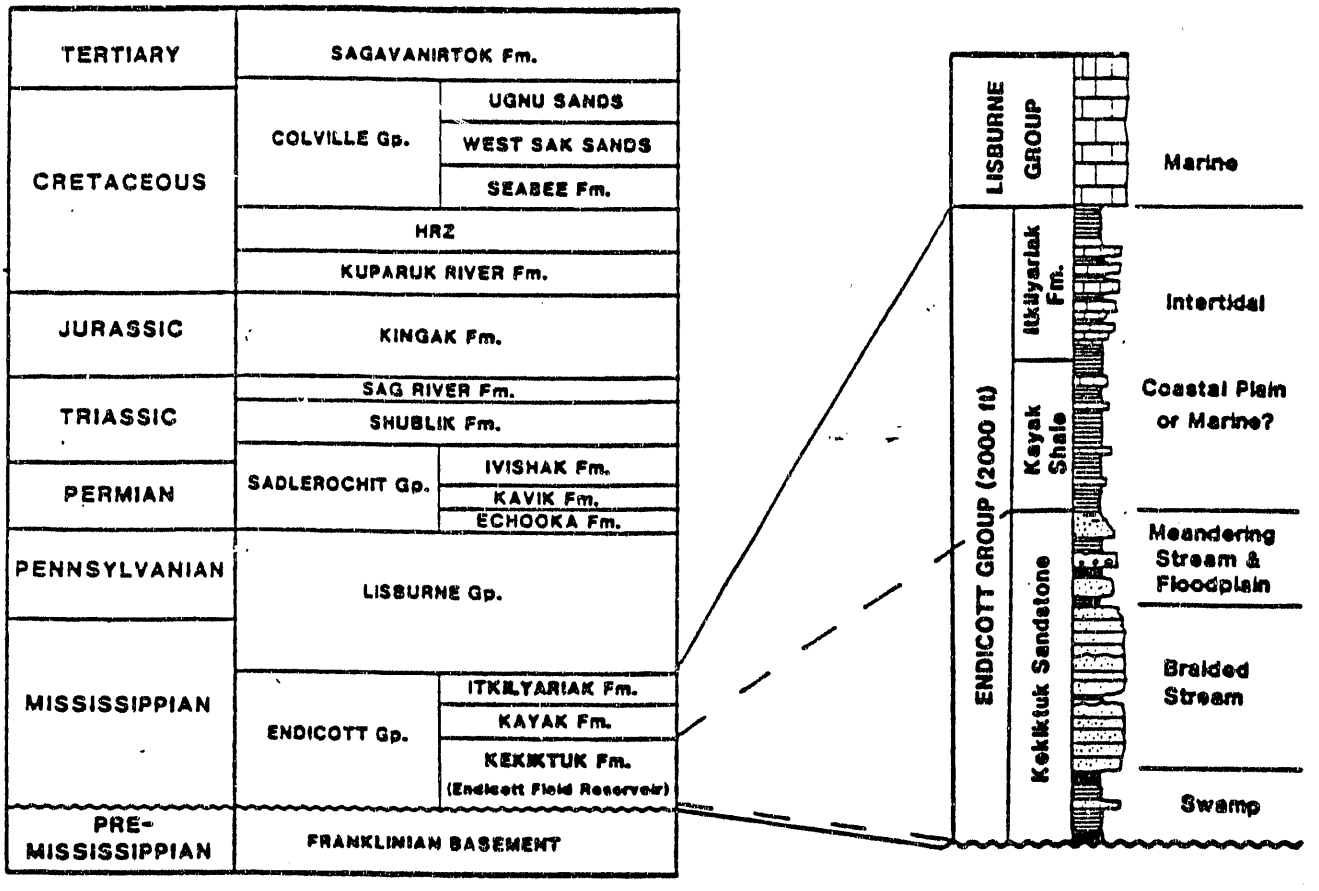

Figure 1.4: Endicott Group Stratigraphic Position and Lithologic Description (Woidneck, et al, 1987)

The comprehensive article by Woidneck et al (1987) provided values of input parameters for log analysis, including reservoir salinity, formation temperature, and the tortuosity and cementation exponents. The primary objective of Endicott well log analysis to date has been to determine the petrophysical properties of each zone as defined in the literature. In general, the Endicott field presents a complicated combination of faulting, structure, and lateral stratigraphic variation. As such, reservoir zones may not represent time stratigraphic units, but rather, as Woidneck et al. (1987) stated, lithostratigraphic units composed of rocks with similar reservoir properties. Although rocks within defined zones may transgress time lines from well-to-well, they possess common reservoir properties unique to each zone and identifiable for correlation and well log analysis. For brevity, individual well names have been abbreviated in this report and are listed in Table 1.2. A map of all wells at Endicott is shown in Figure 1.5. Figure 1.6 shows the Endicott wells which have been analyzed in this report and the locations of cross sections A-A' and B-B'.

1.3 ENDICOTT RESERVOIR DESCRIPTION

1.3.1 Structural Analysis

Cross sections A-A' and B-B' (Figures 1.7 and 1.8) provide evidence of the structural component at Endicott, with dips to the south and west. Since true dip is southwest at 4 to 6 degrees, these cross sections illustrate west and south components of dip only. The Lower Cretaceous Unconformity (LCU) truncates the Kekiktuk throughout much of the field area. Exceptions include western portions of the field, such as the region surrounding Sag Delta 4. The LCU lies at approximately 9425 feet subsea at this well, while the top Kekiktuk lies at 9792 ft subsea.

Cross section A-A' illustrates the impact of the LCU on the Kekiktuk as it truncates into progressively older rocks to the east. While the LCU exhibits only slight (1 to 2 degree) easterly dip, the Kekiktuk exhibits readily observable westward dip. Were the distances between wells scaled to true distances, the dips would appear less exaggerated between Sag Delta 4 and O-16. Similarly, eastward dip at the level of the LCU would also be less pronounced. Faulting may exist between these two wells, however, and, as such, a fault has been dashed in on the cross section.

Table 1.2
Endicott Wells Utilized in Well Log Analysis to Date

Full Well Name	Abbreviated Well Name
1. Duck Island 1	Duck 1
2. Duck Island 2	Duck 2
3. Duck Island 3	Duck 3
4. Sag Delta 4	SD-4
5. Sag Delta 7	SD-7
6. Sag Delta 10	SD-10
7. MPI 2-4/M-19	M-19
8. MPI 1-29/M-25	M-25
9. MPI 2-14/O 16	O-16
10. MPI 1-5/O 20	O-20
11. MPI 2-34/P-14	P-14
12. MPI 2-62/Q-17	Q-17
13. SDI 3-33/K-37	K-37
14. SDI 4-20/M-35	M-35
15. SDI 4-28/P-27	P-27
16. MPI 2-8/K-16	K-16
17. SDI 4-42/P-38	P-38
18. MPI 1-55/R-25	R-25
19. MPI 2-52/S-14	S-14
20. SDI 3-45/M-39	M-39

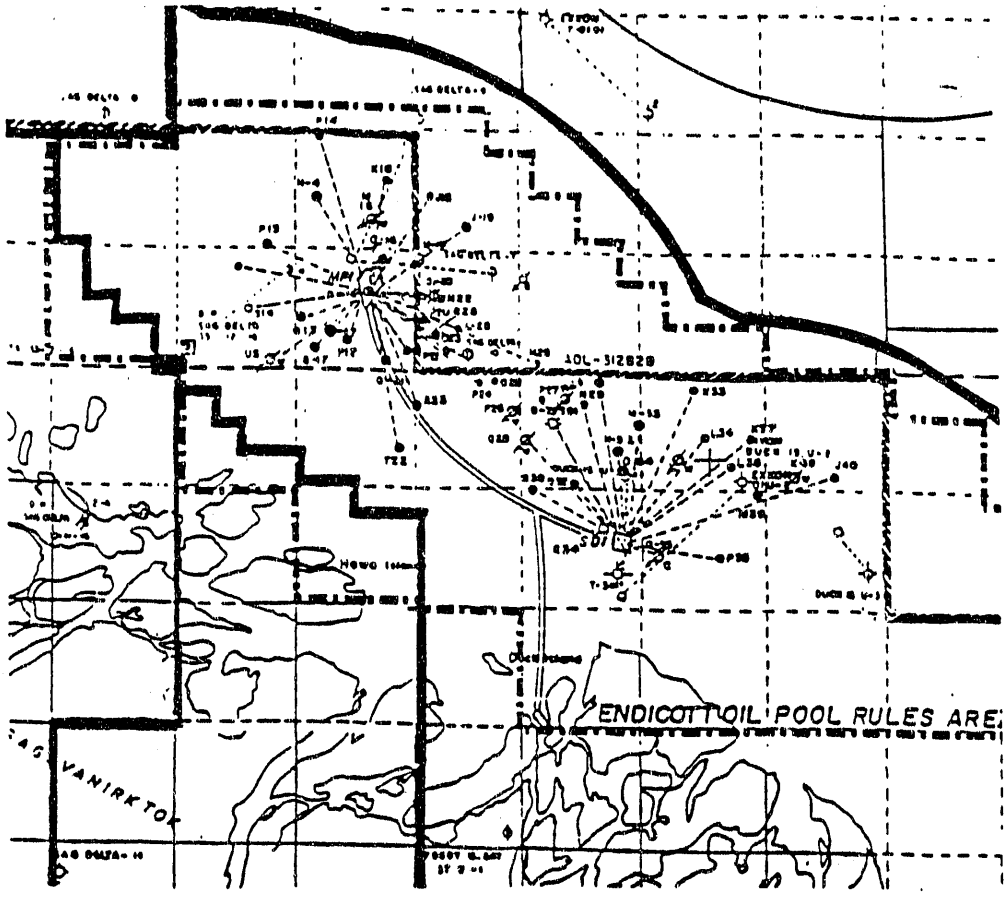

Figure 1.5: Endicott Field Well Location Map (Woidneck, et. al, 1987)

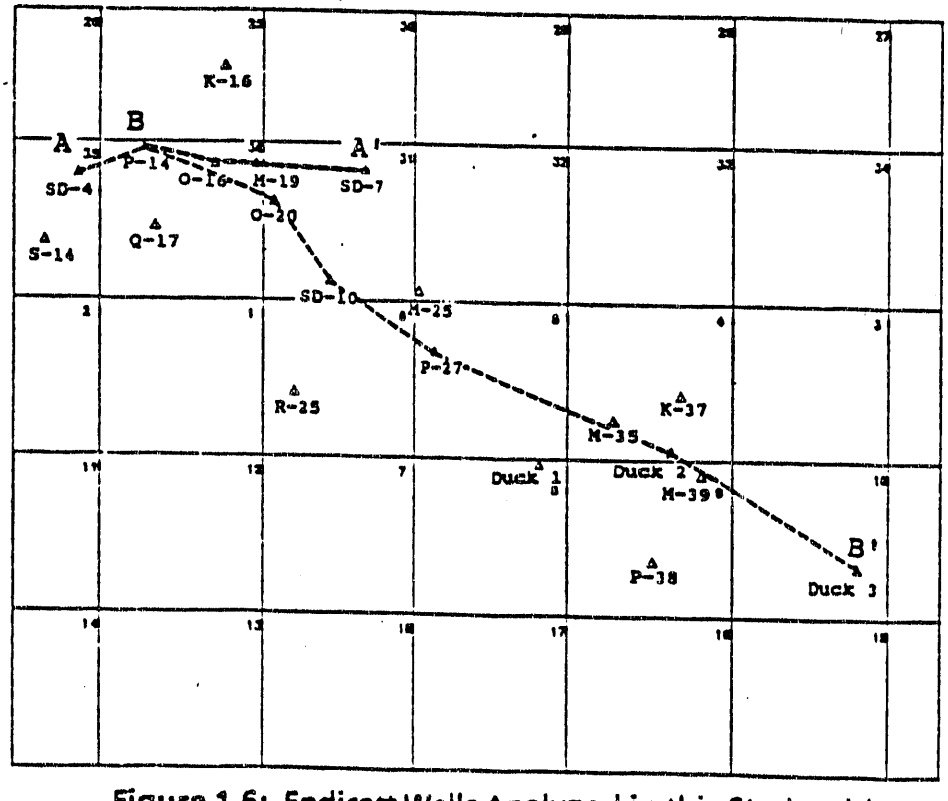

Figure 1.6: Endicott Wells Analyzed in this Study with Cross Sections A-A' and B-B' Plotted

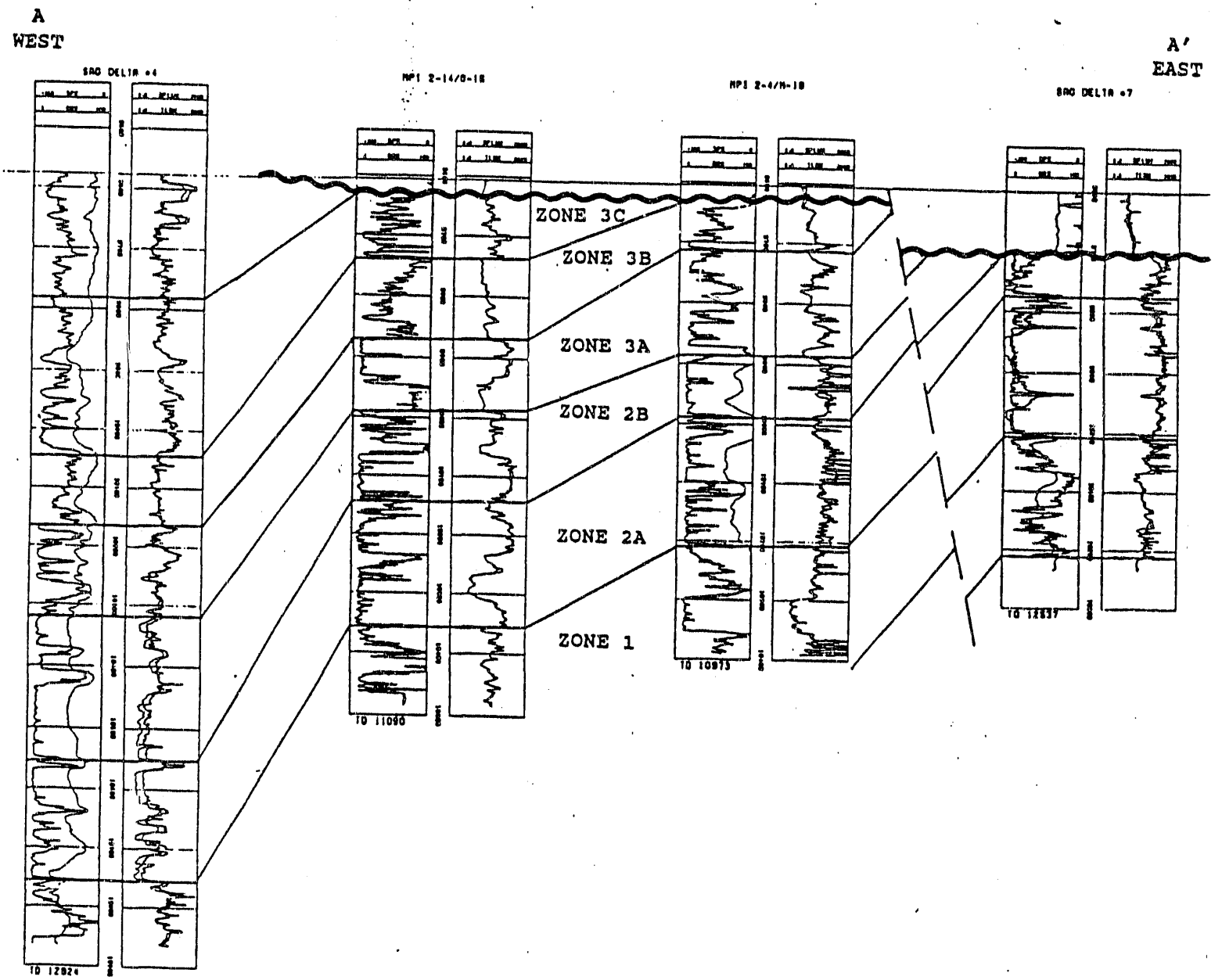

Figure 1.7: Endicott East-West Cross Section A-A'

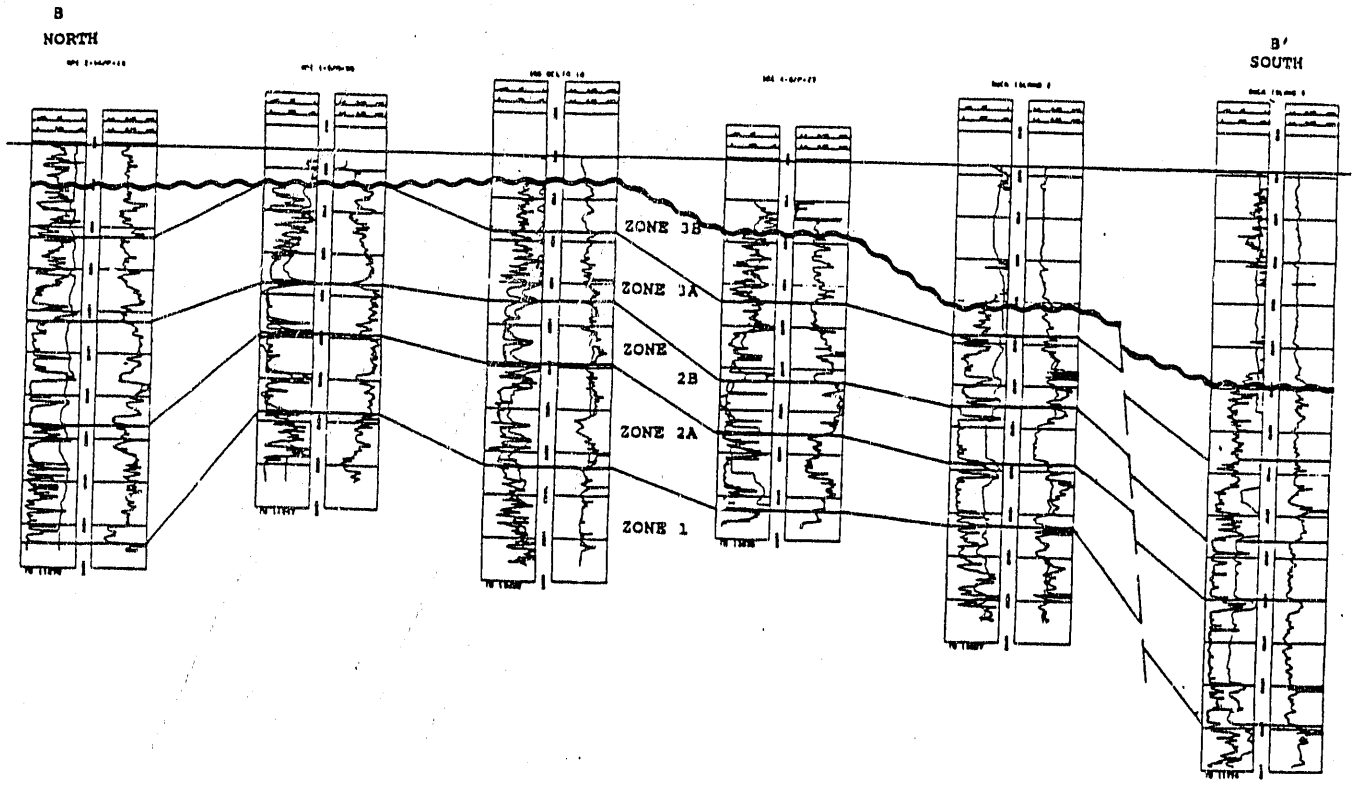

Figure 1.8: Endicott North-South Cross Section B-B'

Kekiktuk structural crest is evident along cross section B-B' at well O-20. The LCU appears relatively flat in the vicinity of this well, but develops slight dip along the southeast portion of the cross section. The analysis does not contradict the possibility of faulting between Duck Island 2 and Duck Island 3; hence a fault is dashed between these wells.

Well P-14 and K-16 are in close proximity to the LCU-cutting Niakuk fault zone. Endicott production ends at the edge of this fault system, approximately one-half mile to the north of the P-14, but continues down-dip and south of the P-14 for several miles to include the major portion of Endicott Field (Figure 1.2).

Well-to-well correlations along the cross sections reflect a relatively consistent pattern of correlatable sands and shales. However, shales tend to be less continuous in the northwestern portion of the field, resulting in increased difficulty in determining subzone tops in this area. Relatively continuous coal markers with consistently high resistivities, low bulk densities, and high interval transit times aided in correlating where shales were less consistent.

Because gradational transitions from one zone to another do occur at Endicott, several of the zonal picks taken from well logs carry a fair degree of uncertainty. Particular difficulty occurred in locating Zone 3B and 2B tops in the P-38, R-25, and S-14 wells. In addition, picks corresponding to the tops of Zone 2A were made with difficulty at the S-14 and M-39 wells. The top of Zone 3C was difficult to precisely determine at the K-16. Finally, the top of Zone 1 was estimated at the K-16, S-14 and M-39 wells, based on log trace character and picks taken from adjacent wells. While these picks carry the greatest uncertainty, determination of picks at other wells occasionally presented some difficulty, although to a lesser degree.

1.3.2 Log-Derived Petrophysical Properties

Effective porosity, water saturation, and net and gross thicknesses are listed in Tables 1.3 through 1.8. Table 1.9 lists weighted averages of porosity and water saturation for each zone. Cut-off values for net pay calculations are 6% for effective porosity, and 40% for water saturation and shale volume. Analysis was performed at one-half foot intervals. In addition to data tabulation, structural contour maps and isopach maps of porosity and water saturation have been generated. Three

dimensional plots are also provided and will be utilized with the contour and isopach maps in future enhanced oil recovery modeling at PDL. Detailed well log analysis of five additional Endicott wells will be incorporated in revised maps and 3-D plots to be presented in the final project report.

Excluding Zone 1 geologic correlations and picks (listed in Table 1.3), data corresponding to Zone 1 have not been tabulated to date for two reasons. First, Zone 1 is not a major producer at Endicott; only two out of the nearly 100 wells produce from this zone. This fits with the low energy, swampy depositional environment characteristic of this zone. Shales and coals are abundant, and sandstones, when present, tend to be fine-grained with low porosities. Second, most wells do not completely penetrate this zone, so that petrophysical analyses, including isopachs and single-valued zonal results cannot be generated.

Overlying Zone 1 is Zone 2, which is subdivided into Zones 2A and 2B by a shale interval. This shale is visible on both cross sections, thinning toward the west of cross section A-A' (Figure 1-7). On the north-south cross section B-B' (Figure 1.8), the shale interval becomes less distinct toward the north, as thin sand stringers tend to interfinger in and out from well to well. Despite this interfingering, the shale remains distinct enough to be employed as a marker bed.

Table 1.4 lists calculated petrophysical values associated with Zone 2A. For the most part, Zone 2A thickness is well over 100 feet, and in one well (the M-19) it exceeds 300 feet. Average porosities vary from a low of 18% to a high of 26%, excluding the O-20 well, while water saturations range between 11% and 51%. The highest porosity value of 26% occurs in the M-19, where the calculated net pay is relatively large--153 ft. Weighted averages of porosity and water saturation given in Table 1.9 are 23% and 50%, respectively.

Zone 2A structure is contoured in Figure 1.9. The selected contouring option utilized in this report estimated grid nodal values as distance-weighted averaged of dips projected from nearby sample data points. The Surf II manual (Sampson, 1984) provides more details on its contouring routines. The surface of Zone 2A generally strikes northwest-southeast, and dips toward the southwest. The K-16 well is responsible for the development of a structural low which noses into Section 25 from southwest to interrupt the otherwise consistent patterns of strike and dip.

TABLE 1.3 Zone 1 Tops at Endicott Field

Well	Subsea depth to Top (ft)	Measured depth to Top (ft)
Duck 1	-10711	12137
Duck 2	-10475	13529
Duck 3	-10850	11468
SD-4	-10752	12694
SD-7	-9947	12170
SD-10	-10277	12878
M-19	-10242	10798
M-25	-10192	13870
O-16	-10300	10875
O-20	-10121	11019
P-14	-10487	11196
Q-17	NDE	NDE
K-37	-10251	13210
M-35	-10437	12142
P-27	-10373	13703
K-16	-10316	12331 (EST)
P-38	NDE	NDE
R-25	NDE	NDE
S-14	-10867	12825 (EST)
M-39	-10519	12810 (EST)

NDE = Not Deep Enough
EST = Estimated

Table 1.4
Petrophysical Properties of Endicott Zone 2A

Well	Subsea depth to Zone 2A (ft)	Measured depth to Zone 2A (ft)	Thickness (ft)	Net Pay (ft)	Avg. Ø (%)	Avg. Sw (%)
Duck 1	-10515	10900	196	10	20	80
Duck 2	-10250	13283	225	75	23	62
Duck 3	-10554	11147	296	16	19	87
SD-4	-10520	12403	232	19	20	80
SD-7	-9721	11874	226	32	21	67
SD-10	-10041	12567	236	133	21	51
M-19	-9929	10460	313	153	26	46
M-25	-9984	13620	208	85	25	51
O-16	-10091	10586	209	139	24	31
O-20	-9927	10800	194	0	--	--100
P-14	-10211	10897	276	171	21	21
Q-17	-10470	10748	99	14	24	68
K-37	-10061	12950	190	140	23	17
M-35	-10277	11934	160	115	21	34
P-27	-10197	13485	176	83	20	48
K-16	-10120	12067	196	69	22	52
P-38	NDE	NDE	--	--	--	--
R-25	NDE	NDE	--	--	--	--
S-14	-10639	12578	232	6	--	100
M-39	-10373	12653	177	27	18	68

NDE = Not Deep Enough

Table 1.5
Petrophysical Properties of Endicott Zone 2B

Well	Subsea depth to Zone 2B (ft)	Measured depth to Zone 2B (ft)	Thickness (ft)	Net Pay (ft)	Avg. Ø (%)	Avg. Sw (%)
Duck 1	-10315	11694	164	36	22	73
Duck 2	-10123	13142	127	21	22	85
Duck 3	-10416	10999	138		18	100
SD-4	-10292	12116	228	10	19	88
SD-7	-9651	11793	70	1	20	85
SD-10	-9894	12377	147	104	22	43
M-19	-9832	10356	97	51	25	53
M-25	-9863	13472	121	76	26	47
O-16	-9933	10372	158	118	26	14
O-20	-9824	10683	103	0	--	100
P-14	-9971	10634	240	189	24	21
Q-17	-10240	10510	230	91	24	58
K-37	-9910	12752	151	147	24	9
M-35	-10131	11746	146	64	25	50
P-27	-10057	13311	140	117	26	9
K-16	-10030	11944	90	79	23	17
P-38	-10513	11820 (EST)	NDE	--	--	--
R-25	NDE	NDE	--	--	--	--
S-14	-10445	12364	194	0	21	98
M-39	-10239	12499	134	77	19	51

NDE = Not Deep Enough
EST = Estimated

The contour plot of Zone 2A porosity (Figure 1.10) shows highest values in the central and northwest portions of the mapped area, but the distribution of values shows a high degree of randomness. Water saturations also vary from well-to-well across the mapped southeast edge. Generally lower values are found in the northwest and central regions (Figure 1.11). 3-D plots of porosity and water saturation (Figures 1.12 and 1.13) tend to reflect a poor correlation between high porosities and low water saturations.

Zoned 2B average porosity is somewhat lower than that corresponding to Zone 2A (20% versus 23%, respectively, as listed in Table 1.9). Average water saturation remains essentially unchanged at 51%, compared to 50% for Zone 2A. Excluding the Duck Island Well 3 and Well O-20, the values of water saturation range from a low of 9% at the P-27 and K-37 wells to a high of 88% at the Sag Delta 4.

Contour maps depicting structure of Zone 2A and 2B (Figures 1.9 and 1.14) show strong similarities. These similarities are also reflected in their generally unchanging interval thicknesses on cross sections A-A' and B-B' (Figures 1.7 and 1.8). Interval thicknesses do vary enough, however, to result in slightly less dip at the level of Zone 2B, as compared with Zone 2A. In contrast to Zone 2A, a reasonably good correlation exists between Zone 2B higher porosities and low water saturations. Zone 2B porosity and water saturation contour maps show this, as do corresponding 3-D plots (Figures 1.15-1.18). The bar graphs of Zone 2B porosity and water saturation (Figure 1.19) also highlight the relatively good correlation between lower porosity and higher water saturation associated with this zone. The corresponding bar graph for Zone 2A (Figure 1.20) reflects the poor correlation between lower porosities and high water saturations.

Zone 3 is derived from a more mature environment of deposition as compared to Zone 2. Meandering stream sand sequences predominate in the former zone as compared to sheetlike geometries associated with braided stream deposits in the latter (Woidneck, et al, 1987). Overlapping point bars with good interconnectivity exist in Zone 3, and help to explain why the highest Endicott porosities are found in this zone. The structural contour map of the top of Zone 3A (shown in Figure 1.21) strongly resembles the structural contour maps of Zones 2A and 2B. The zone shallows toward the northwest as is expected, and dips south and west away from the

M-19 and O-20 wells. Also, this map show a continuation of the trend toward progressively shallower dips up section through the Kekiktuk zones.

Zone 3A porosities range from a low of 18% in the Sag Delta 4 to a high of 34% in the M-25 (Table 1.6). The thickness-weighted average porosity for this zone is 28% and is the highest of any of the zones (Table 1.9). Figure 1.19 shows the trend of higher porosities toward the central region of the map area with lowest values occurring in the northwest. A region of very similar porosities (around 22%) exists in the northwest but consistently higher porosities occur in the southeast (Figure 1.22).

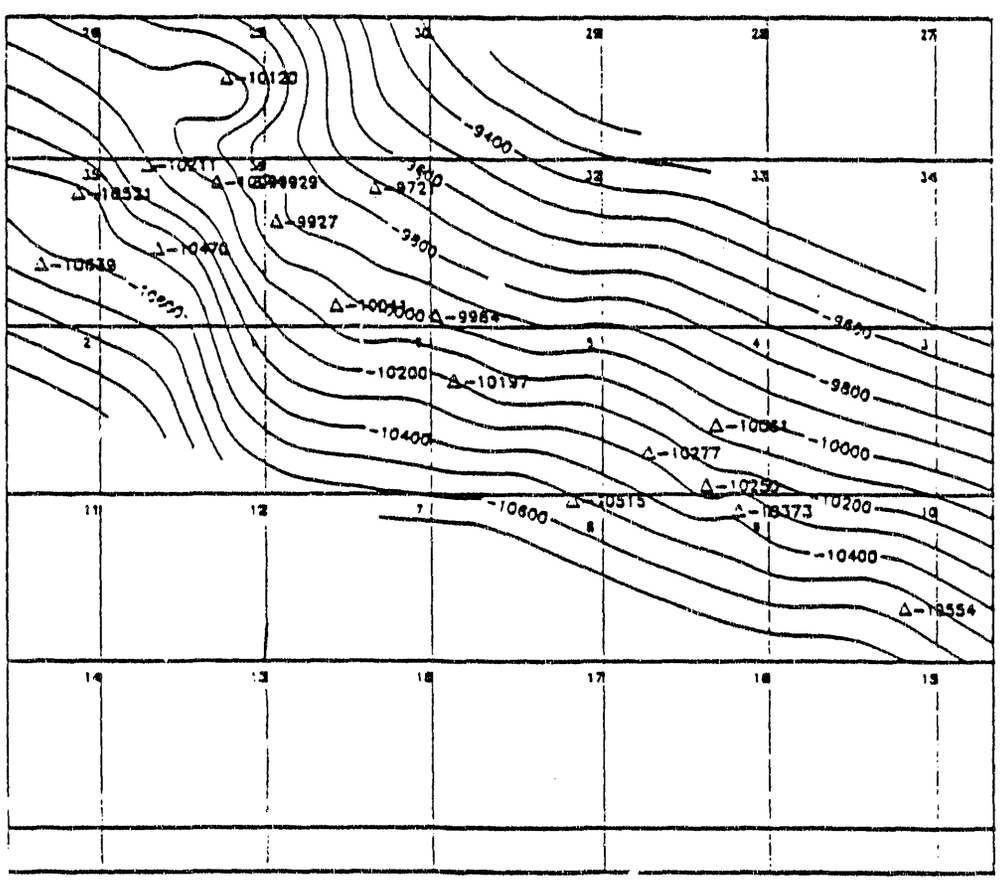

Figure 1.9: Top Zone 2A Structure Contour Map C.I. 50'

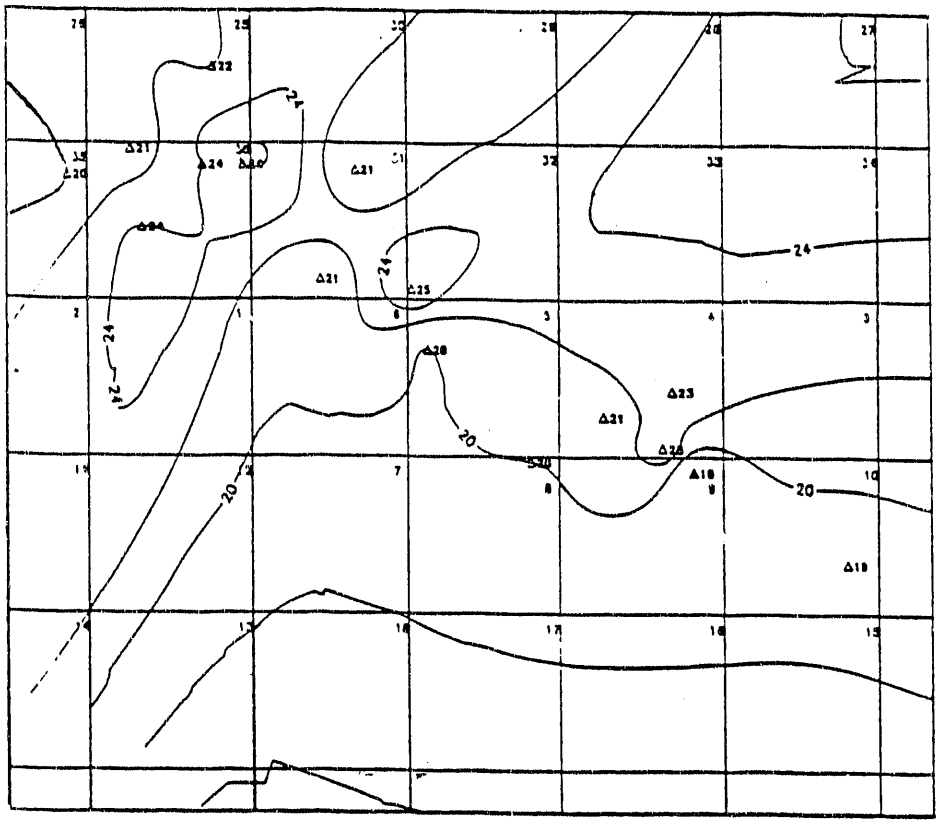

Figure 1.10: Zone 2A Porosity Contour Map C.I. 2%

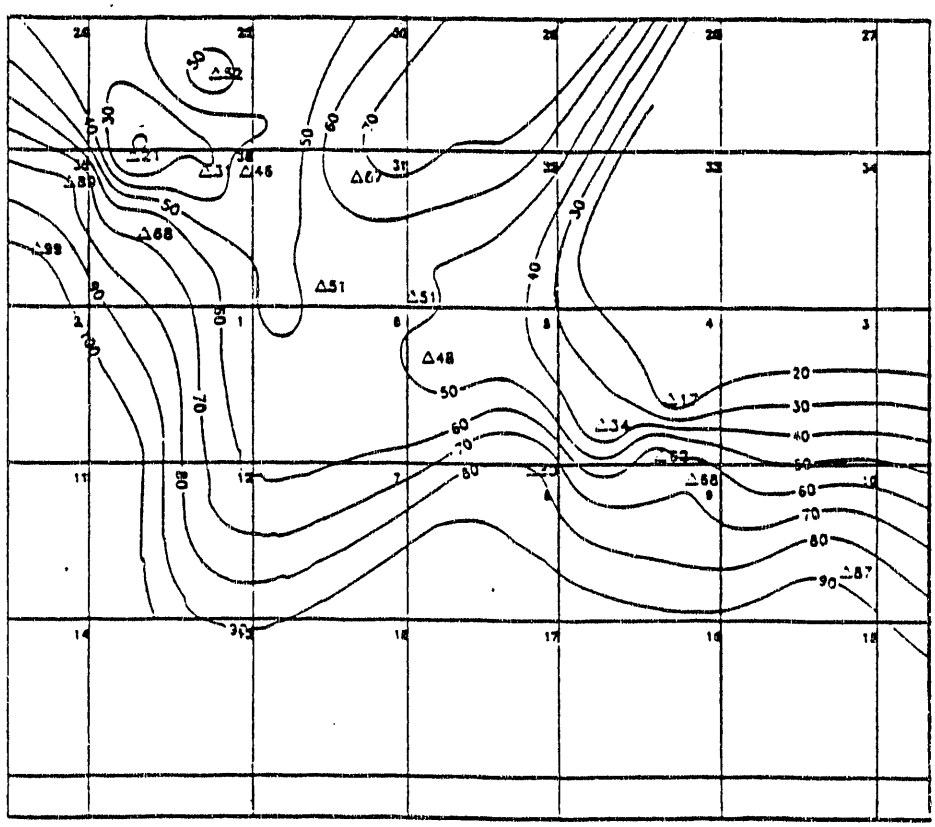

Figure 1.11: Zone 2A Water Saturation Contour Map C.I. 10%

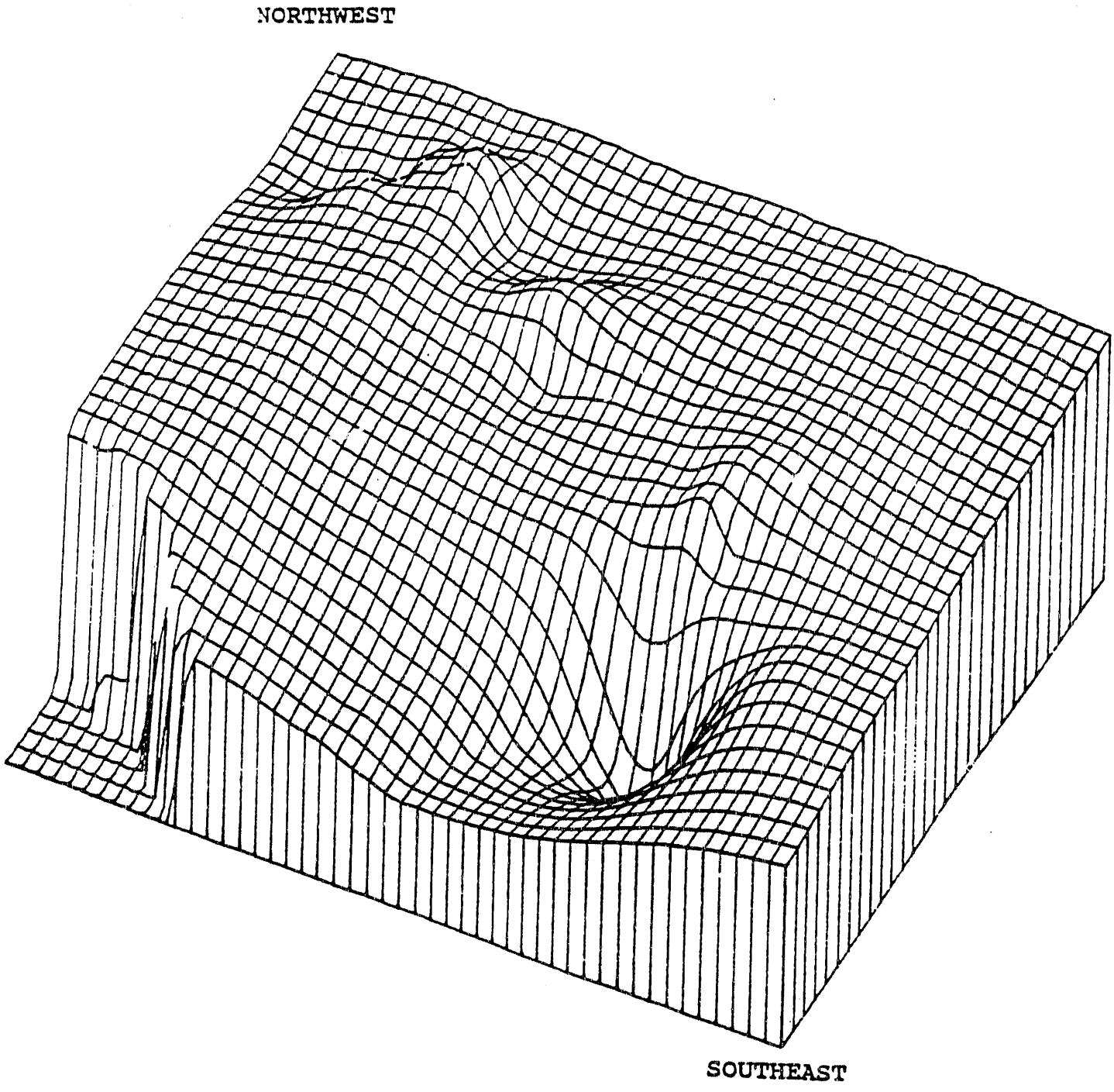

Figure 1.12: Zone 2A 3-D Porosity Isopach

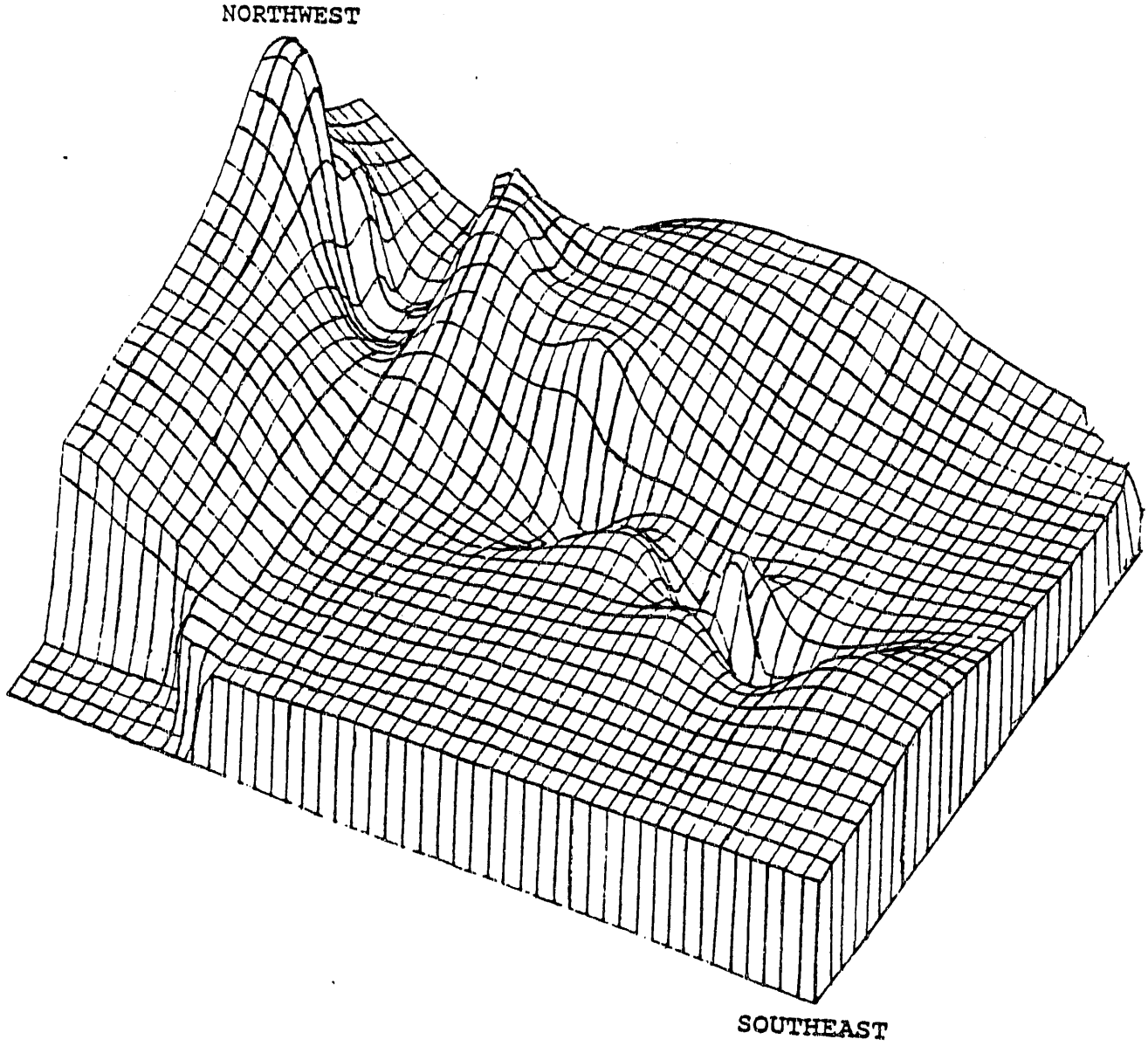

Figure 1.13: Zone 2A 3-D Water Saturation Isopach

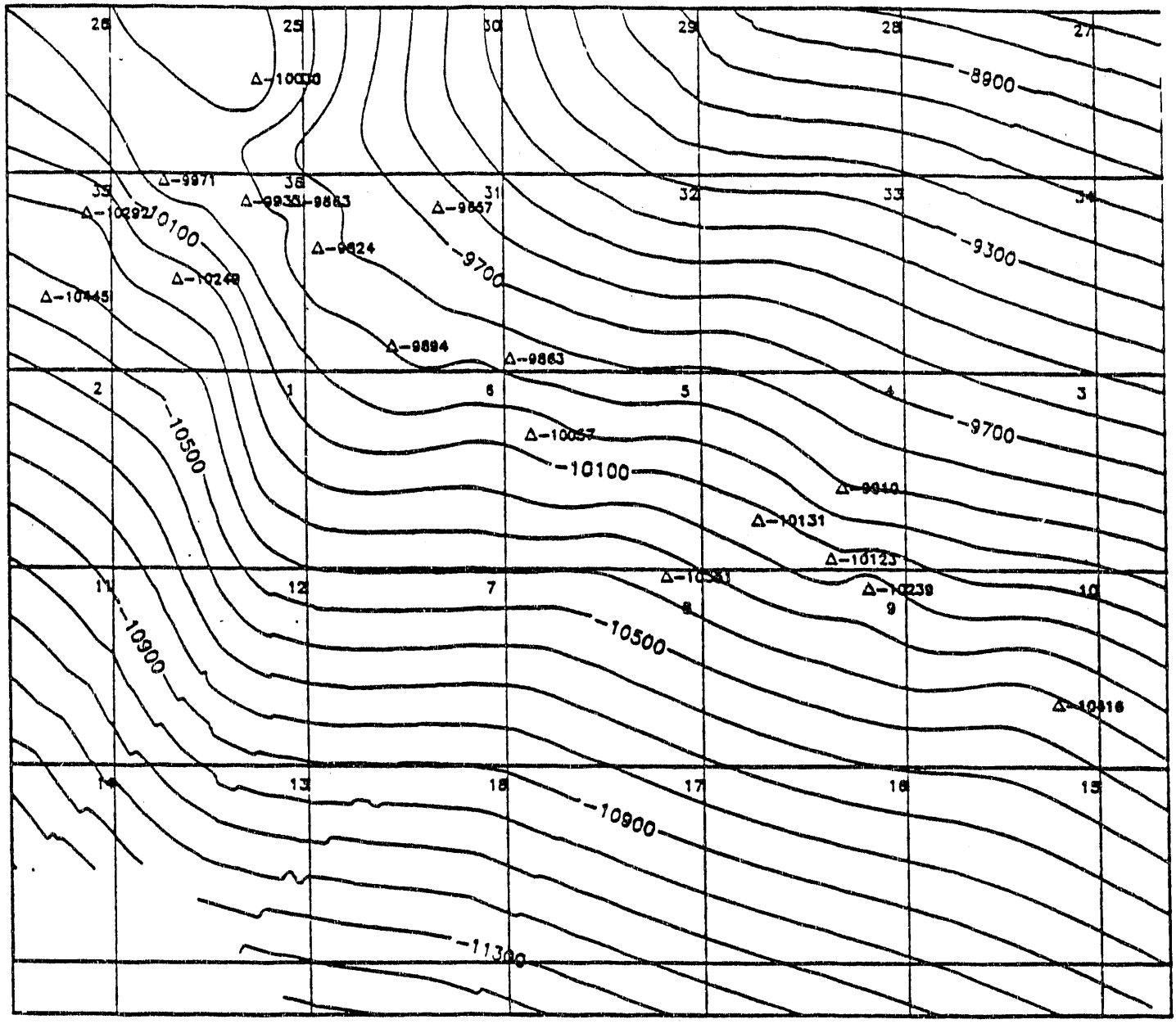

Figure 1.14: Zone 2B Structure Contour Map C.I. 50'

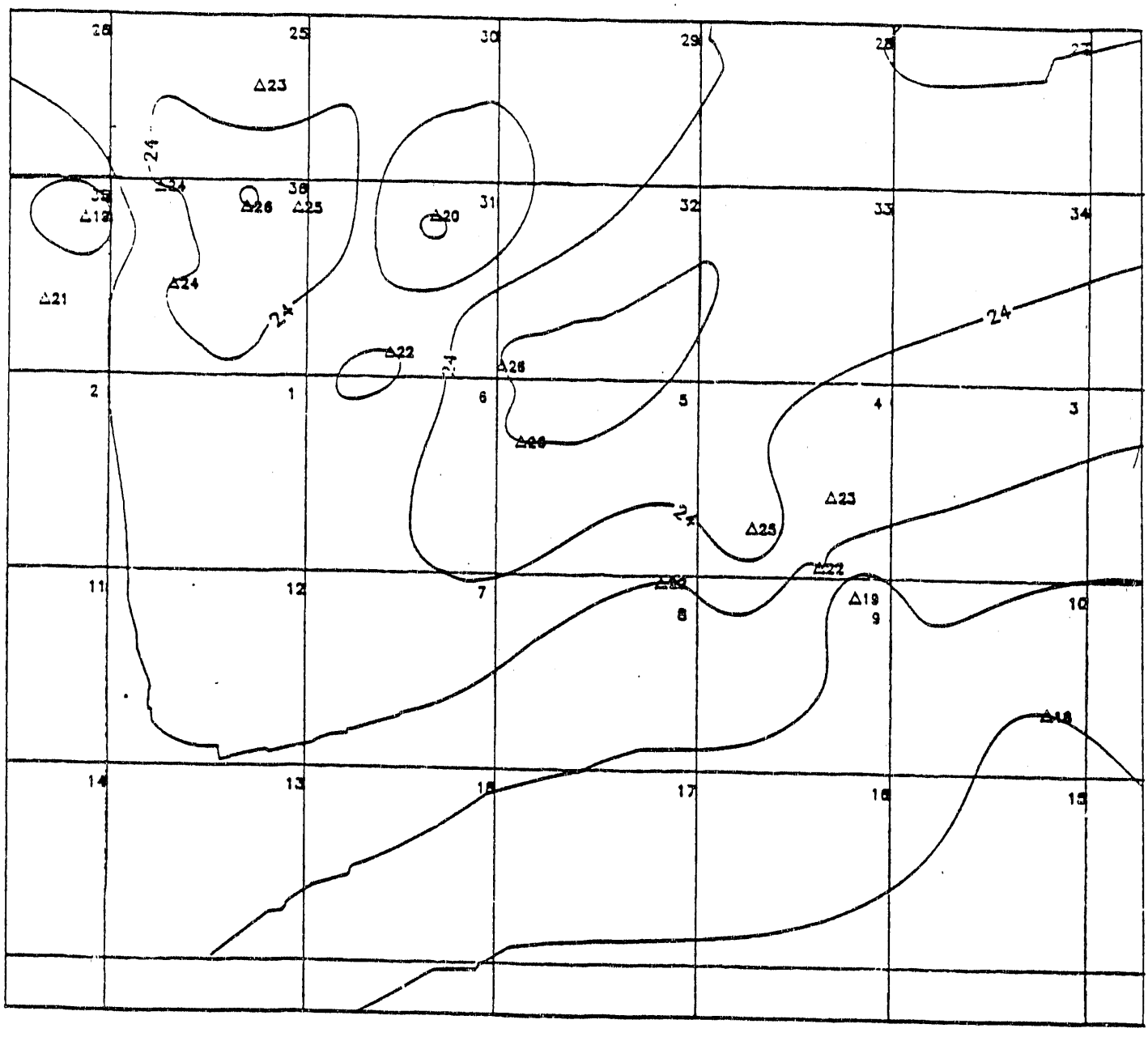

Figure 1.15: Zone 2B Porosity Contour Map C.I. 2%

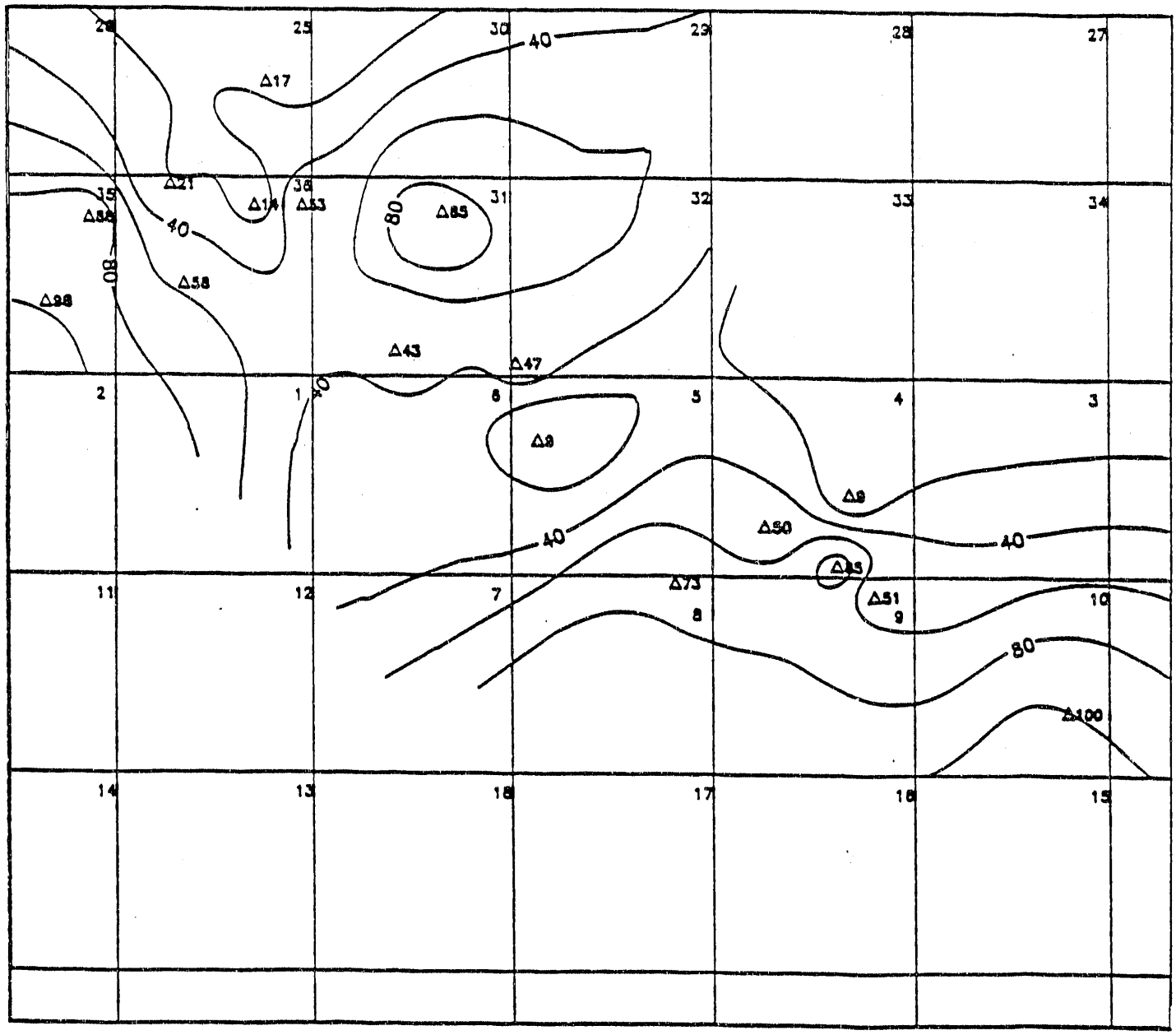

Figure 1.16: Zone 2B Water Saturation Contour Map C. I. 20%

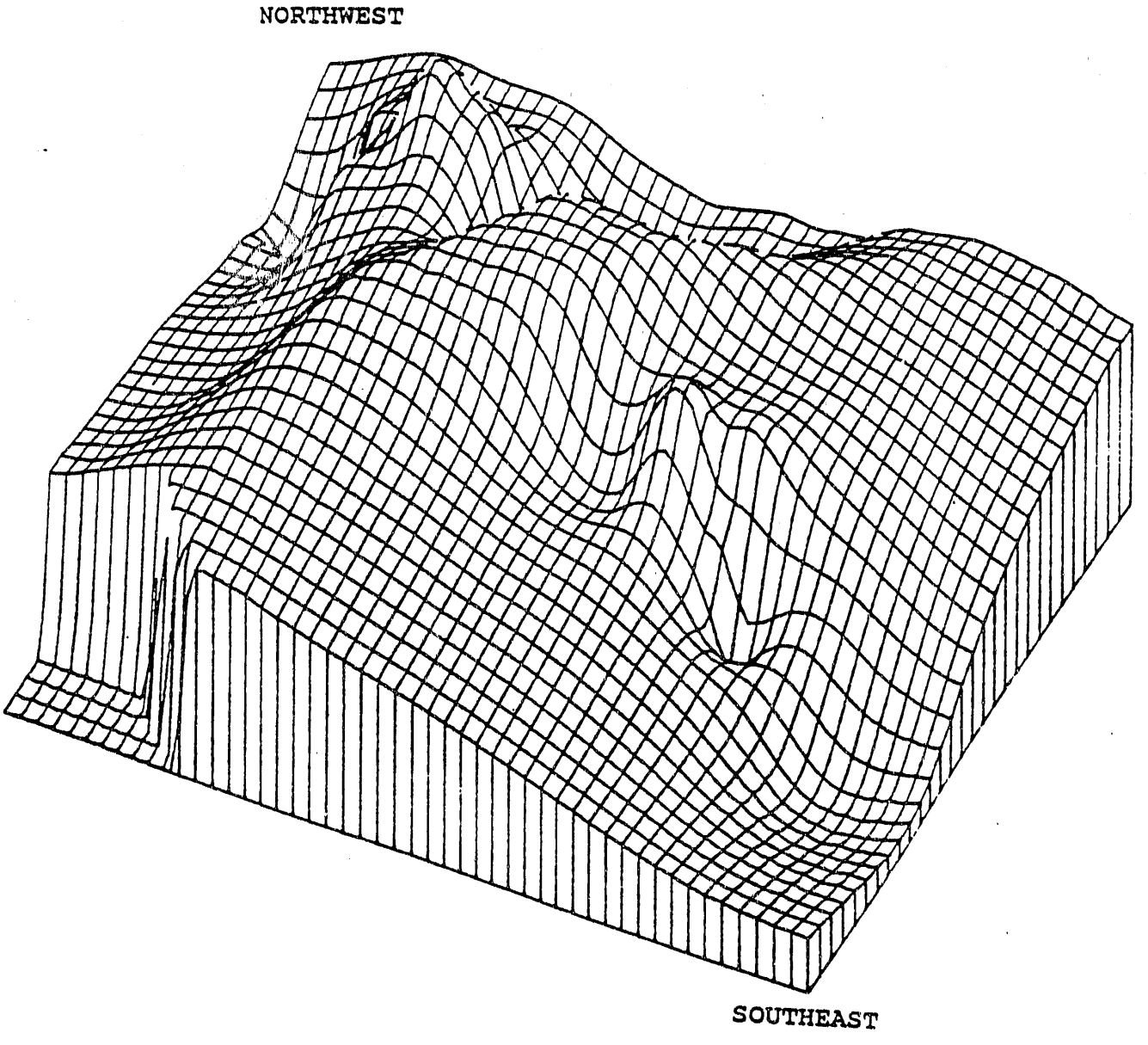

Figure 1.17: Zone 2B 3-D Porosity Isopach

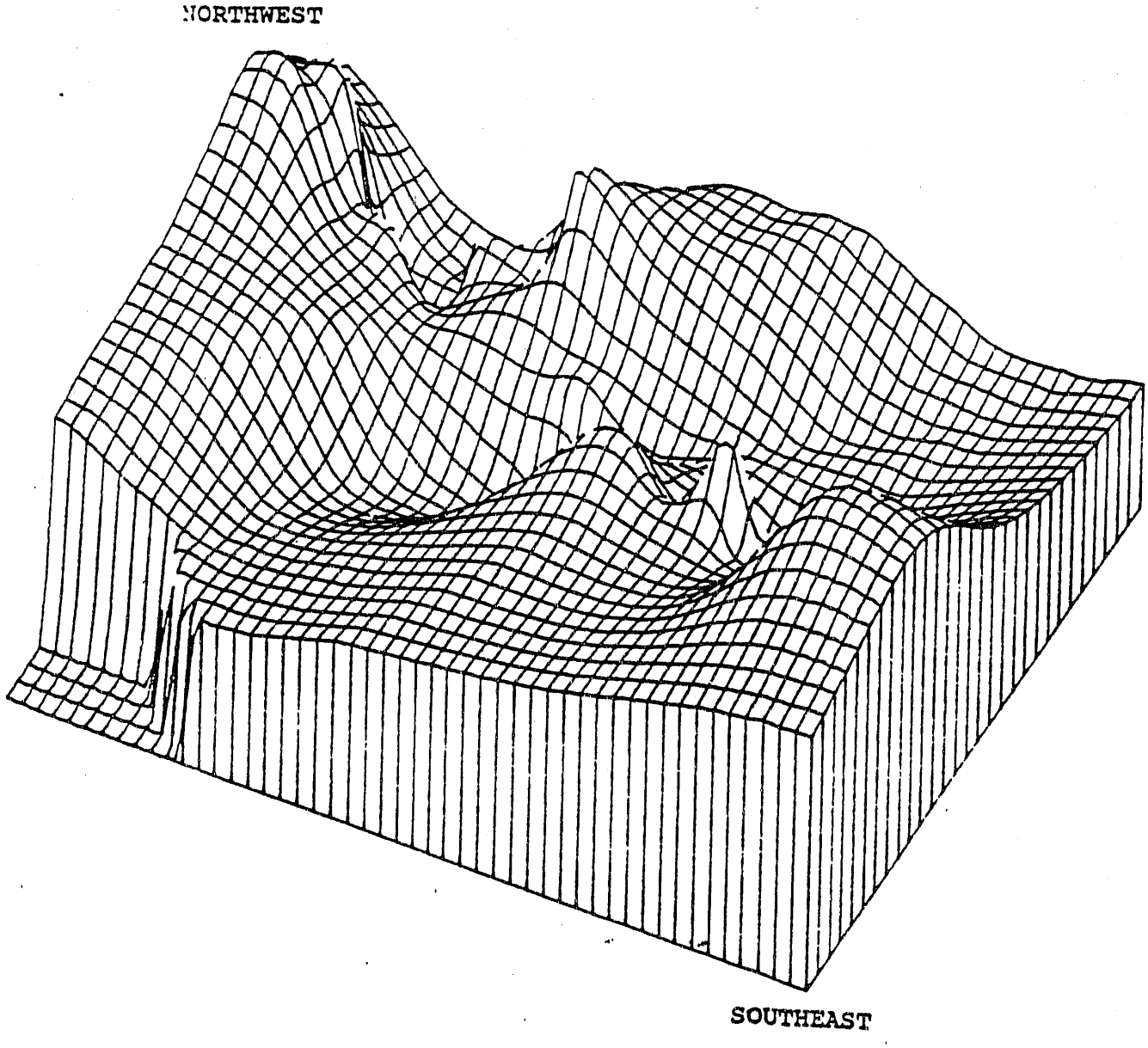

Figure 1.18: Zone 2B 3-D Water Saturation Isopach

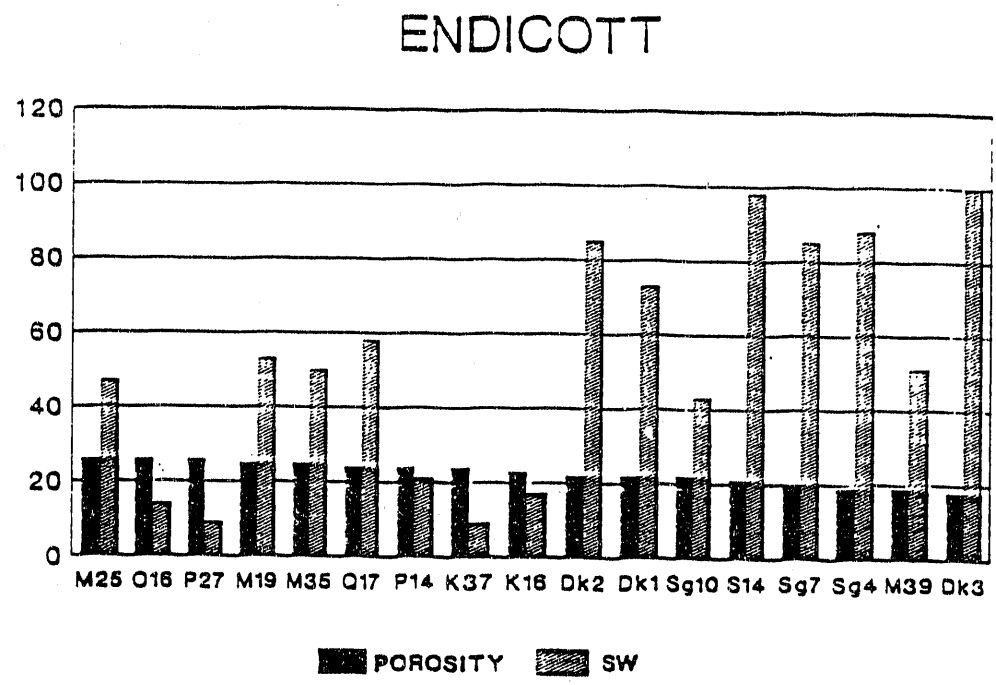

Figure 1.19: Porosity - Sw: Zone 2B

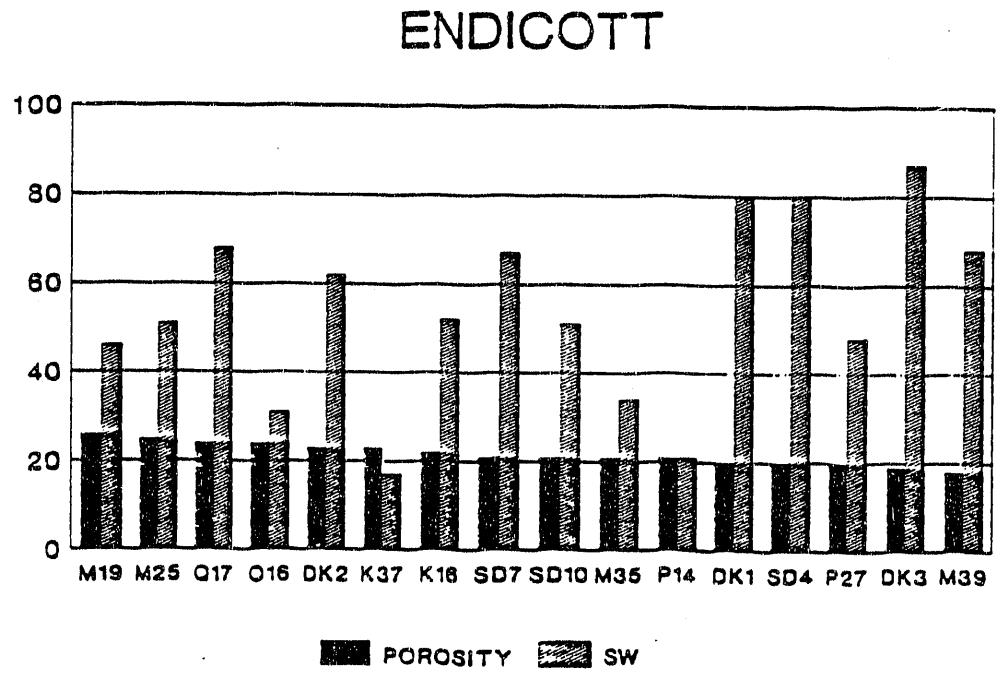

Figure 1.20: Porosity - Sw: Zone 2A

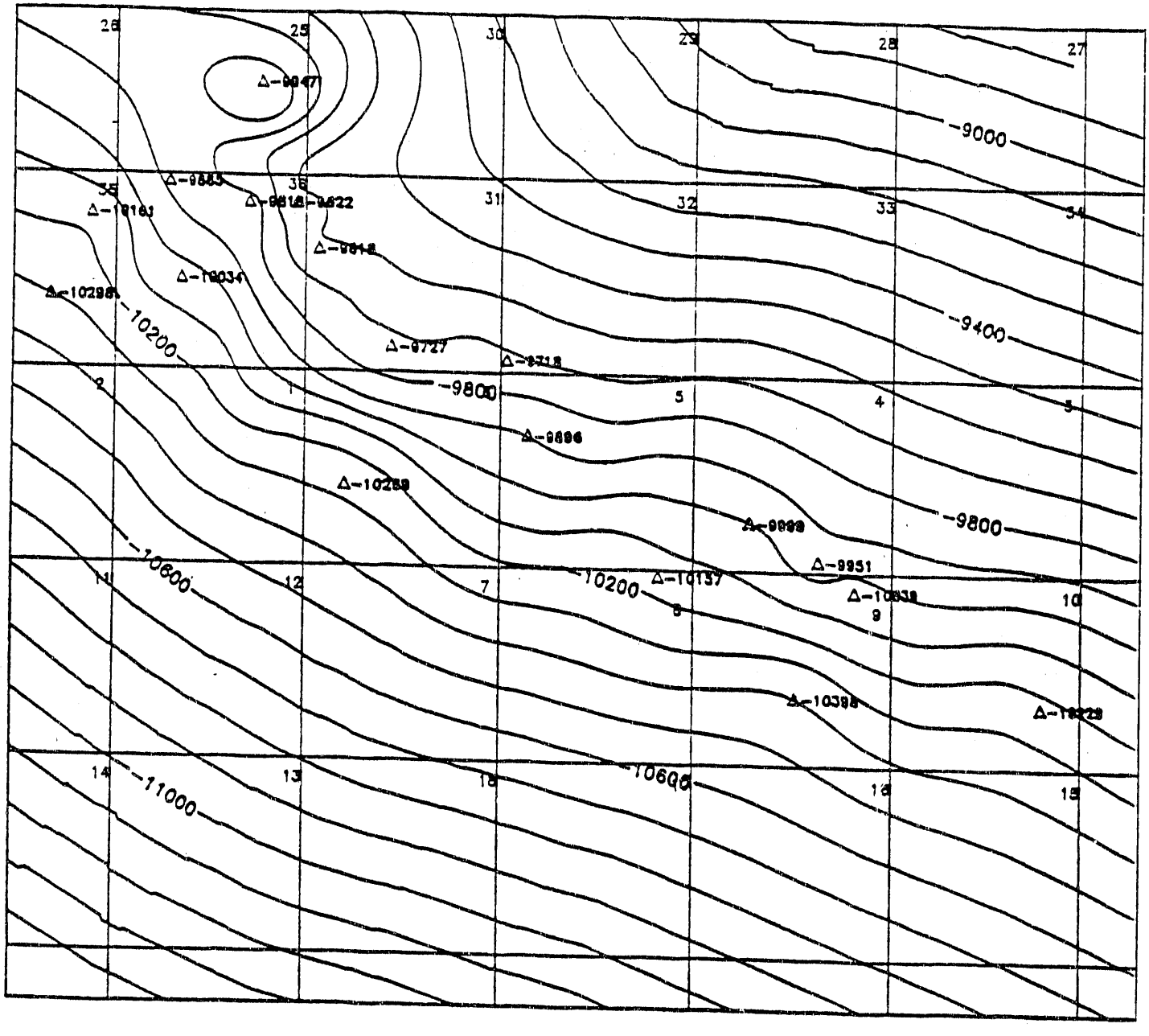

Figure 1.21: Top Zone 3A Structure Contour Map C.I. 50'

In contrast, water saturations vary widely across the area but show highest values in the northwest and southeast (Figure 1.23). They range from a minimum of 13% at the P-27 to a high of 84% at the S-14. These porosity and water saturation patterns can also be seen in 3-D plots of Zone 3A porosity and water saturation (Figures 1.24 and 1.25). Because several wells exhibit a combination of relatively high porosities and low water saturations in Zone 3A, it is potentially the most prolific hydrocarbon-producing zone at Endicott field.

Zone 3B, being shaly in most of the mapped area, yields comparatively low values of net pay, ranging from 7 to 61 feet (Table 1.7). Porosities within non-shaly intervals are similar to those in Zone 2. The highest porosity (36%) occurs in Duck Island 3 while the lowest value (11%) is found in the O-16. The average porosity in Zone 3B is 16% versus 28% in Zone 3A. Water saturations in Zone 3B are considerably higher than in Zone 3A. The average water saturation in Zone 3B is 59%, considerably higher than the 39% calculated for Zone 3A.

No Zone 3B net pay is observed in four wells: Duck Island 2, M-19, R-25, and S-14. This is due to the high shale volumes at these wells. At those depth points where shale volumes are greater than the cut-off limit, LOGCALC sets the porosities to 0% and then excludes these points from net pay calculations. LOGCALC also sets water saturation to 100% at such points. A visual inspection of Zone 3B log traces confirms overwhelming shale content in the Duck Island 2 and Q-17 wells. At the M-19, R-25 and S-14, Zone 2B also consists primarily of shale, but some shaly sands are present.

The structure of Zone 3B shown in Figure 1.26 conforms to the general structural trend of the underlying Kekiktuk zones. Also, this map shows a continuation of the trend of progressively shallower dips up section through the Kekiktuk zones. Figure 1.27 shows that porosities are generally constant from northwest to southeast, and decrease toward the southwest. The most notable exception to this pattern occurs at the Duck Island 3, where a high porosity of 36% produces a contoured porosity high in its vicinity. Water saturations (Figure 1.28) vary dramatically across the area and show no similar directional trend of consistent values. Between the Duck Island 2 and Duck Island 3, porosities double from 18% to 36%. Values of water saturation vary substantially over short distances, especially near Duck Island 2 and the Q-17 wells. Overall, Zone 3B is of poorer reservoir quality than the other zones, which is predictable considering its higher shale content. Production from Zone 3B does

occur in about 15% of the Endicott wells, although no well produces entirely from this zone.

Zone 3C provides only a limited number of wells for analysis, as it is truncated by the LCU along the north-south axis of the reservoir. The structural contour map of the top of Zone 3C (Figure 1.29) indicates southwest dip. This zone's production is derived primarily from 28 wells located along the western, or down dip, flank of the field. Additional production occurs from two wells within the Niakuk fault zone, but on the upthrown side of the northernmost Niakuk fault. Porosity and water saturation are shown in Figures 1.30 and 1.31 and they illustrate increasing porosity combined with increasing water saturation southwestward with best values in the northwest.

Notwithstanding the relatively limited amount of data associated with this horizon, average values of porosity and water saturation are computed to be 17% and 41%, respectively. Both porosity and water saturation are generally lower than in other zones. Highest porosity is 22% and is found in the K-16 and the Sag Delta 4 (Table 1.8). The lowest value of porosity is 13% and is found in the Duck Island 1. Water saturation ranges from a high of 48% in the S-14 to a low of 22% in Sag Delta 4. Analysis of additional down dip wells would probably yield higher porosities assuming the effects of upward fining sands in Zone 3C to be less predominant lower down the section.

Figures 1.29 through 1.32, show the 3-D plots of net pay thicknesses corresponding to the formation subzones. Zones 2A and 2B (Figures 1.32 and 1.33) indicate net pay to generally increase from southeast to northwest. Considerable differences exist between net pay thicknesses of wells P-14 and Sag Delta 4, as indicated most dramatically in Figure 1.30. For example, Zone 2B net pay is 189 feet at well P-14 and diminishes to just 10 feet at Sag Delta 4. Such a rapid change in sand thickness over a short distance is possible in a braided stream environment. For example, depositionally, reverse eddies from active channels can carry silt and clay into connected, but abandoned older channels and then dump it as velocities rapidly drop. This results in silt and clay traps juxtaposed against sand deposits (Selley, 1978).

Table 1.6
Petrophysical Properties of Endicott Zone 3A

Well	Subsea depth to Zone 3A (ft)	Thickness (ft)	Net Pay (ft)	Avg. Ø (%)	Avg. Sw (%)
Duck 1	-10157	194	94	27	38
Duck 2	-9951	172	81	30	44
Duck 3	-10229	187	43	31	45
SD-4	-10161	131	36	18	50
SD-7	NP	--	--	--	--
SD-10	-9727	167	55	25	43
M-19	-9622	210	45	24	63
M-25	-9718	145	46	34	50
O-16	-9816	117	71	22	19
O-20	-9618	206	12	22	58
P-14	-9885	86	49	22	18
Q-17	-10034	206	90	22	24
K-37	NP	--	--	--	--
M-35	-9999	132	110	33	16
P-27	-9896	161	78	33	13
K-16	-9947	83	49	23	15
P-38	-10398	115	25	31	42
R-25	-10269	NDE	--	--	--
S-14	-10298	147	0	20	84
M-39	-10039	200	100	31	10

NP = Not Present
NDE = Not Deep Enough

Table 1.7
Petrophysical Properties of Endicott Zone 3B

Well	Subsea depth to Zone 3B (ft)	Gross Thickness (ft)	Net Pay (ft)	Avg. Ø (%)	Avg. Sw (%)
Duck 1	-9978	179	5	15	45
Duck 2	-9878	73	0	18	100
Duck 3	-10053	176	22	36	51
SD-4	-10000	161	10	14	44
SD-7	NP	--	--	--	--
SD-10	-9631	96	16	12	75
M-19	-9587	35	0	13	99
M-25	NP	NP	--	--	--
O-16	-9681	135	7	11	62
O-20	-9580	38	14	18	57
P-14	-9767	118	15	13	51
Q-17	-9964	70	--	--	100
K-37	NP	--	--	--	--
M-35	-9850	149	61	20	49
P-27	-9724	172	35	14	47
K-16	-9838	109	5	17	40
P-38	-10173	225	4	15	72
R-25	-10123	146	0	--	100
S-14	-10160	138	0	12	72
M-39	-9943	96	11	15	33

NP = Not Present

Table 1.8
Petrophysical Properties of Endicott Zone 3C

Well	Subsea depth to Zone 3C (ft)	Gross Thickness (ft)	Net Pay (ft)	Avg. Ø (%)	Avg. Sw (%)
Duck 1	-9791	187		13	42
Duck 2	NP	--	--	--	--
Duck 3	NP	--	--	--	--
SD-4	-9792	208	107	18	22
SD-7	NP	--	--	--	--
SD-10	NP	--	--	--	--
M-19	NP	--	--	--	--
M-25	NP	--	--	--	--
O-16	-9545	136	51	17	33
O-20	NP	--	--	--	
P-14	-9662	105	41	16	31
Q-17	-9752	212	84	18	33
K-37	NP	--	--	--	--
M-35	NP	--	--	--	--
P-27	NP	--	--	--	--
K-16	-9677	161	115	22	25
P-38	-9919	254	36	14	46
R-25	-9895	228	5	20	70
S-14	-9931 (EST)	229	28	16	48
M-39	NP	--	--	--	--

NP = Not Present
EST = Estimated

Table 1.9

Weighted Zone Averages of Porosity and Water Saturation at Endicott Field

	Avg. Porosity (%)	Avg. Water Saturation (%)
Zone 3C	17	41
Zone 3B	16	59
Zone 3A	28	39
Zone 2B	20	51
Zone 2A	23	50

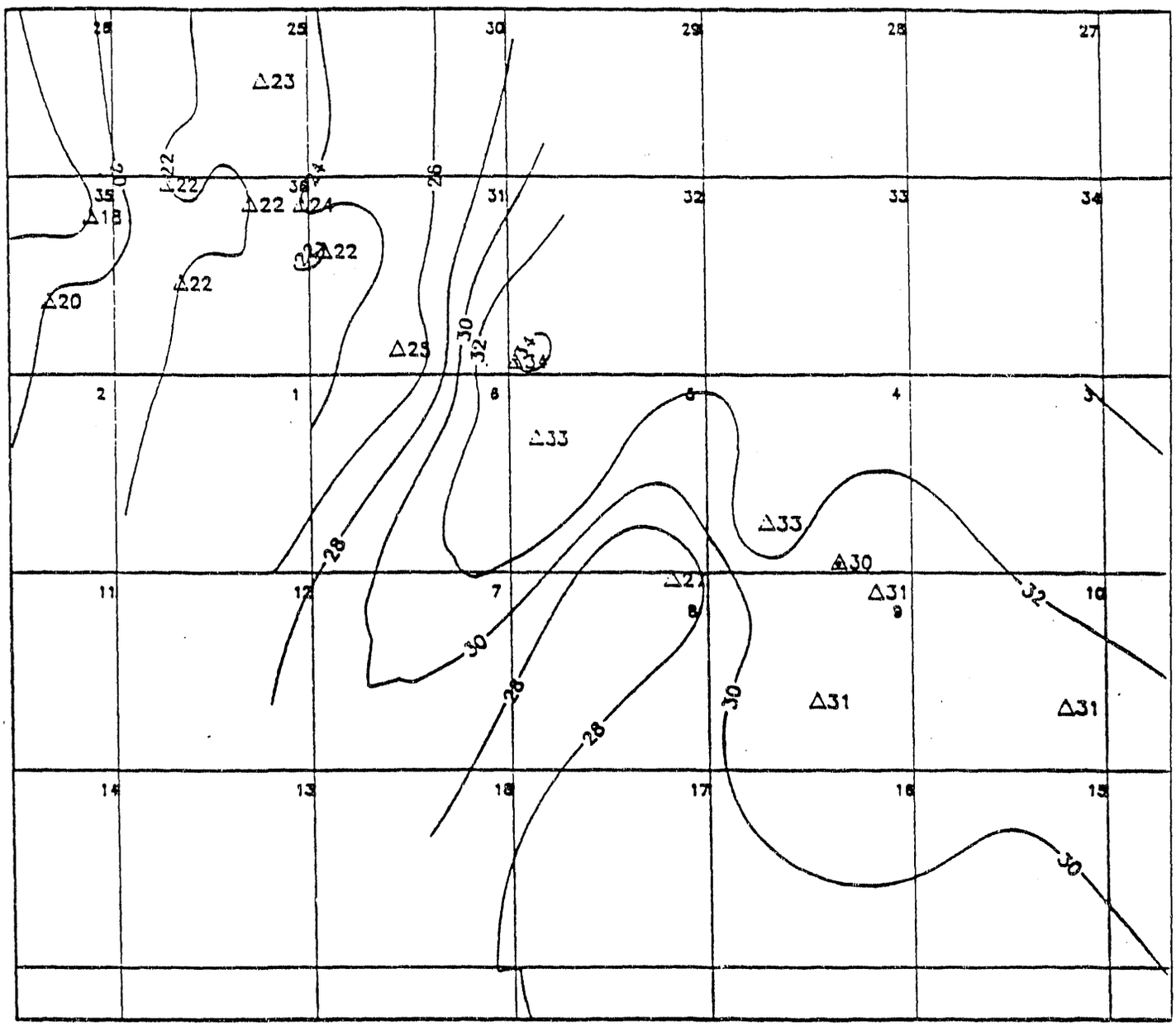

Figure 1.22: Zone 3A Porosity Contour Map C.I. 2%

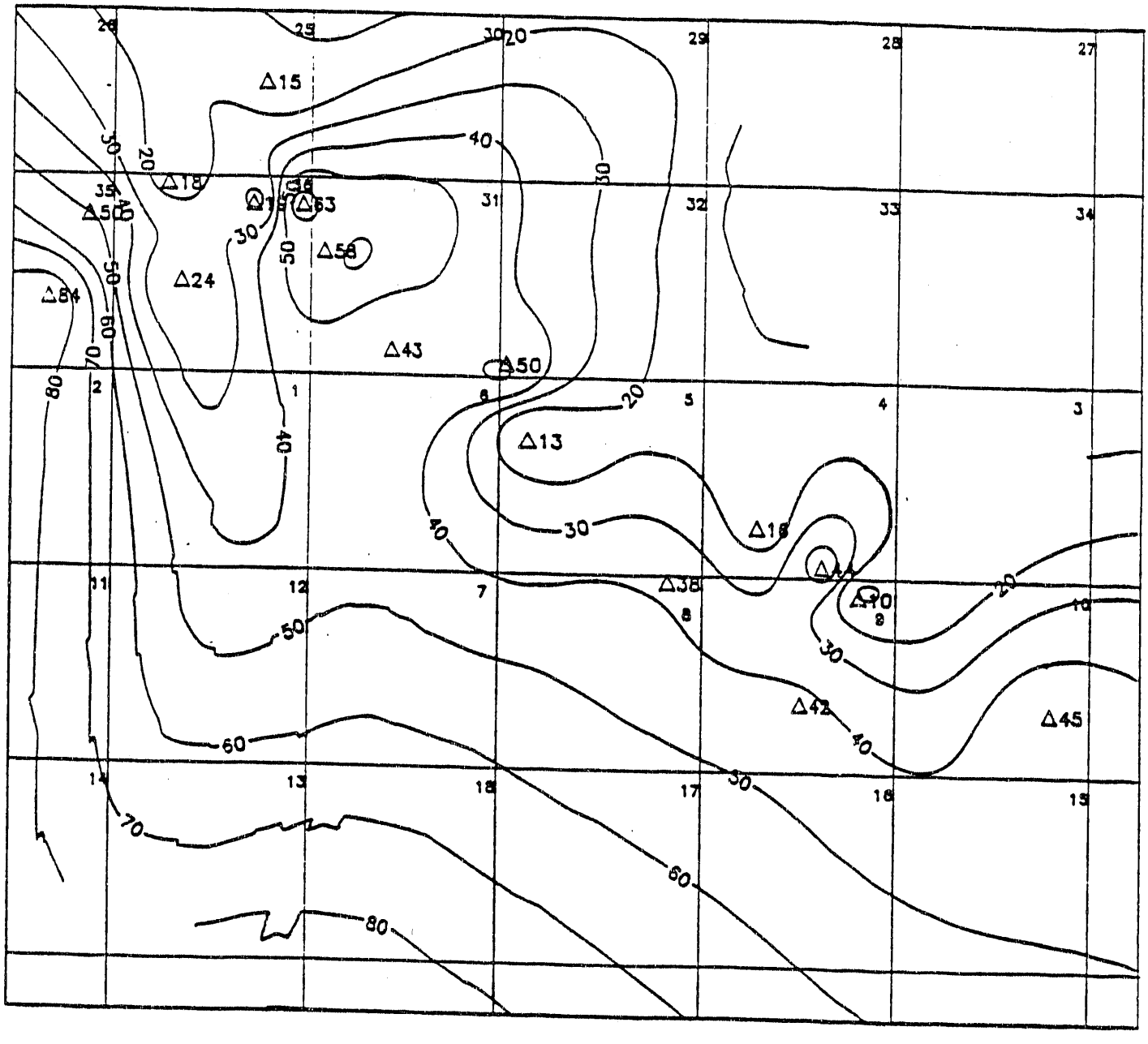

Figure 1.23: Zone 3A Water Saturation Contour Map C.I. 10%

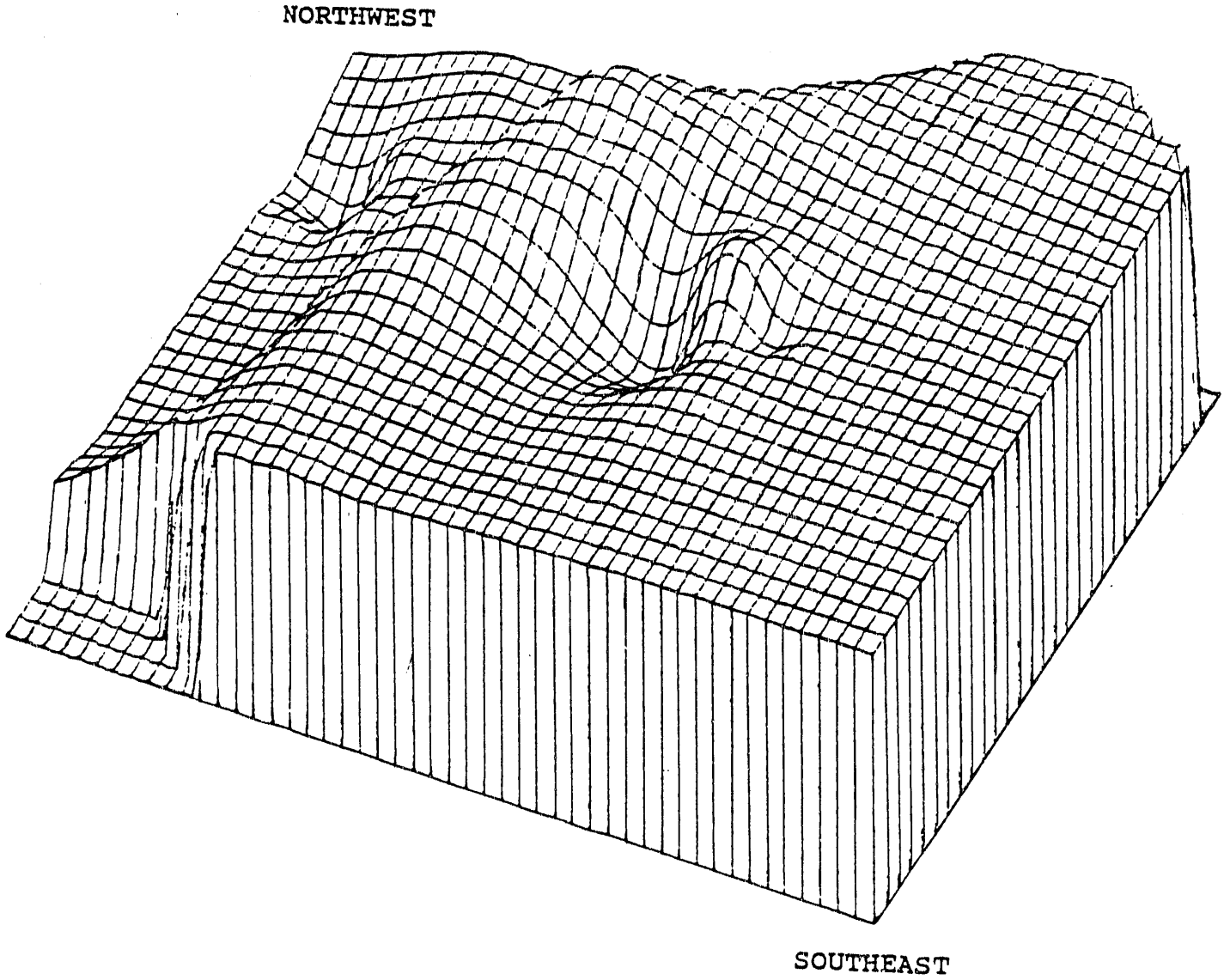

Figure 1.24: Zone 3A 3-D Porosity Isopach

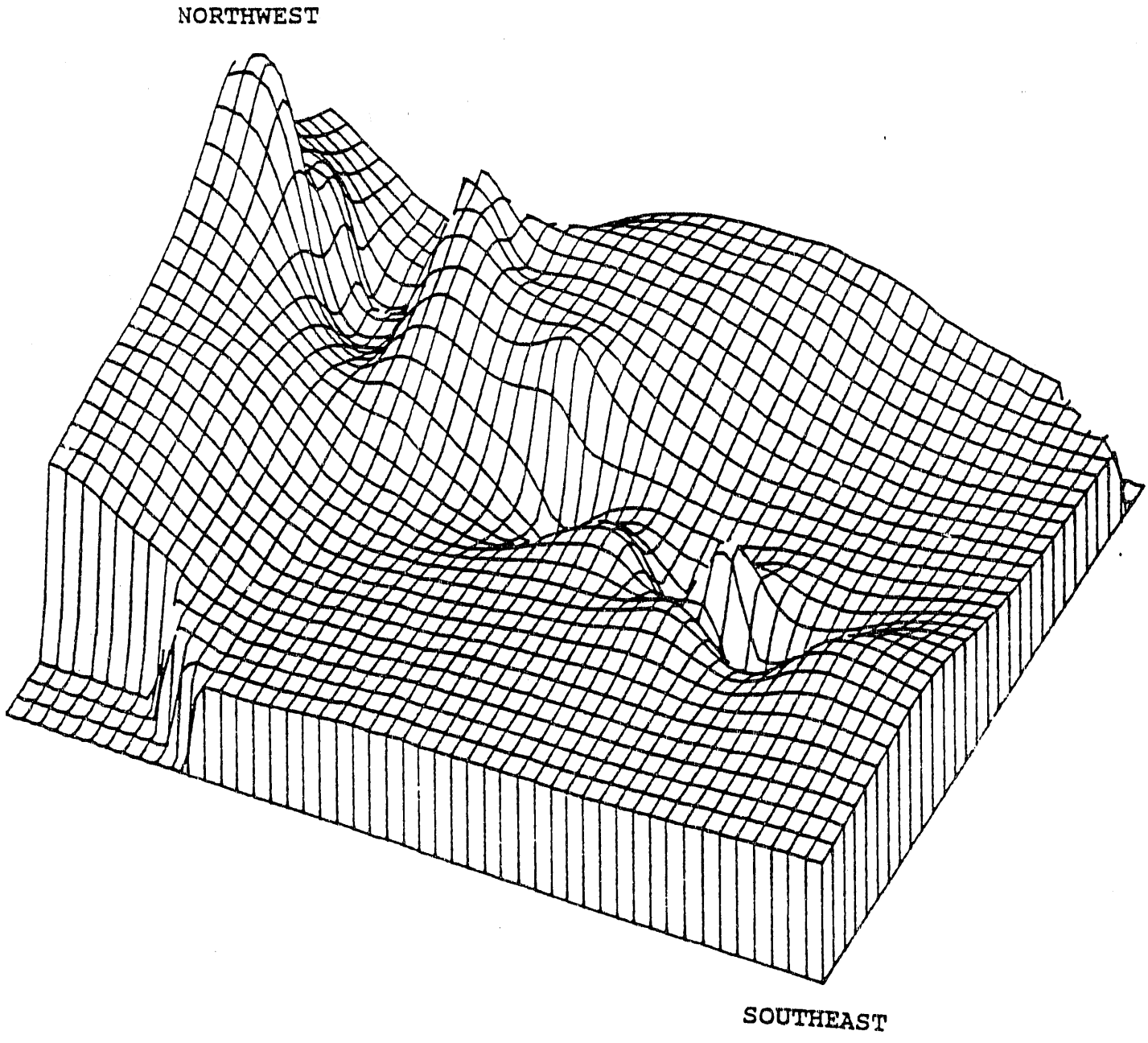

Figure 1.25: Zone 3A 3-D Water Saturation Isopach

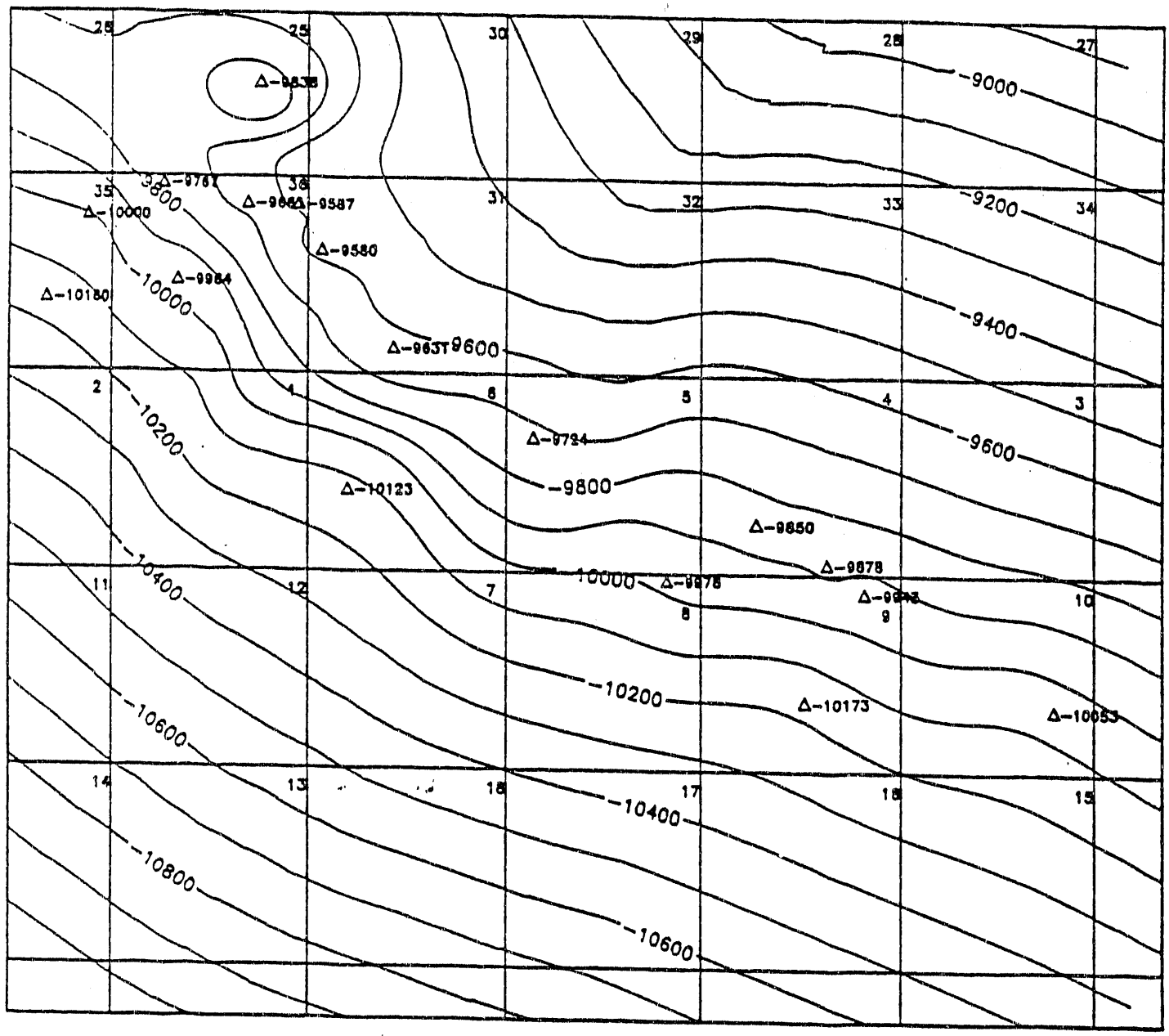

Figure 1.26: Top Zone 3B Structure Contour Map C.I. 50'

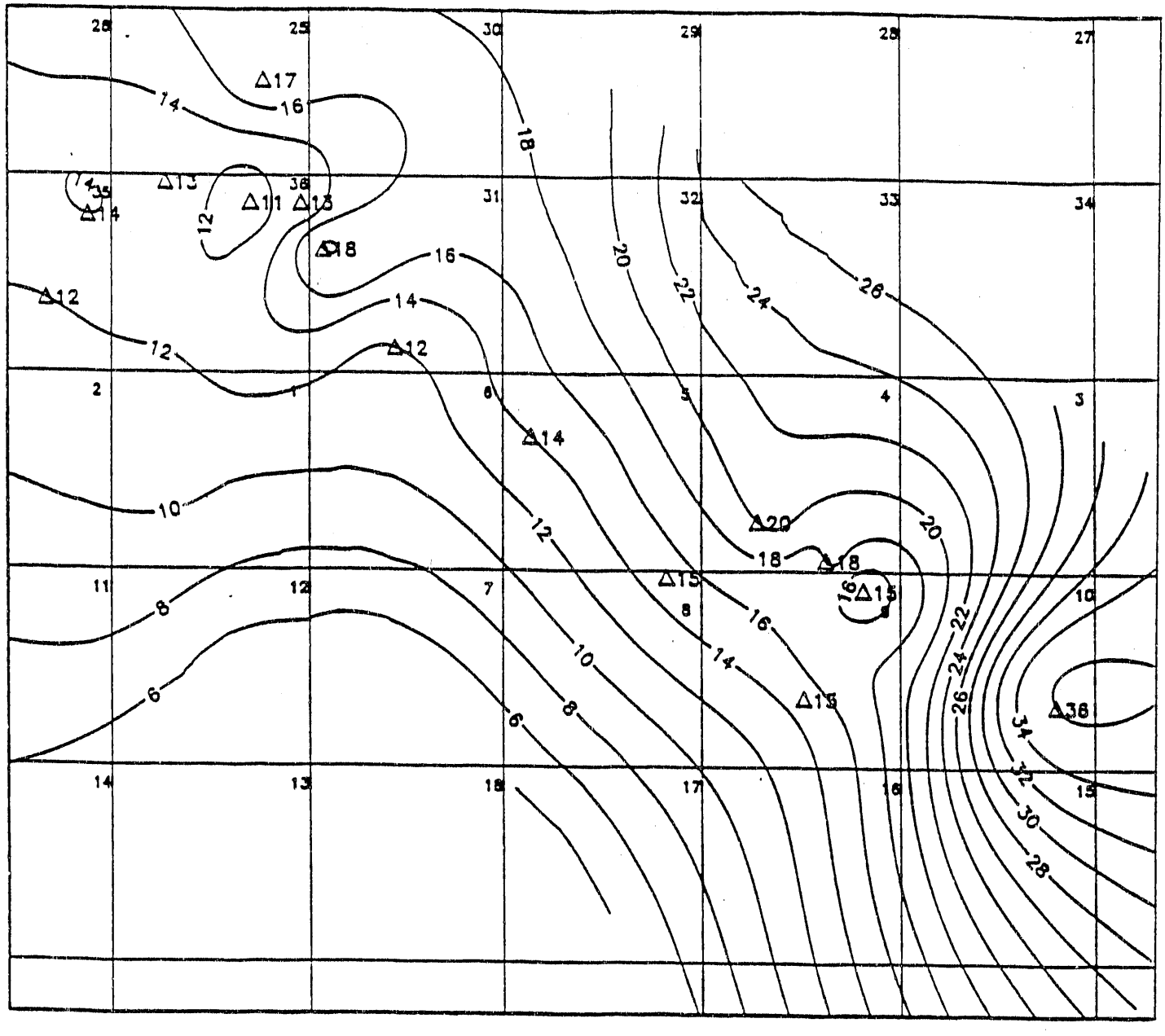

Figure 1.27: Zone 3B Porosity Contour Map C.I. 2%

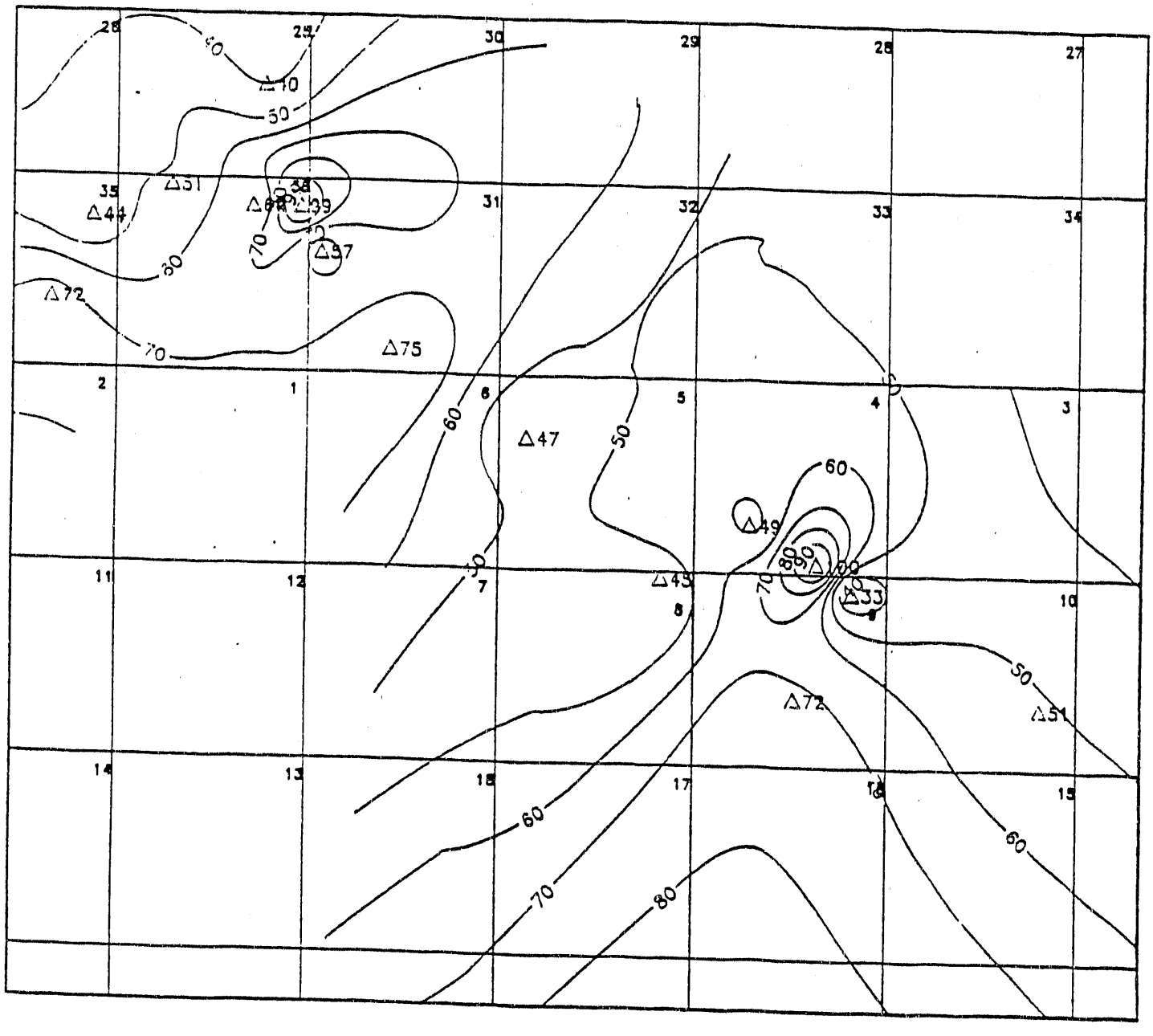

Figure 1.28: Zone 3B Water Saturation Contour Map C.I. 10%

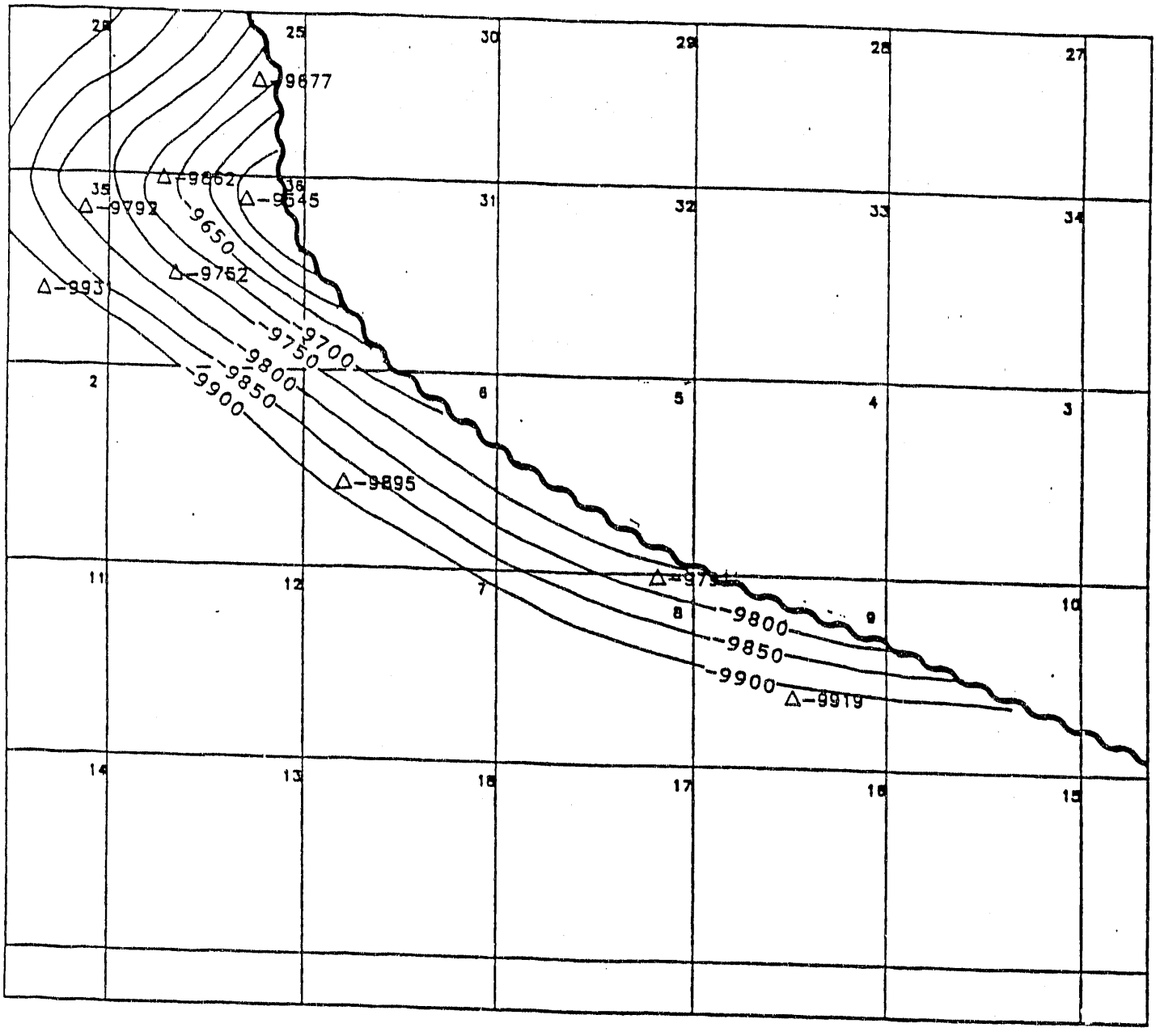

Figure 1.29: Top Zone 3C Structure Contour Map C.I. 50'

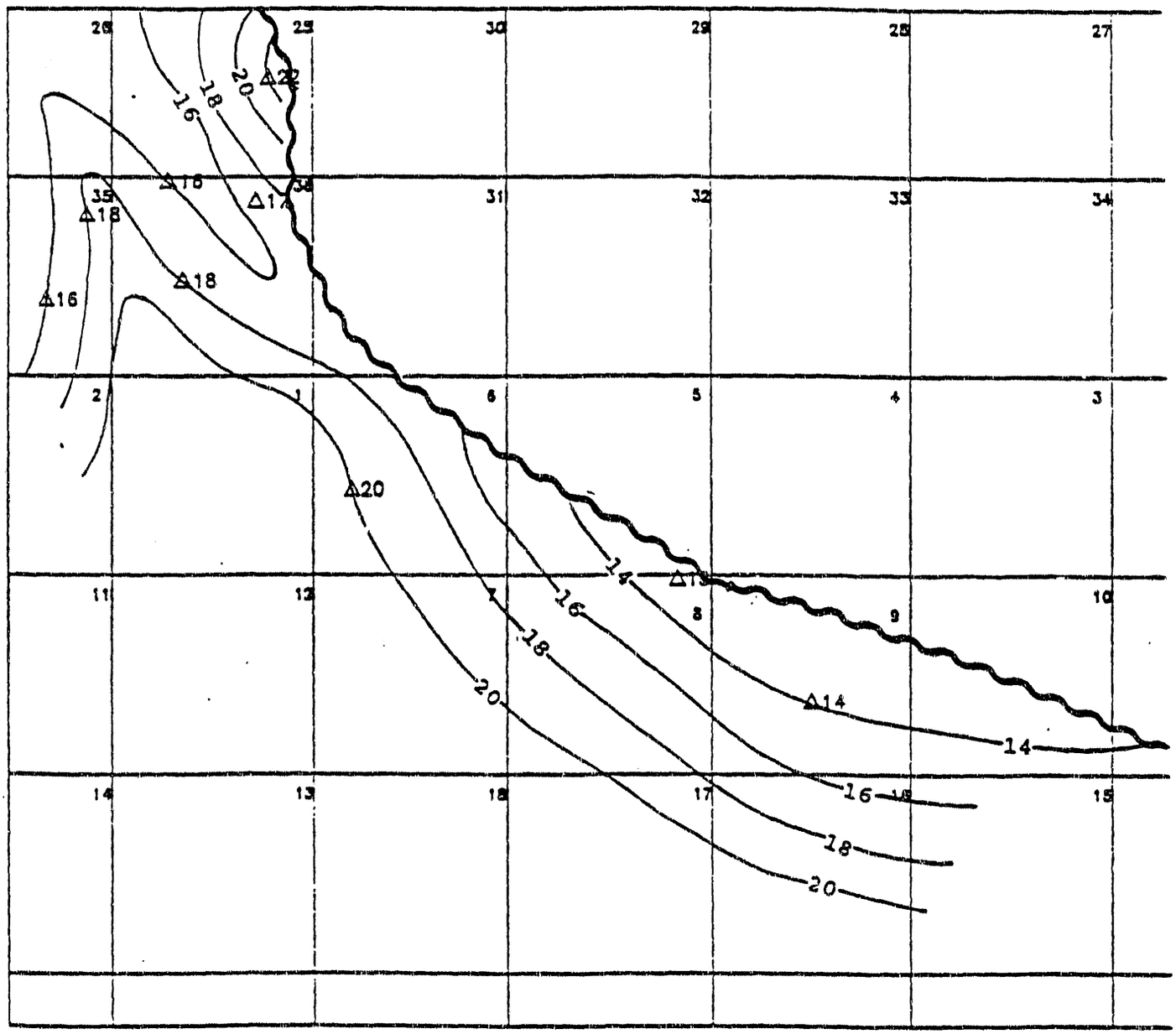

Figure 1.30: Zone 3C Porosity Contour Map C.I. 2%

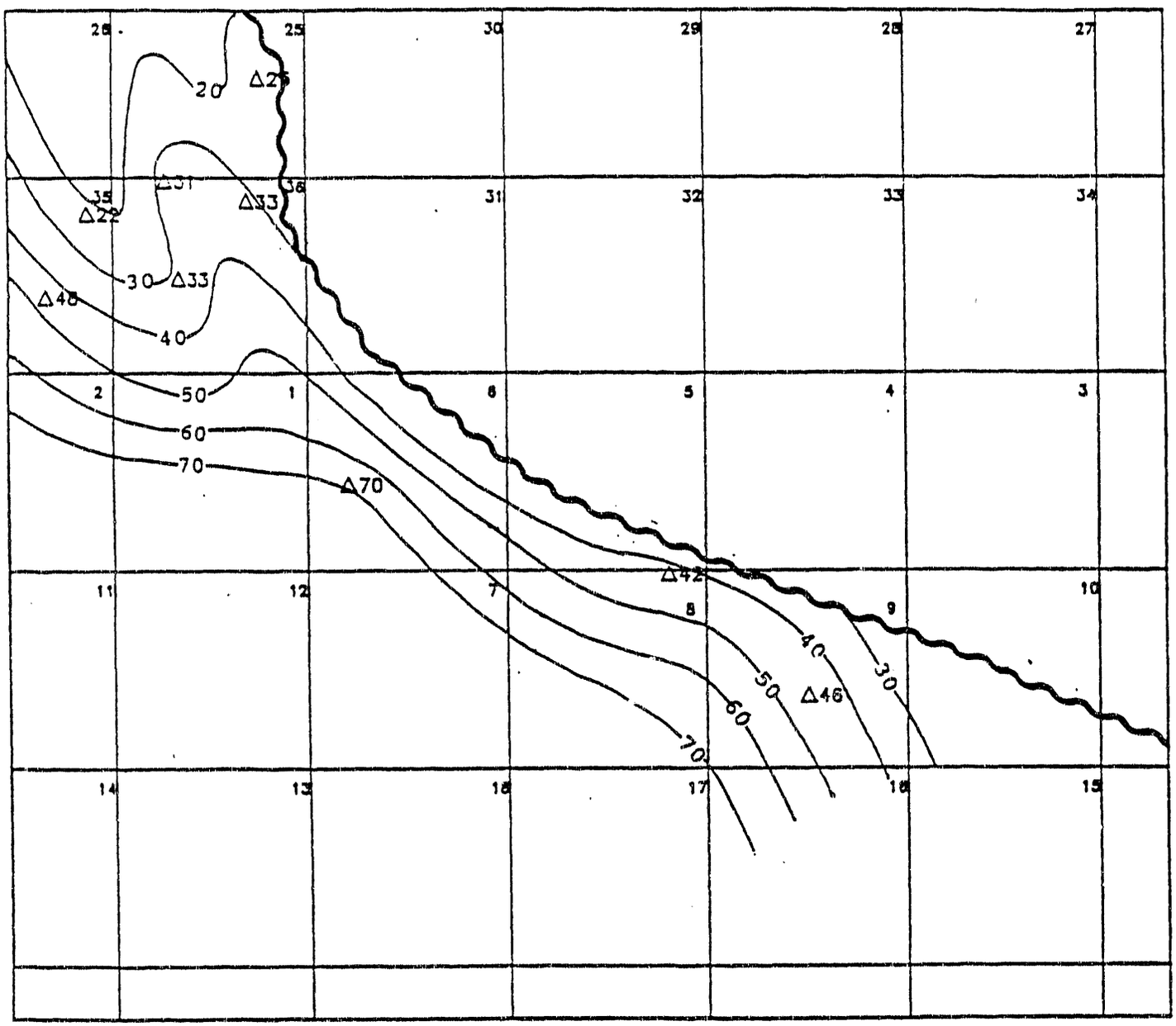

Figure 1.31: Zone 3C Water Saturation Contour Map C.I. 2%

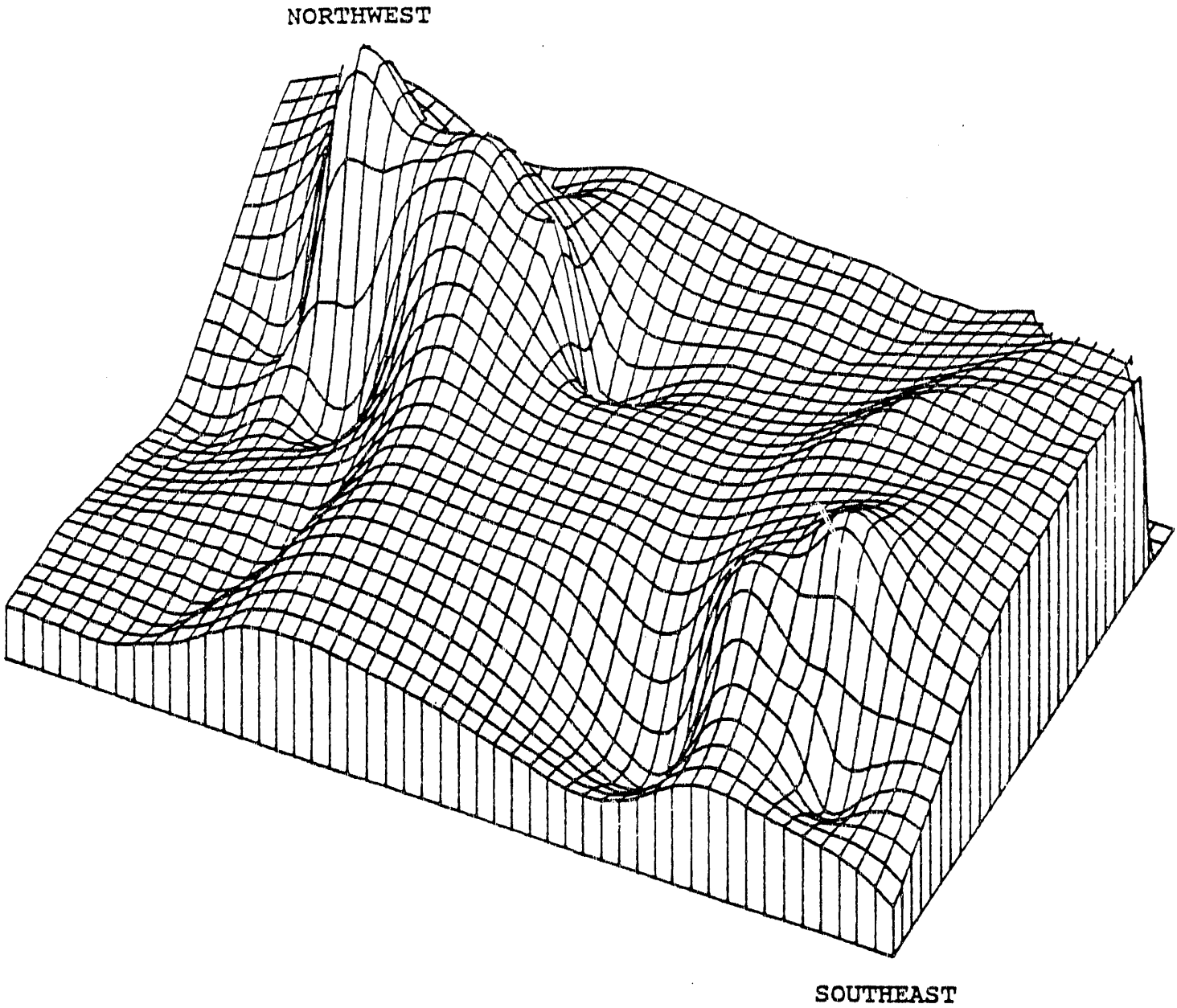

Figure 1.32: Zone 2A 3-D Net Pay Isopach

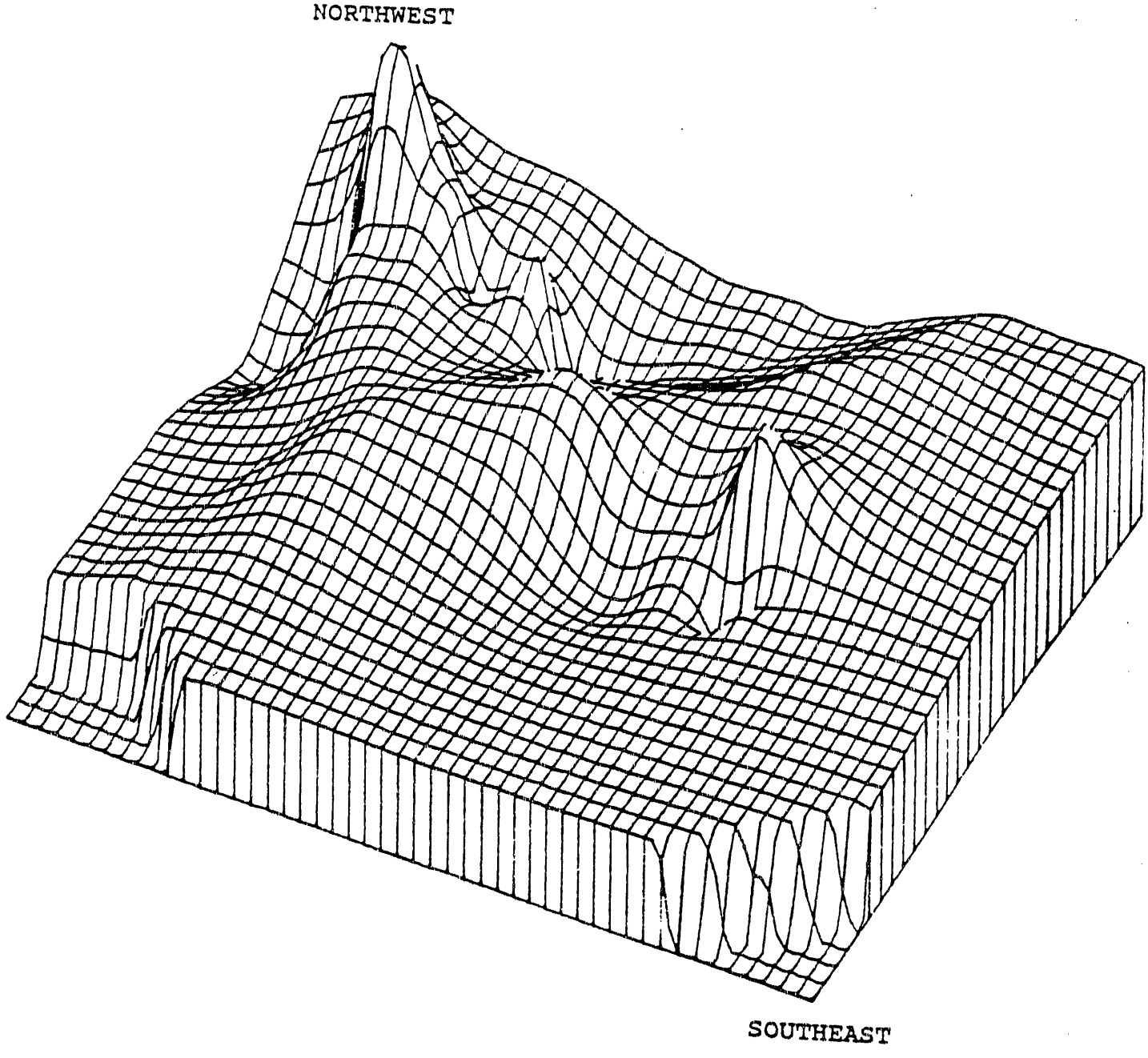

Figure 1.33: Zone 2B 3-D Net Pay Isopach

Net pay trends in Zone 3 (Figures 1.34 and 1.35) show a reversal of the trend in Zone 2. Generally, higher values of net pay occur in Zone 3 in the southeast, contrasting with lower Zone 2 values there, while thicknesses decrease toward the northwest. A region of consistently high net pay occurs from west to east but migrates northward in Zone 3B as compared to Zone 3A. This may be representative of lateral migration of a meandering stream channel and associated deposition over time.

1.4 FUTURE ENDICOTT RESERVOIR CHARACTERIZATION

A thorough assessment of log trace character is planned in order to better understand the depositional environments at each analyzed well. This will include, as much as possible, descriptions of individual sand facies within each sand package, including identification of channel lag deposits, point bar deposits, overbank floodplain material, etc.

An effort to determine clay mineralogy with the aid of core analyses is under consideration. Identification and location of faults within Endicott field using available seismic data is also being considered. Subsequent to completion of well log analyses at Endicott, the resulting reservoir characterization data will be utilized in enhanced oil recovery modeling at PDL.

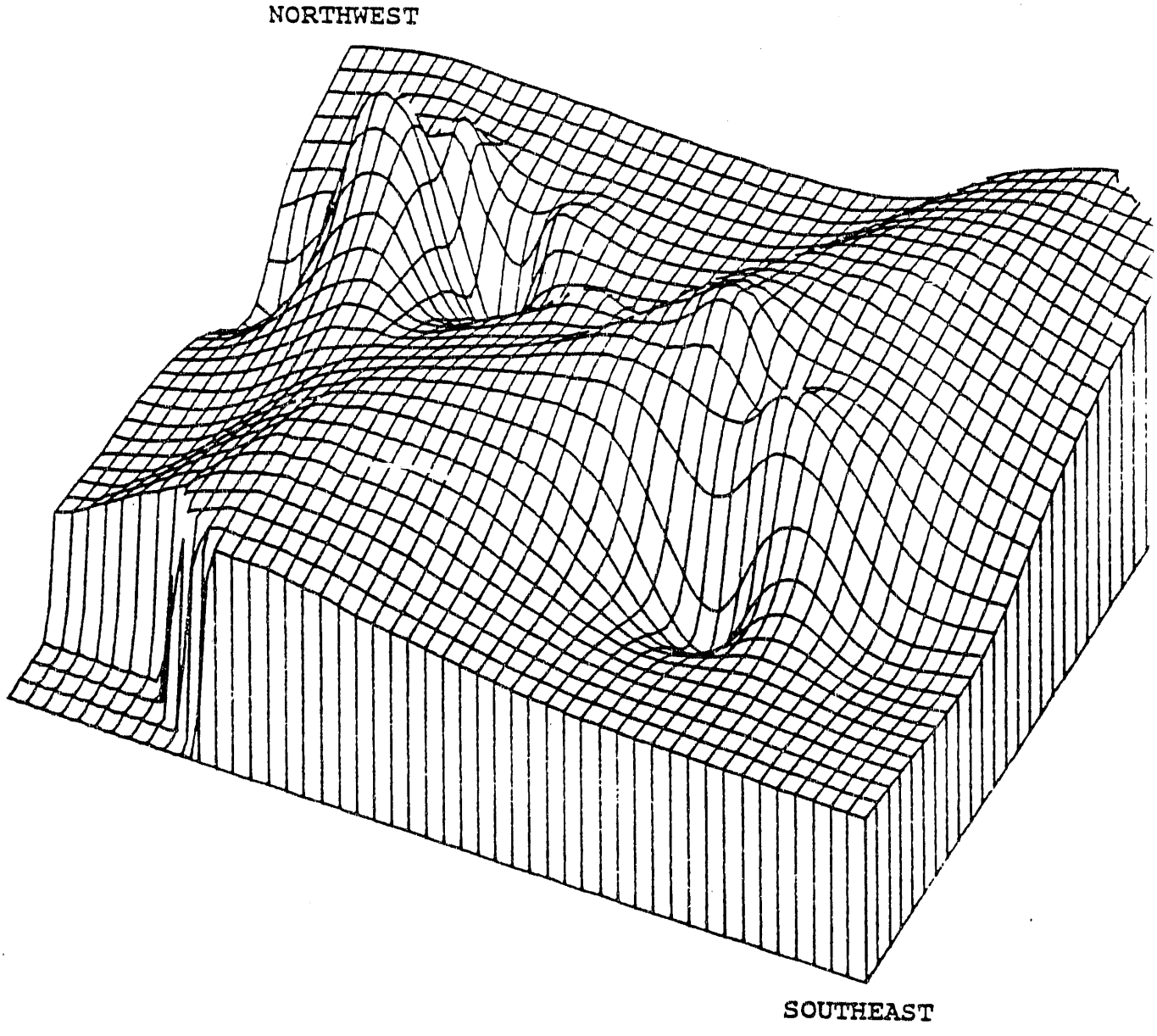

Figure 1.34: Zone 3A 3-D Net Pay Isopach

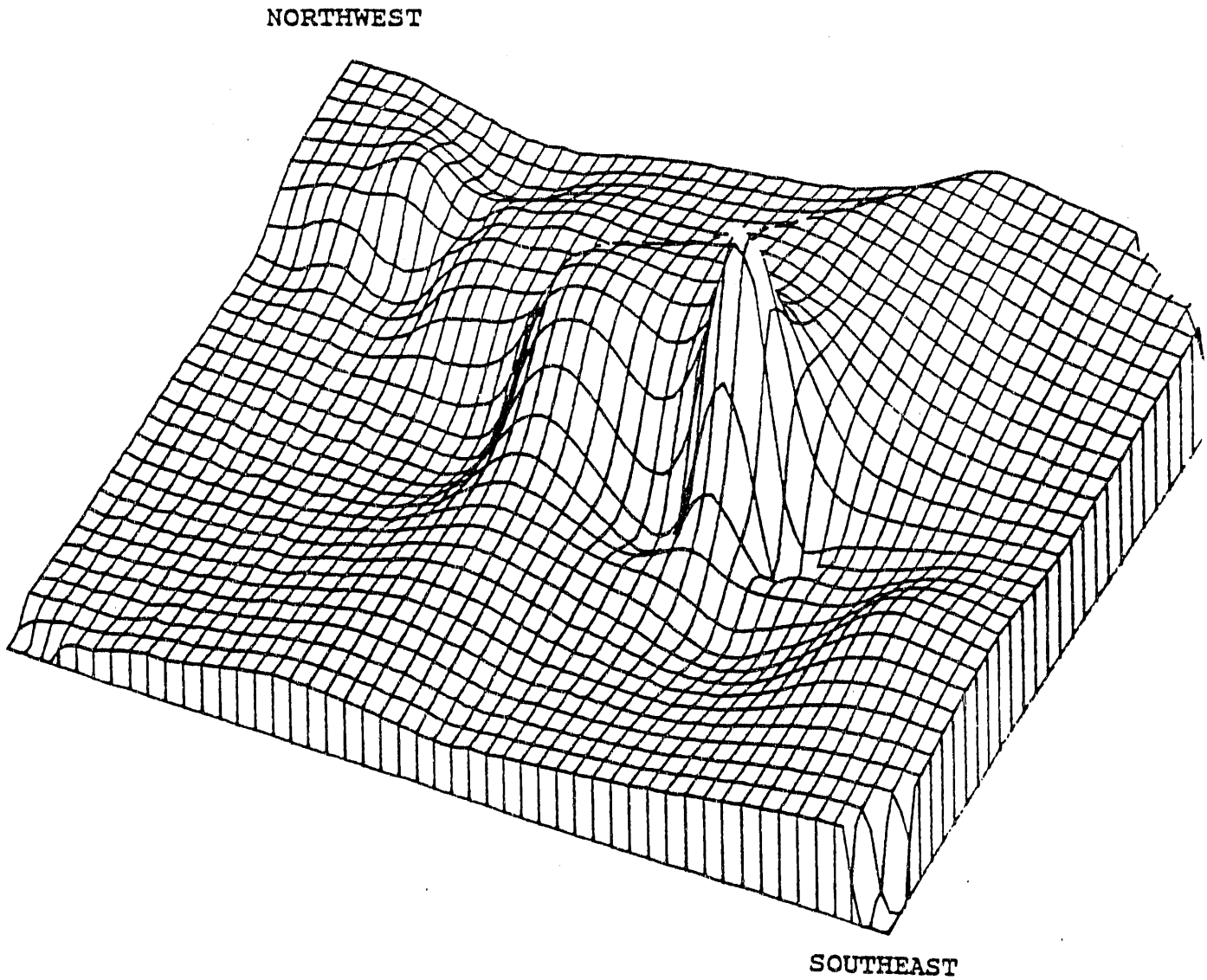

Figure 1.35: Zone 3B 3-D Net Pay Isopach

1.5 NOMENCLATURE

AOGCC	=	Alaska Oil and Gas Conservation Commission
HRZ	=	Highly Radioactive Zone
LCU	=	Lower Cretaceous Unconformity
MWD	=	Measured Well Depth
NDE	=	Not Deep Enough
NP	=	Not Present
TVD	=	True Vertical Depth

1.6 REFERENCES

1. Bird, K. J., 1987, The Framework Geology of the North Slope of Alaska as Related to Oil-Source Rock Correlations, in Alaskan North Slope Geology, Vol. 1, Page 121.

2. Curtis, M. I. and Huxley, D. B., 1985, First Arctic Offshore Field, Endicott, on Decade Long Way to Production: Oil and Gas Journal, Vol. 83, No. 13, Pages 64-70.

3. Melvin, J., 1987, Sedimentological Evolution of the Mississippian Kekiktuk Formation, Sagavanirktok Delta Area, North Slope, Alaska, in Alaskan North Slope Geology, Vol. 1, Page 60.

4. Sampson, R. J., Surface II Graphics System, Computer Sciences Section, Kansas Geological Survey, Lawrence, Kansas, Pages 91-98.

5. Selley, R. C. (1978), Ancient Sedimentary Environments (2d Ed.): Ithaca, New York, Cornell University Press, Page 287.

6. Woidneck, K., Behrman, P., Soule, C., and Wu, J., 1987, Reservoir Description of The Endicott Field, North Slope, Alaska, in Alaskan North Slope Geology, Vol. 1, Pages 43-59.

CHAPTER 2.0

PETROGRAPHIC CHARACTERISTICS OF SELECTED STRATIGRAPHIC HORIZONS: UGNU SWPT #1 AND WEST SAK SWPT #1

2.1 INTRODUCTION

This petrographic work is part of the reservoir characterization project being carried out under the aegis of the Petroleum Development Laboratory, University of Alaska Fairbanks, to obtain increased understanding of the West Sak and Ugnu (Brookian) petroleum reservoirs of northern Alaska. It is viewed as a key aspect of PDL's reservoir characterization effort, since it is intended to provide direct, substantive physical characterization, i.e. mineralogy, textural features/relationships of the rocks. In turn, relating this work to and integrating the results with other geological, petrophysical and engineering information will provide a synergistic appreciation of the characteristics of these potentially important reservoirs.

The present report is a preliminary presentation of petrographic analyses of thirty samples of core material from selected stratigraphic horizons representing the West Sak and the Ugnu intervals in the ARCO Ugnu Single-Well Production Test (SWPT) #1 and West Sak SWPT #1 wells, Northern Alaska. These samples were intended to be representative of the spectrum of lithologies, and attendant apparent petrophysical characteristics, i.e. reservoir/seal qualities, observed megascopically. Wireline logs also were used to guide sample selection.

Other aspects, geological, petrophysical, engineering, subsequently will be integrated with this and other petrographic work presently in progress.

A technical paper representing a preliminary synthesis of this analysis was presented at the Annual Meeting of the American Association of Petroleum Geologists in Dallas, Texas in April, 1991. A copy of the abstract of this paper (Mowatt, Ogbe, Kamath and Sharma, 1991) is included as an appendix to the present report.

2.2 PETROGRAPHIC ANALYSES

Quantitative petrographic analysis was carried out on each of 20 thin-sections. Since many of the samples were, at best, semi-consolidated--cemented, as it were, by

viscous hydrocarbon material in situ, several problems are inherent here. Sample integrity, especially in terms of textural relationships, becomes a serious concern. This involves the entire series of events from initial perturbation of in situ materials during drilling through sample recovery, handling, transportation, and ultimately preparation as petrographic thin-sections. Thus, though the resultant observed mineralogic compositions likely at least somewhat closely resemble those originally extant in situ, textural relationships are an entirely different matter. Somewhat surprisingly, however, serious disruptions were not apparent in many instances in the present work, particularly in those samples of inherently low reservoir quality, i.e. the more coherent and/or finer-grained samples. For those samples of apparently better reservoir quality with higher porosities, less proportions of finer-grained constitutions, etc., varying amounts of disruptions of original textures were all too evident in thin-section. However, with these caveats, and an awareness of certain limitations, appreciable potentially useful information remains to be gleaned from petrographic study of these materials.

The present focus has been on the West Sak and Ugnu SWPT wells, and immediately adjacent horizons in terms of reservoir characterization. Similar investigations of other wells should lead to increased understanding of areal relationships which will be fundamental to effective recovery of hydrocarbons as a development geology-engineering concern.

In addition, petrographic characterization keyed to wireline log responses will provide critical information as to efficient, substantive utilization of wireline logs during subsequent development work.

2.3 SAMPLE DESCRIPTIONS

The following pages contain descriptions of 30 samples analyzed petrographically. First, the 18 samples obtained from Ugnu SWPT #1 are described. Second, the 12 samples from the West Sak SWPT #1 are described. Additional photomicrographs of each sample are on file at PDL, and selected ones will be included as part of the final project report, subsequent to project completion.

2.3.1 Ugnu SWPT #1 Samples

A. Ugnu SWPT #1, 3532' (below West Sak Zone).

Description:

Lithic Wacke. Framework grains (33%) : predominately very fine-fine sand-sized, with trace amounts of medium sand-sized materials, poorly-moderately sorted, angular/subangular/subrounded, consisting of quartz (48%), feldspars (4%, plagioclase and potassium feldspars), lithic fragments (44%) and other minor-trace constituents, including micas, chlorite, glauconite, organic materials.

Detrital matrix (46%) as patches-streaks-layers-clasts of silt/clay-rich material. Rock exhibits sedimentary layering and is also moderately burrowed.

Visible porosity (shown in blue) estimated as 19%, principally as semi-pervasive intergranular (associated especially with burrows); moderately-highly effective.

Some microporosity, associated with silt-clay. Cement not apparent, but trace amounts of pyrite are present.

This sample has undergone slight apparent compaction.

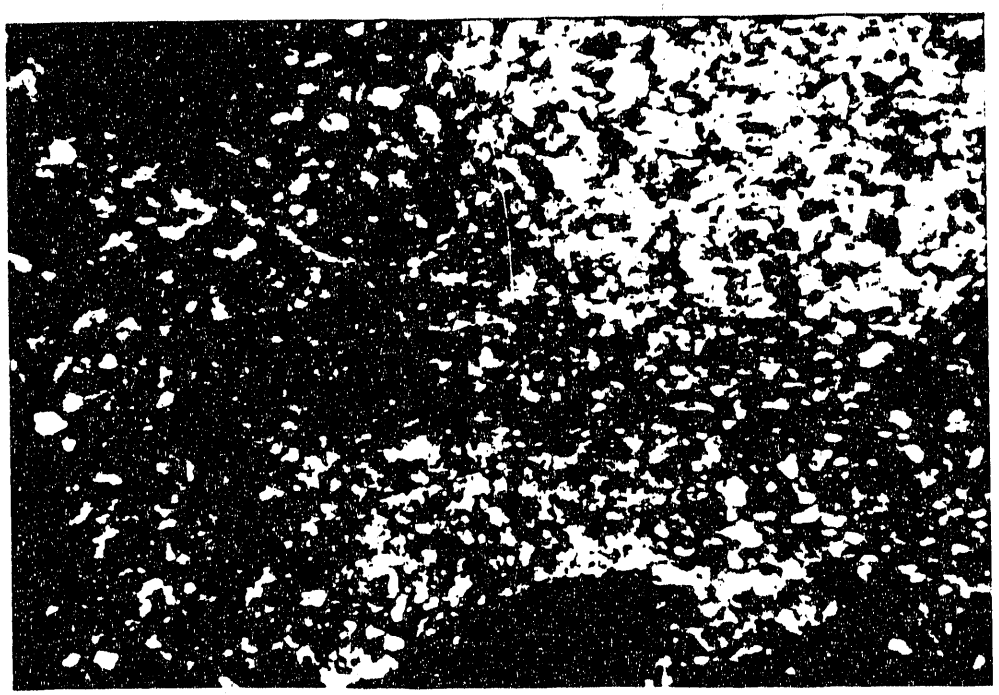

Figure 2.1: Ugnu SWPT #1, 3532' (50 x PL)

B. Ugnu SWPT #1, 3526' (West Sak Sands).

Description:

Lithic Wacke. Framework grains (48%): predominately very fine sand-sized, with minor amounts of fine sand-sized materials, poorly-moderately sorted, angular/subangular, consisting of quartz (40%), feldspar (3%; plagioclase and potassium feldspar), lithic fragments (53%), and other minor-trace constituents, including micas, chlorite, glauconite, iron-oxide opaque minerals, and organic materials.

Detrital matrix (33%) as patches-streaks of silt-clay rich material. Rock exhibits sedimentary layering, and is slightly-moderately burrowed.

Visible porosity (shown in blue) estimated as 18%, principally as semi-pervasive intergranular; highly effective. Some (?) of this may be an artifact of thin-section preparation.

Some microporosity, associated with silt-clay. Cement not apparent, but some of the iron-oxide material may be diagenetic (?).

This sample has undergone slight apparent compaction.

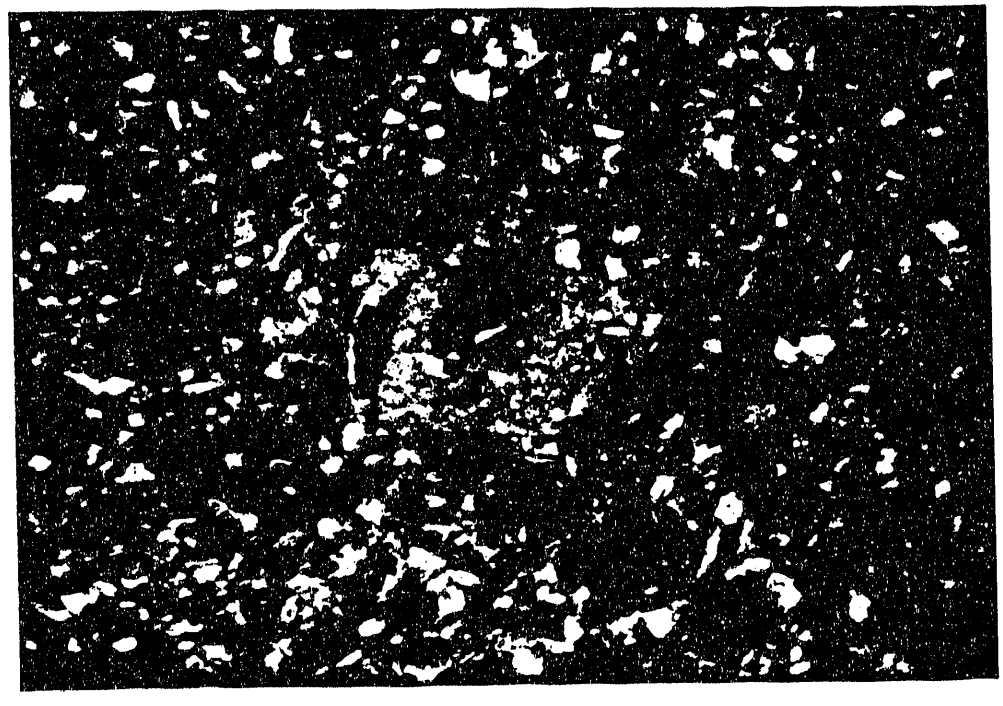

Figure 2.2: Ugnu SWPT #1, 3526' (50 x PL)

C. Ugnu SWPT #1, 3507' (West Sak Zone).

Description:

Lithic Wacke. Framework grains (43%): range from very coarse to fine-sand-sized, with subordinate amounts of granule-pebble-sized fossil materials, very poorly sorted, angular/subangular/subrounded, consisting of quartz (39%), feldspars (3%, plagioclase and potassium feldspars.), lithic fragments (56%), and other minor-trace constituents, including micas, chlorite, glauconite, opaque iron-oxide minerals, and organic materials.

Detrital matrix ("54%"?) difficult to elucidate; could also include clay cements. It does include residential hydrocarbon material in this analysis and thus, is at least in part equivalent to "porosity". The relative amounts of matrix versus porosity are not rigorously determinable in this thin-section.

Some, at least, is microporosity, associated with clays. Cement as such is not apparent, although the hydrocarbon material as well as perhaps at least some of the "matrix" clays could represent cement in this sample. Most likely, at least an appreciable proportion of the "matrix/porosity" here represents effective intergranular pore space.

This sample has undergone slight apparent compaction. The rock fabric is indeterminate due to specimen disaggregation, but appears to have been massive.

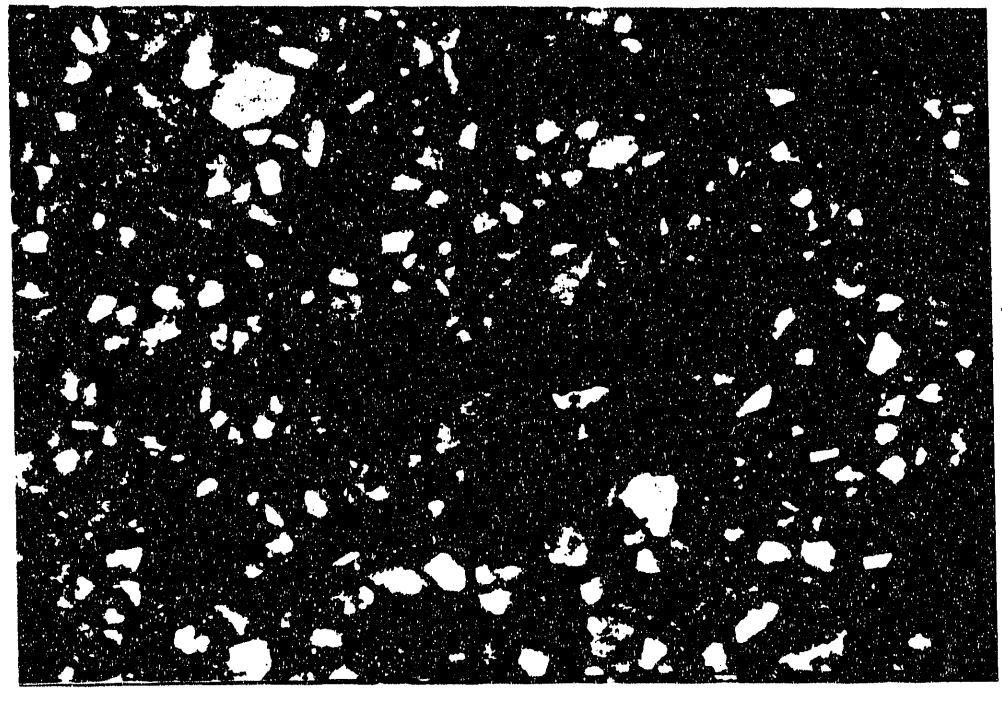

Figure 2.3: Ugnu SWPT #1, 3507' (50 x PL)

D. Ugnu SWPT #1, 3497' (West Sak Zone).

Description:

Lithic Wacke/Siltstone. Framework grains (30%): predominately very fine sand-sized, with subordinate amounts of fine sand-sized materials, poorly-moderately sorted, angular/subangular/subrounded, consisting of quartz (40%), feldspars (3%; plagioclase and potassium feldspars), lithic fragments (50%), and other minor-trace constituents, including micas, chlorite, glauconite, opaque iron-oxide minerals, and organic materials.

Detrital matrix (56%) as lenses-patches-streaks of silt-clay materials. Rock is strongly burrowed with coarser grains filling burrows.

Visible porosity (shown in blue) estimated as 9%, principally as intergranular, and associated in large part with burrow-filling grains. It may be only moderately effective, thus, although on the order of 30% within the burrows.

Also sample shows is some microporosity associated with silt-clay. Cement not apparent, although some of the iron-oxides may be diagenetic. This sample has undergone slight apparent compaction.

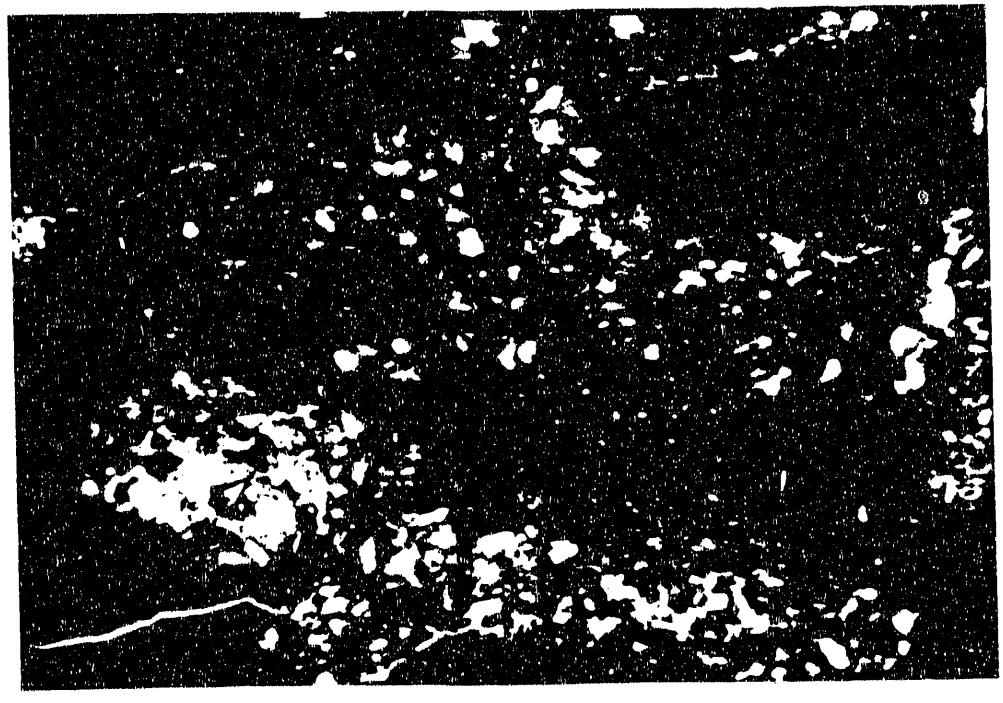

Figure 2.4: Ugnu SWPT #1, 3497' (50 x PL)

E. Ugnu SWPT #1, 3493' (West Sak Zone).

Description:

Litharenite. Framework grains (66%): predominately very fine sand-sized, with trace amounts of fine sand-sized materials, well-very well sorted, angular/subangular/subrounded, consisting of quartz (30%) feldspars (3%; plagioclase and potassium feldspars), lithic fragments (64%), and other minor-trace constituents, including micas, chlorite, glauconite, opaque iron-oxide minerals, and organic materials.

Detrital matrix (16%) as vague patchy areas/layers of clay materials. At least some may (?) represent, rather, diagenetic clay cement.

Visible porosity (shown in blue) estimated as 17%, principally as pervasive intergranular; highly effective. A moderate amount of microporosity, associated with clays. Cement not apparent, although at least a portion of "matrix" clay material may well be rather diagenetic clay cement.

This sample has undergone slight apparent compaction.

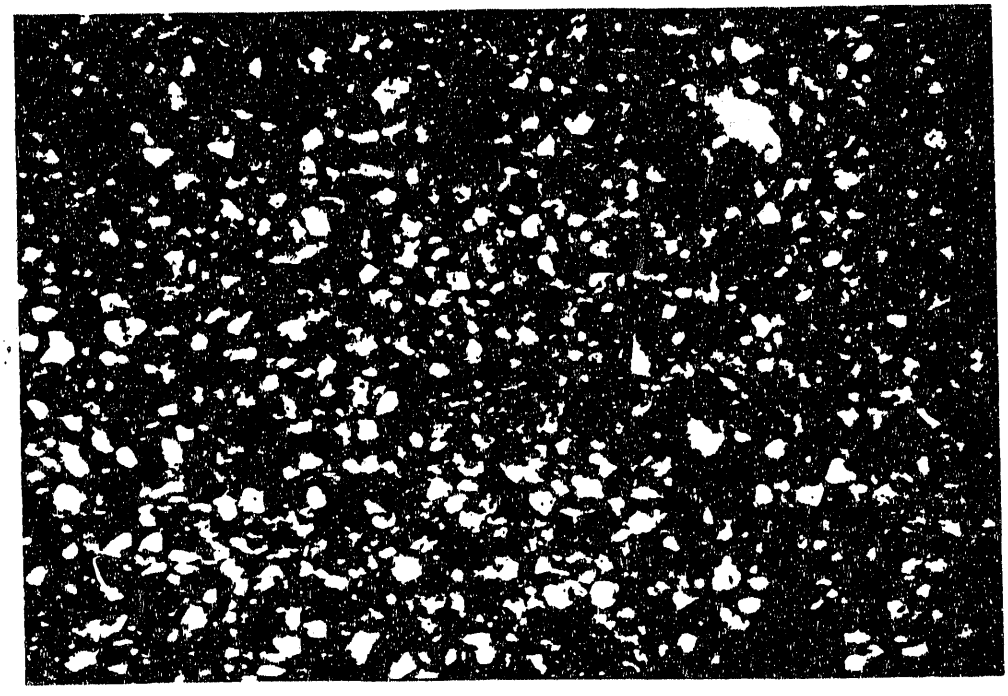

Figure 2.5: Ugnu SWPT #1, 3493' (50 x PL)

F. Ugnu SWPT #1, 3457' (West Sak Zone).

Description:

Lithic Wacke/Siltstone. Framework grains (38%): predominantly very fine sand-sized, with subordinate amounts of fine and medium sand-sized materials, poorly-moderately sorted, angular/subangular/subrounded, consisting of quartz (40%), feldspars (6%; plagioclase and potassium feldspars), lithic fragments (50%), and other minor-trace constituents, including micas, chlorite, glauconite, and organic materials.

Detrital matrix (55%) as patchy areas of silt-clay. Rock is moderately burrowed.

Visible porosity (shown in blue) estimated as 5%, principally as intergranular, patchy; moderately-poorly effective. Some microporosity, associated with clay. Cement not apparent, although some of the "matrix" clay may represent diagenetic material. Minor pyrite, with euhedral crystal faces, is authigenic-diagenetic.

This sample has undergone slight apparent compaction.

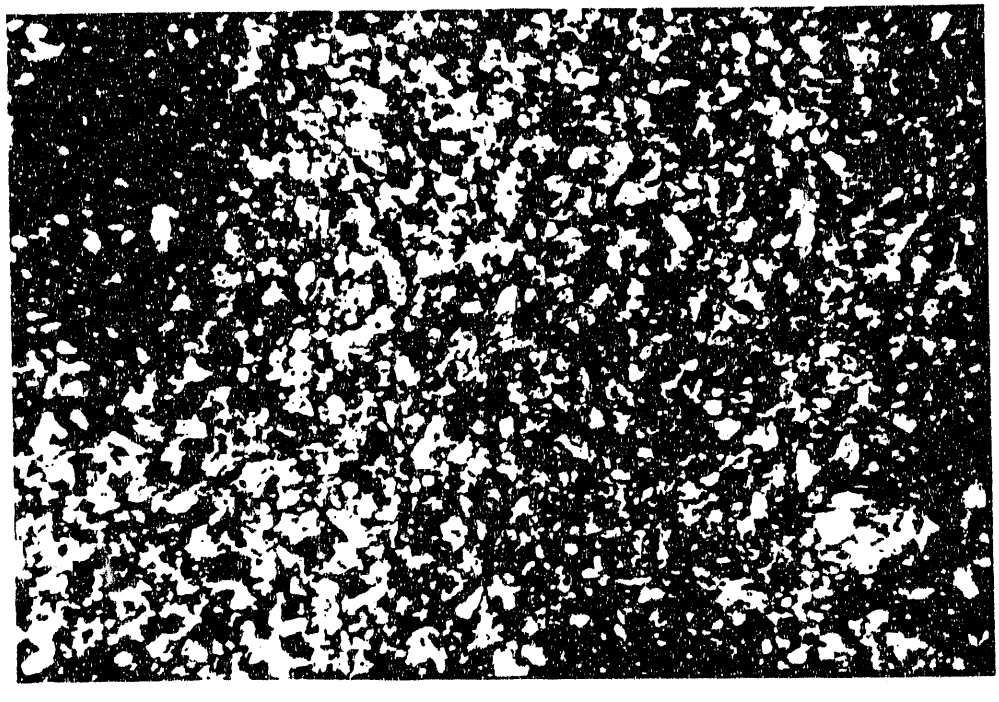

Figure 2.6: Ugnu SWPT #1, 3457' (50 x PL)

G. Ugnu SWPT #1, 3452' (West Sak Zone).

Description:

Litharenite. Framework grains (63%): predominantly fine sand-sized, with trace amounts of medium and coarse sand-sized materials, well-very well sorted, angular/subangular/subrounded, consisting of quartz (37%), feldspars (4%; plagioclase and potassium feldspars), lithic fragments (56%), and other minor-trace constituents, including micas, chlorite, glauconite, and organic materials.

Detrital matrix (11%) as vague patches among framework grains. Some, at least, may, rather, represent intergranular clay "cement." Vague sedimentary layering.

Visible porosity (shown in blue) estimated as 26%, principally as pervasive intergranular; highly effective. Some microporosity, associated with clays. Cement not apparent, although at least some of the clays present may well represent diagenetic "cement". Minor pyrite present, appears to be of authigenic-diagenetic origin. This sample has undergone slight apparent compaction.

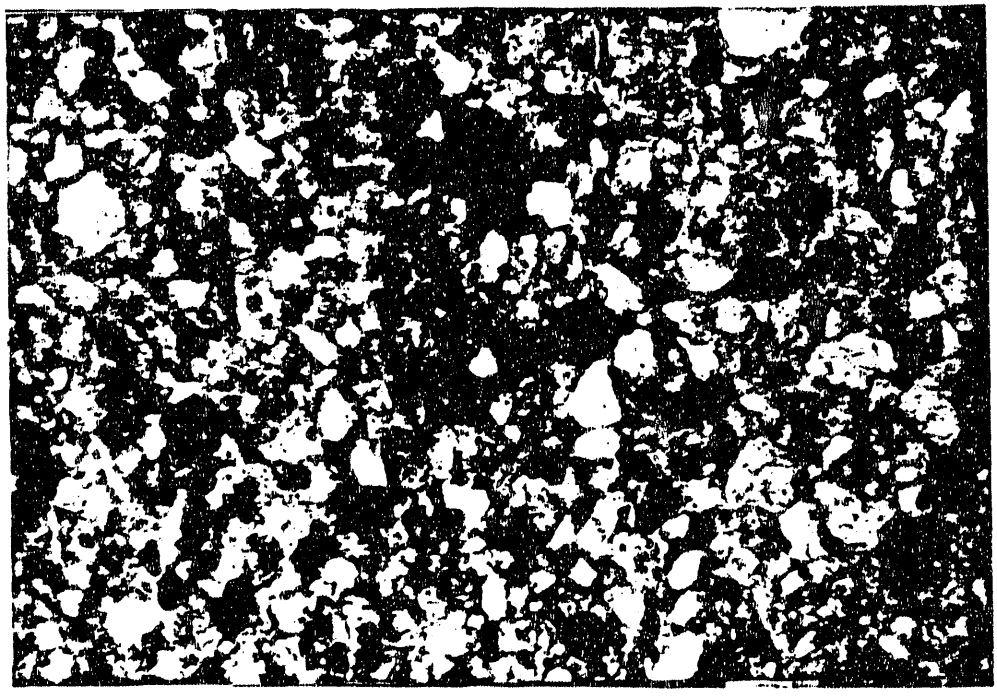

Figure 2.7: Ugnu SWPT #1, 3452' (50 x PL)

H. Ugnu SWPT #1, 3425' (West Sak Zone).

Description:

Litharenite. Framework grains (70%): predominantly very fine sand-sized, with subordinate-trace amounts of fine, medium, and coarse sand-sized materials, well-very well sorted, angular/subangular/subrounded, consisting of quartz (30%), feldspars (3%; plagioclase and potassium feldspars), lithic fragments (65%), and other minor-trace constituents, including micas, chlorite, glauconite, and organic materials.

Detrital matrix (6%) as vague layers-zones containing clay materials. Vague sedimentary layering.

Visible porosity (shown in blue) estimated as 23%, principally as pervasive intergranular; highly effective.

Some microporosity, associated with clays. Cement not apparent. At least some of the clays may represent diagenetic "cement". Minor pyrite, of authigenic-diagenetic origin.

This sample has undergone slight apparent compaction.

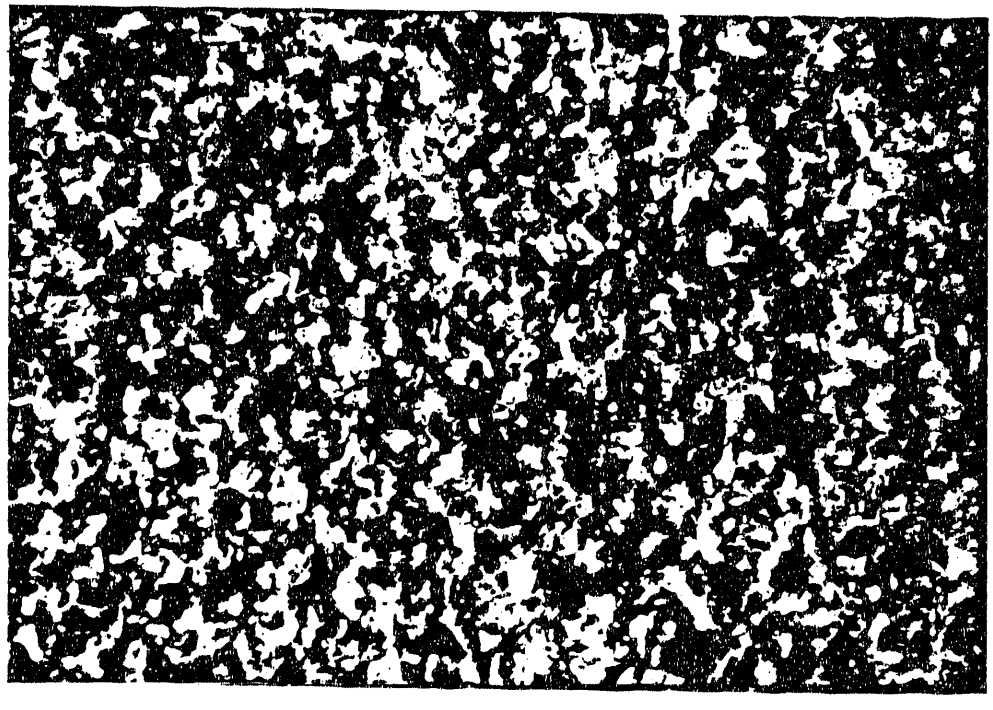

Figure 2.8: Ugnu SWPT #1, 3425' (50 x PL)

I. Ugnu SWPT #1, 3422' (West Sak Zone).

Description:

Litharenite (or Lithic Wacke?). Framework grains (66%): predominantly fine sand-sized, with trace amounts of medium and coarse sand-sized materials, well (poorly?) sorted, angular/subangular/subrounded, consisting of quartz (40%), feldspars (5%; plagioclase and potassium feldspars), lithic fragments (50%), and other minor-trace constituents, including micas, chlorite, glauconite, opaque iron-oxide minerals, and organic materials.

Detrital matrix (a minimum of 18%) as clays intergranular to framework grains, associated with residual hydrocarbon material. These clays may, rather, be diagenetic in origin. Alternatively, they might represent thorough mixing due to burrowing of organisms. Vague sedimentary layering.

Visible porosity (shown in blue) estimated as up to 15%, principally as intergranular; probably moderately-highly (?) effective.

Moderate amount of microporosity, associated with clays. Cement not apparent, although at least a portion of the "matrix" clays might, rather, represent "cement" of diagenetic origin.

This sample has undergone slight apparent compaction.

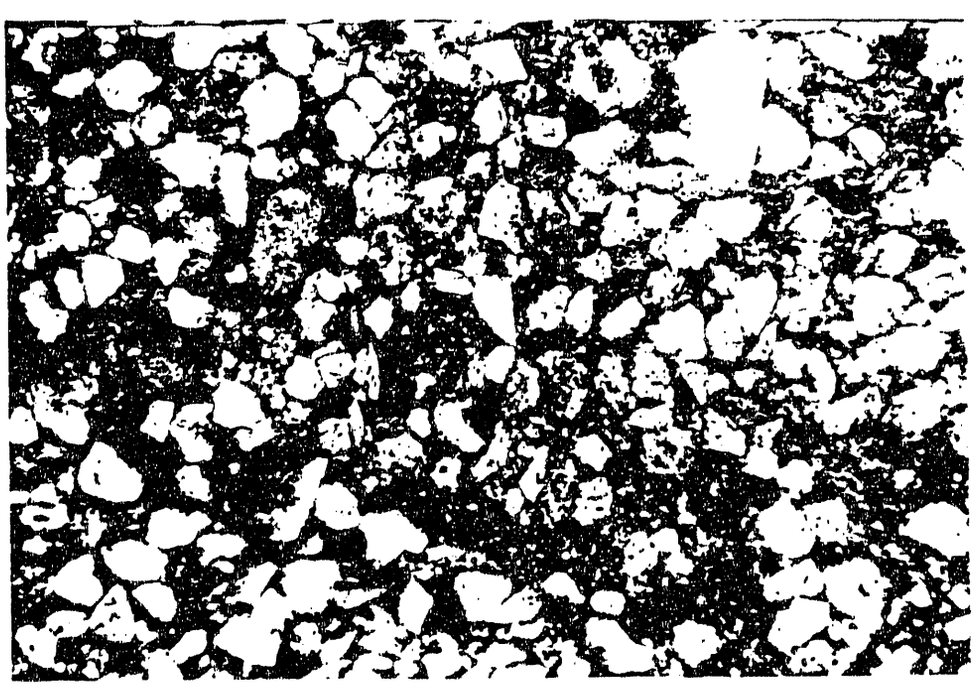

Figure 2.9: Ugnu SWPT #1, 3422' (50 X PL)

J. Ugnu SWPT #1, 3412' (above West Sak Zone).

Description:

Sandy Siltstone. Sand-size grains (27%): predominantly very fine sand-sized; rock is poorly-very poorly sorted, angular/subangular, consisting of quartz (45%), feldspars (5%; plagioclase and potassium feldspars), lithic fragments (46%), and other minor-trace constituents, including micas, chlorite, glauconite, opaque iron-oxide minerals, and organic materials.

Detrital matrix (66%) in silt-clay-rich layers-patches. Moderately burrowed.

Visible porosity (shown in blue) estimated as 7%, principally as intergranular to burrow-filling grains; burrowed areas are patchy; porosity of poor effectiveness.

Some microporosity, associated with clays. Cement not apparent.

This sample has undergone slight apparent compaction.

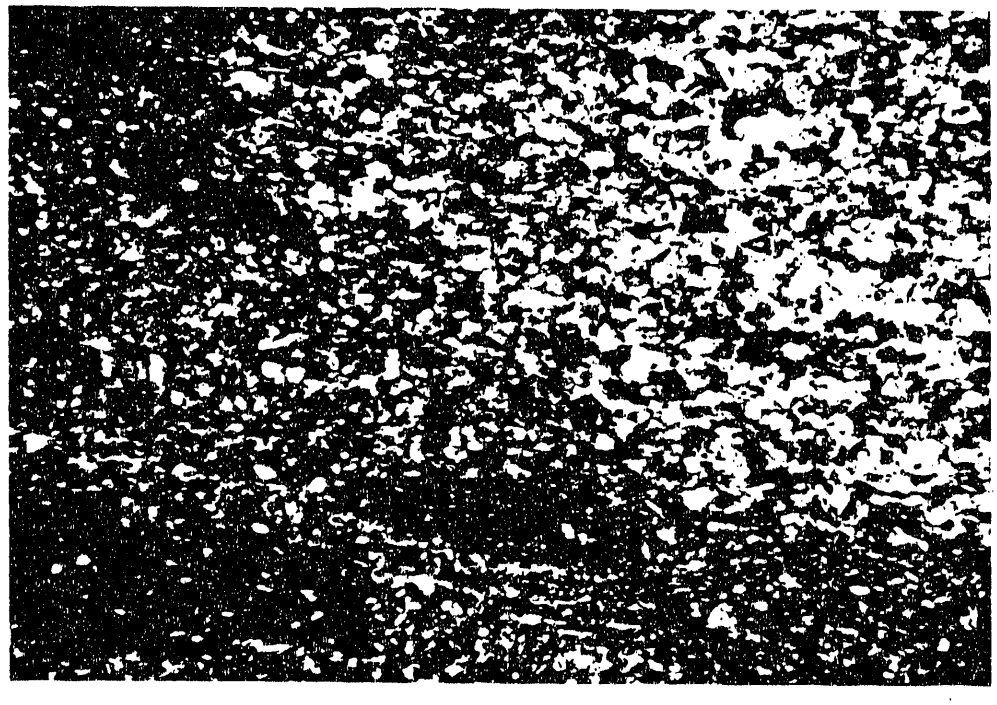

Figure 2.10: Ugnu SWPT #1, 3412' (50 X PL)

K. Ugnu SWPT #1, 3264' (lower Ugnu (?) Zone.)

Description:

Lithic Wacke. Framework grains (59%): predominantly fine and very fine sand-sized, with trace amounts of medium and coarse sand-sized materials, poorly-very poorly sorted, angular/subangular/subrounded, consisting of quartz (32%), feldspars (4%; plagioclase and potassium feldspars), lithic fragments (60%), and other minor-trace constituents, including micas, chlorite, glauconite, opaque iron-oxide minerals, and organic materials (flakes, some recognizable plant fragments)

Detrital matrix (28%) of silt-clay, patchy. Fair sedimentary layering. Moderately burrowed.

Visible porosity (shown in blue) estimated as 13%, principally as intergranular, particularly in burrowed areas. Effectiveness: fair-poor.

Appreciable microporosity, associated with clays. Cement not apparent, although some of the clays might represent diagenetic clay "cement".

This sample has undergone slight apparent compaction.

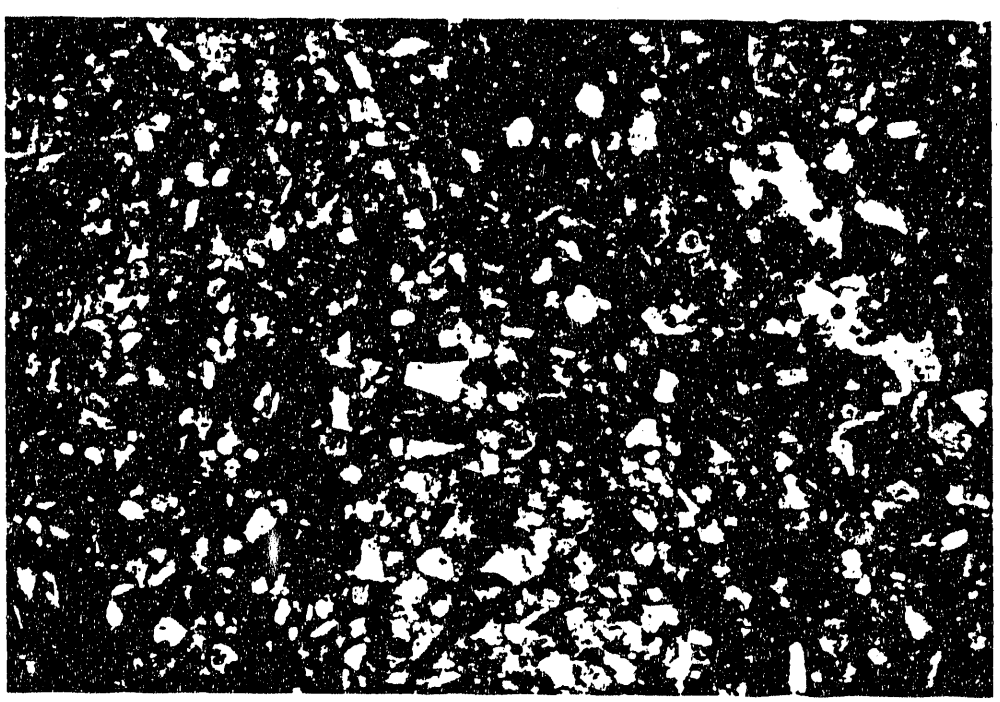

Figure 2.11: Ugnu SWPT #1, 3264' (50 X PL)

L. Ugnu SWPT #1, 3241' (Lower Ugnu (?) Zone).

Description:

Siltstone. Sand-sized grains (14%): predominantly very fine; fine; and medium sand-sized, poorly-very poorly sorted, angular/subangular/subrounded, consisting of quartz (50%), feldspars (2%; plagioclase and potassium feldspars), lithic fragments (44%), and other minor-trace constituents, including micas, chlorite, glauconite (in burrow), opaque iron-oxide minerals, and organic materials (including recognizable plant fragments)

Detrital matrix (75%) of silt-clay, semi-pervasive, streaky-patchy with sedimentary layering. Moderately burrowed.

Visible porosity (shown in blue) estimated as 11%, principally as intergranular to burrow-filling grains (coarser).

Effectiveness: poor-fair parallel to layering, poor perpendicular to layering.

Appreciable microporosity, associated with clays. Cement not apparent, some iron-oxide could be authigenic/diagenetic.

This sample has undergone slight apparent compaction.

Figure 2.12: Ugnu SWPT #1, 3241' (50 X PL)

M. Ugnu SWPT #1, 3235' (Lower Ugnu (?) Zone).

Description:

Lithic Wacke. Framework grains (39%): predominantly very fine sand-sized, with subordinate amounts of fine, medium, coarse, very coarse sand-sized materials, poorly-very poorly sorted, angular/subangular/subrounded, consisting of quartz (37%), feldspars (3%; plagioclase and potassium feldspars), lithic fragments (53%), and other minor-trace constituents, including micas, chlorite, glauconite, opaque iron-oxide minerals, and organic materials (5%)

Detrital matrix (46%) of silt-clay, as patches-streaks, and clasts of siltstone-mudstone. Vague sedimentary layering. Strongly burrowed.

Visible porosity (shown in blue) estimated as 16%, principally as intergranular, particularly associated with burrow-filling coarser grains. Effectiveness: moderate.

Moderate microporosity, associated with clays. Cement not apparent, although some of the clays could represent diagenetic material. Pyrite (2-5%) associated with burrows as authigenic/diagenetic material.

This sample has undergone slight apparent compaction.

N. Ugnu SWPT #1, 3235' (Lower Ugnu (?) Zone).

Description:

Sandy Siltstone. Sand-size grains (31%): predominantly very fine, fine, and medium sand-sized, with trace amounts of coarse sand-sized materials, very poorly (bimodally?) sorted, angular/subangular/subrounded, consisting of quartz (30%), feldspars (10%; plagioclase and potassium feldspars), lithic fragments (38%), and other minor constituents, including micas, chlorite, glauconite, epidote, opaque iron-oxide minerals (4%), and organic materials (15%; including recognizable plant fragments).

Detrital matrix (57%) of silt-clay, semi-pervasive/lense-like/patchy-fair sedimentary layering. Moderately burrowed.

Visible porosity (shown in blue) estimated as 12%, principally as intergranular, particularly associated with burrow-filling grains of coarser material. Effectiveness: fair-poor.

Fair amount of microporosity, associated with clays. Cement not apparent.

This sample has undergone slight apparent compaction.

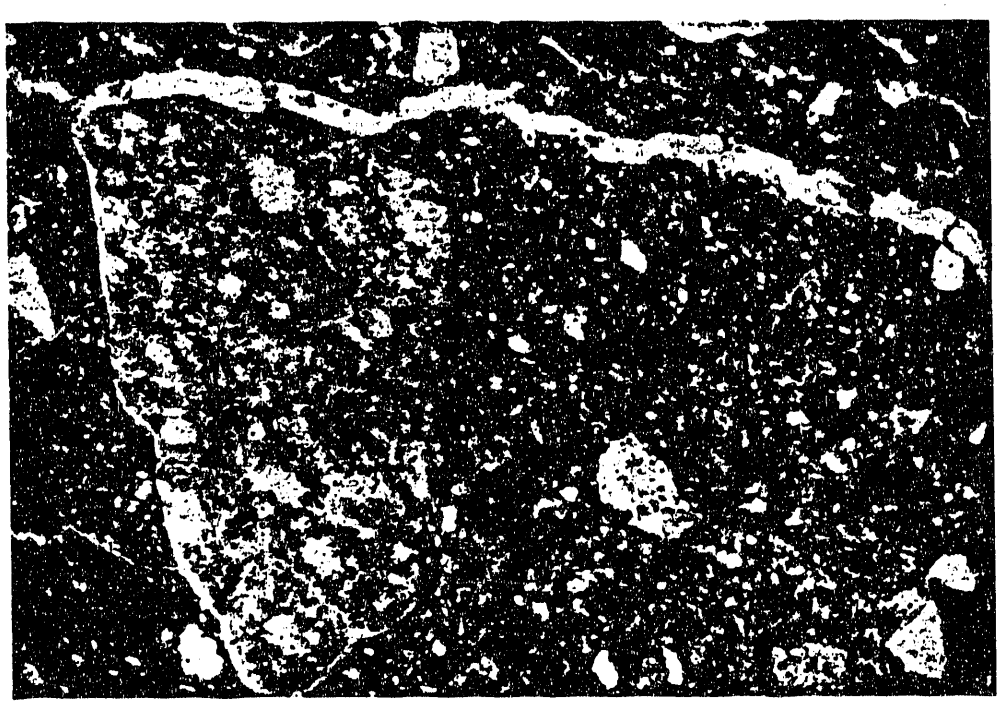

Figure 2.13: Ugnu SWPT #1, 3235' (50 x PL)

O. Ugnu SWPT #1, 3174' (Lower (?) Ugnu Zone).

Description:

Lithic Wacke. Framework grains (47%): predominantly coarse sand-sized, with subordinate amounts of medium sand-sized materials, (rock is biomodally sorted), angular/subangular/subrounded, consisting of quartz (23%), feldspars (14%; plagioclase and potassium feldspars), lithic fragments (62%), and other minor-trace constituents, including micas, chlorite, glauconite, opaque iron-oxide minerals, and organic materials

Detrital matrix (41%) of semi-pervasive silt-clay among framework grains.

Visible porosity (shown in blue) estimated as 13%, principally as intergranular, with an appreciable proportion as microporosity, associated with clays. Effectiveness: low.

Moderate microporosity, associated with clays. Cement consists of traces of quartz overgrowths on some framework grains; some of the "matrix" clays might, rather, represent diagenetic clay "cement".

This sample has undergone slight apparent compaction.

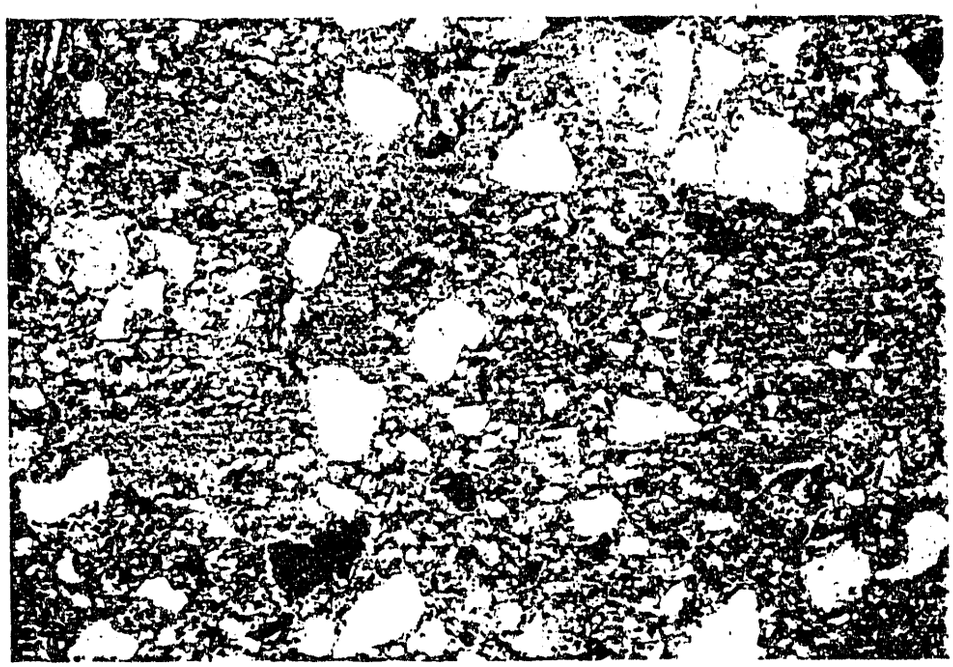

Figure 2.14: Ugnu SWPT #1, 3174' (50 x PL)

P. Ugnu SWPT #1, 3128' (Lower (?) Ugnu Zone;

Description:

Siltstone. Sand-size grains (10%): predominantly very fine sand-sized, moderately sorted, angular/subangular, consisting of quartz (59%), feldspars (18%; plagioclase and potassium feldspars), lithic fragments (4%), and other minor-trace constitutents, including micas, chlorite, glauconite, opaque iron-oxide (10%) minerals, organic (7%) materials and patches of residual hydrocarbons.

Detrital matrix (79%) principally of silt, with subordinate clay. Vague sedimentary layering.

Visible porosity (shown in blue) estimated as 11%, principally as micro-porosity, with intergranular porosity as well. Effectiveness: marginal-fair(?). Cement not apparent.

This sample has undergone slight apparent compaction.

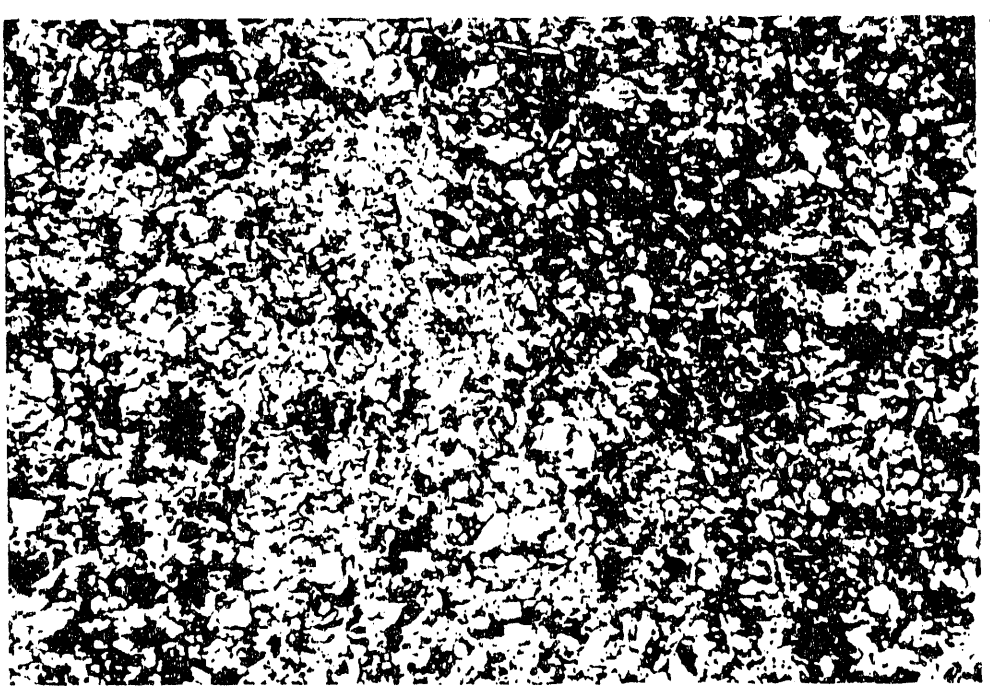

Figure 2.15: Ugnu SWPT #1, 3235' (50 x PL)

Q. Ugnu SWPT #1, 3112' (Lower (?) Ugnu Zone).

Descript'on:

Lithic Wacke. Framework grains (51%): predominantly fine sand-sized, with subordinate amounts of medium and coarse sand-sized materials, moderately sorted, angular/subangular/subrounded, consisting of quartz (38%), feldspars (13%; plagioclase and potassium feldspars), lithic fragments (45%), and other minor-trace constitutents, including micas, chlorite, glauconite(?), opaque iron-oxide minerals, and organic materials (3%).

Detrital matrix (26%) intergranular to framework grains, and as layers enriched in silt clay.

Visible porosity (shown in blue) estimated as 24%, principally as intergranular, with an appreciable component of microporosity as well.

Effectiveness: good-fair. Cement not apparent. However, an appreciable proportion of the "matrix" clays might well, rather, represent diagenetic "cement".

This sample has undergone slight apparent compaction.

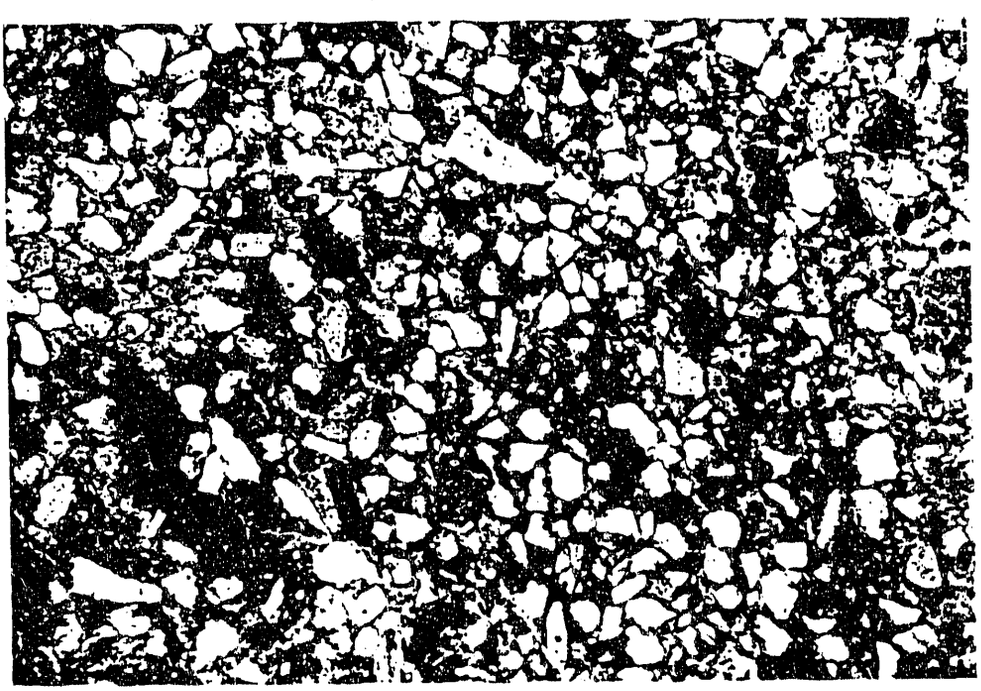

Figure 2.16: Ugnu SWPT #1, 3112' (50 X PL)

R. Ugnu SWPT #1, 3059' (Lower Ugnu Zone).

Description:

Litharenite. Framework grains (54%): predominantly coarse sand-sized, with trace amounts of very fine-sized materials, (rock is well/bimodally(?) sorted), angular/subangular/subrounded, consisting of quartz (18%), feldspars (4%; plagioclase and potassium feldspars), lithic fragments (77%), and other minor-trace constitutents, including micas, glauconite and epidote. There is appreciable residual hydrocarbon material as well.

Detrital matrix (46%) questionable/optically indeterminate; much of this may, rather, represent hydrocarbon-occupied pore space(?). Some clay material is recognizable.

Visible porosity is optically indeterminate, but could be on the order of as much as 30 + % of the specimen. Such porosity would be principally intergranular, with some associated minor microporosity. Effectiveness: good-fair. Cement not apparent, although some/much of the "matrix" clays which are present may well represent diagenetic "cement".

This sample has undergone slight apparent compaction.

Figure 2.17: Ugnu SWPT #1, 3059' (50 x PL)

S. Ugnu SWPT #1, 3013' (Upper Ugnu Zone).

Description:

Lithic Wacke. Framework grains (39%): predominantly very fine sand-sized, with trace amounts of fine sand-sized materials, poorly sorted, angular/subangular, consisting of quartz (49%), feldspars (2%; plagioclase and potassium feldspars), lithic fragments (45%), and other minor-trace constitutents, including micas, chlorite, glauconite, opaque iron-oxide minerals, and organic materials (4%).

Detrital matrix (55%) as patches rich in clay-silt. Vague sedimentary layering. Moderately burrowed(?).

Visible porosity (shown in blue) estimated as 7%, principally as intergranular, microporosity; perhaps some secondary dissolution of some framework grains. Effectiveness: low. Cement not apparent.

This sample has undergone slight apparent compaction.

T. Ugnu SWPT #1, 2996' (upper Ugnu Zone).

Description:

Litharenite. Framework grains (64%): predominantly very fine sand-sized, with trace amounts of fine and medium sand-sized materials, well sorted, angular/subangular/subrounded, consisting of quartz (50%), feldspars (2%; plagioclase and potassium feldspars), lithic fragments (47%), and other minor-trace constituents, including micas, chlorite, glauconite(?). Also appreciable residual hydrocarbons.

Detrital matrix (37%?) questionable/optically indeterminate, due to presence of hydrocarbon material. Some clay material is recognizable, but much of the "matrix" here may, rather, represent porosity, which thus could be on the order of as much as 30%, or greater. This would be principally intergranular, with some microporosity.

Effectiveness: good. Cement not apparent, although at least some of the intergranular clay as is actually present may well represent diagenetic clay "cement".

This sample has undergone slight apparent compaction.

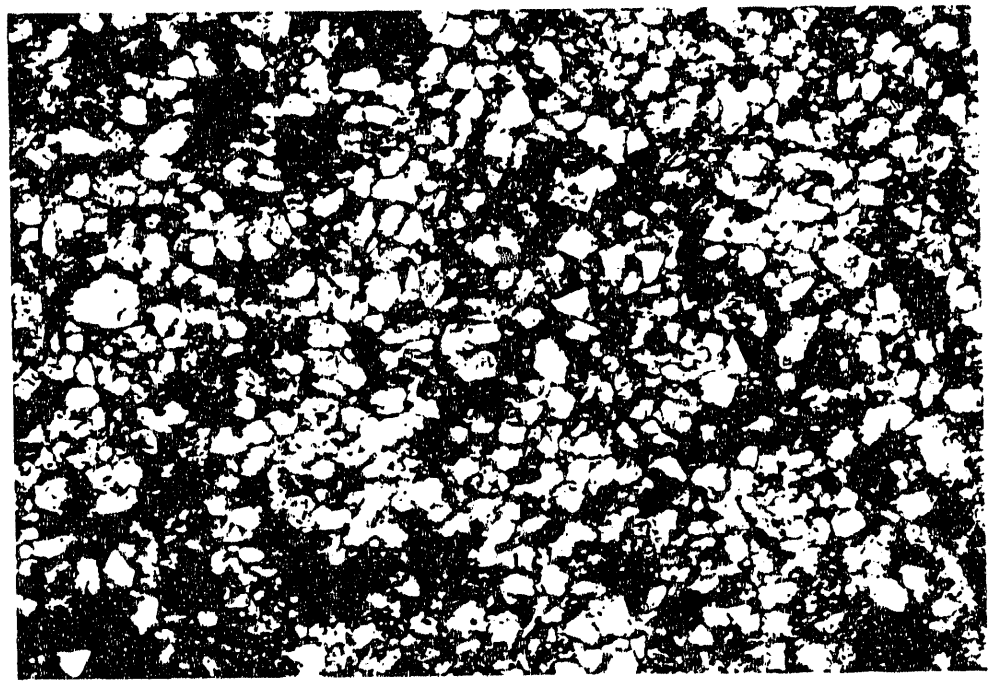

Figure 2.18: Ugnu SWPT #1, 3996' (50 x PL)

2.3.2 West Sak SWPT #1 Samples

The following are the results of the Petrographic analyses on the 11 Samples obtained from West Sak SWPT #1.

A. West Sak SWPT #1, 3960' (below West Sak Zone).

Description:

Litharenite. Framework grains (72%): predominantly very fine sand-sized, with subordinate amounts of fine sand-sized materials, well sorted, angular, consisting of quartz (30%), feldspars (3%; plagioclase and potassium feldspars), lithic fragments (64%), and other minor-trace constitutents, including micas, opaque iron-oxide minerals, glauconite, and organic materials.

Detrital matrix (10%) as streaks-patches, richer in clays. Fair-good sedimentary layering.

Visible porosity (shown in blue) estimated as 15%, principally as semi-pervasive intergranular; moderately effective.

Moderate microporosity, associated with clays. Cement not apparent, although at least some of the clays might well represent diagenetic "cement".

This sample has undergone slight-moderate apparent compaction.

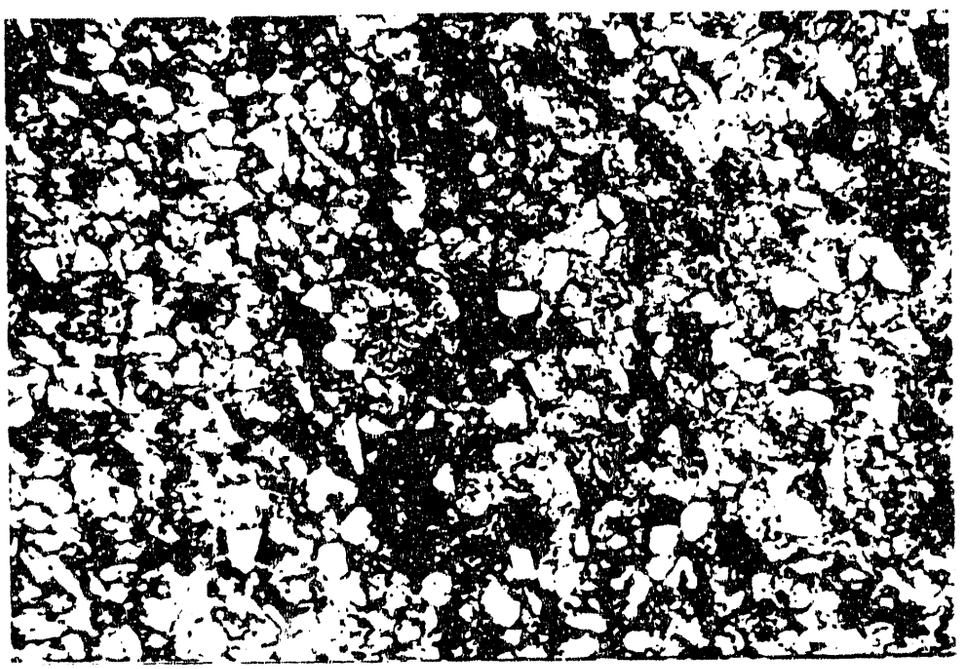

Figure 2.19: West Sak SWPT #1, 3960' (50 x PL)

B. West Sak SWPT #1, 3923' (below West Sak Zone).

Description:

Lithic Wacke. Framework grains (58%): predominantly very fine sand-sized, with subordinate amounts of fine and medium sand-sized materials, moderately-poorly sorted, very angular/angular/subangular, consisting of quartz (40%), feldspars (5%; plagioclase and potassium feldspars), lithic fragments (50%), and other minor-trace constitutents, including micas, chlorite, glauconite, and organic materials.

Detrital matrix (37%) as lenses-streaks-patches, richer in silt-clays. Fair sedimentary layering, with moderate burrowing.

Visible porosity (shown in blue) estimated as 5%, principally as patchy intergranular; poorly effective.

Moderate microporosity, associated with clays. Cement not apparent., although some of the clays might well represent diagenetic "cement". Irregular patches of iron-oxide minerals (after sulphides?) are scattered within rock.

This sample has undergone slight apparent compaction.

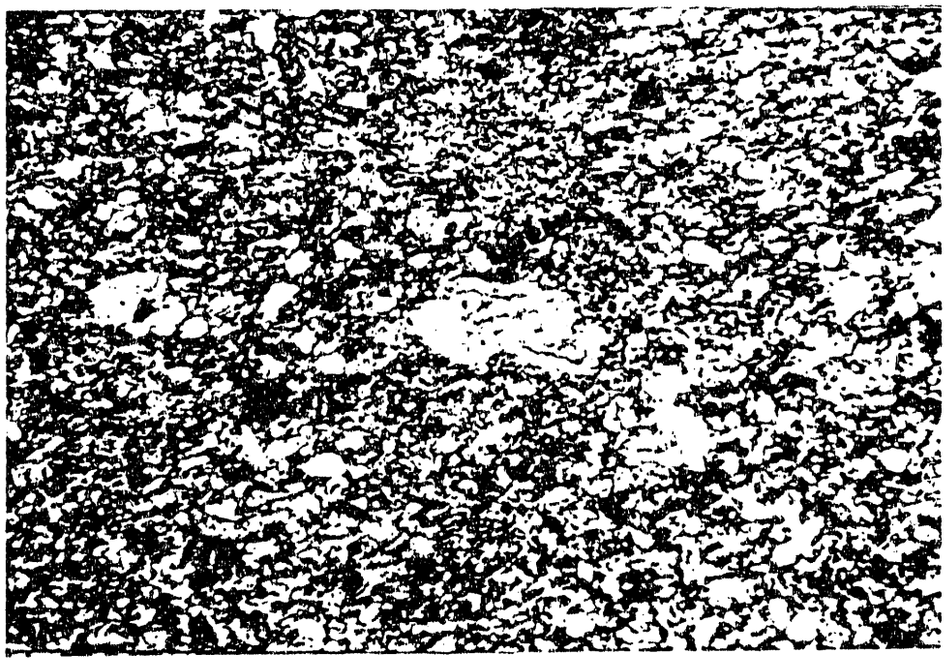

Figure 2.20: West Sak SWPT #1, 3923' (50 x PL)

C. West Sak SWPT #1, 3917' (below West Sak Zone).

Description:

Siltstone. Sand-size grains (35%): predominantly fine and very fine sand-sized, with trace amounts of medium sand-sized materials, poorly sorted, angular/subangular, consisting of quartz (46%), feldspars (7%; plagioclase and potassium feldspars), lithic fragments (44%), and other minor-trace constitutents, including micas, chlorite, glauconite, and organic materials.

Detrital matrix (59%) of silt and clays. Fair sedimentary layering, with streaks-patches of sand-size grains. Moderately burrowed.
Visible porosity (shown in blue) estimated as 3%, principally as intergranular to sand-size grains in burrow fillings. Discontinuous-poorly effective.
Microporosity, associated with clays. Cement not apparent., although some of the clays might represent diagenetic "cement". Pyrite (3%) as framboids, aggregates, irregular masses, some in excess of 1.0 mm in size; of authigenic/diagenetic origin.

This sample has undergone slight apparent compaction.

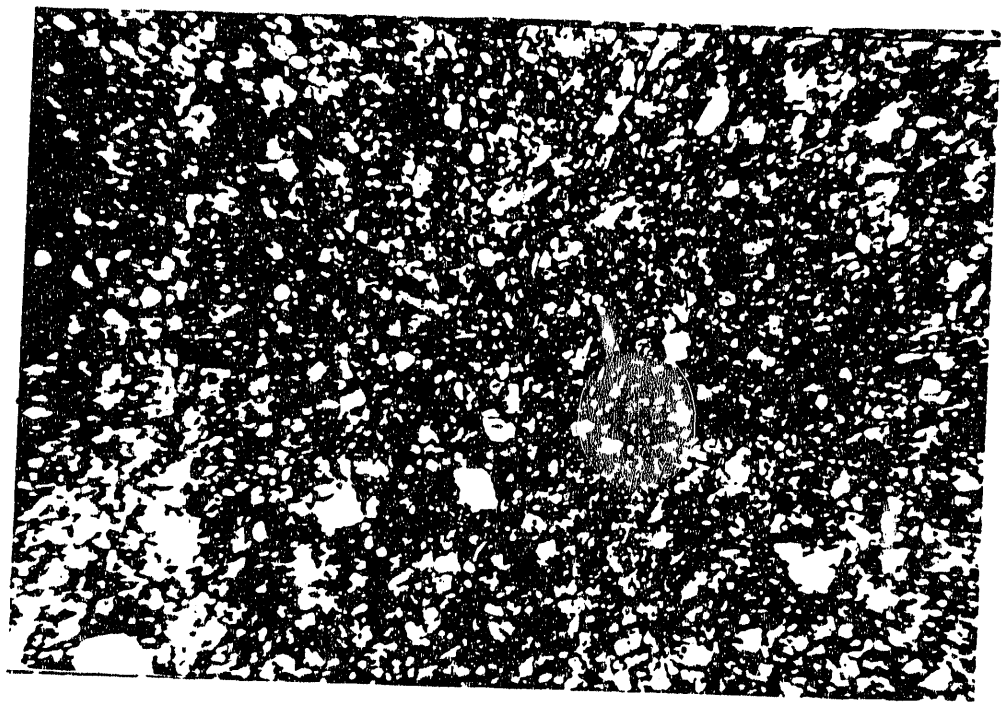

Figure 2.21: West Sak SWPT #1, 3917' (50 x PL)

D. West Sak SWPT #1, 3953' (below West Sak Zone).

Description:

Lithic Wacke/Siltstone. Framework grains (43%): predominantly very fine sand-sized, with subordinate amounts of fine and medium sand-sized materials, poorly, sorted; angular/subangular/subrounded, consisting of quartz (48%), feldspars (3%; plagioclase and potassium feldspars), lithic fragments (46%), and other minor-trace constitutents, including micas, chlorite, glauconite, and organic materials (pervasive, evenly distributed; plant fragments, etc.).

Detrital matrix (46%) as streaks-patches of silt and clay-rich material. Fair sedimentary layering, moderately burrowed.

Visible porosity (shown in blue) estimated as 4%, principally as inter-granular to sand-size grains in burrow fillings. Discontinuous, and poorly effective

Microporosity, associated with clays. Cement not apparent., although some of the clays might represent diagenetic "cement". Pyrite (3%) as authigenic/diagenetic aggregates; irregular/sub-euhedral; some as large as 2.5 mm, some, at least, associated with burrows.

This sample has undergone slight apparent compaction.

Figure 2.22: West Sak SWPT #1, 3953' (50 x PL)

E. West Sak SWPT #1, 3812' (West Sak Zone).

Description:

Lithic Wacke. Framework grains (60%): predominantly very fine sand-sized, with trace amounts of fine sand-sized materials, poorly sorted, angular/subangular/subrounded, consisting of quartz (35%), feldspars (3%; plagioclase and potassium feldspars), lithic fragments (58%), and other minor-trace constitutents, including micas, chlorite, glauconite, and organic materials (including recognizable plant fragments).

Detrital matrix (33%) pervasive. Fair sedimentary layering. Moderately burrowed.

Visible porosity (shown in blue) estimated as 6%, principally as patchy areas, intergranular; some, at least, associated with burrows; poorly effective.

Microporosity, associated with clays. Cement not apparent, some clay might represent diagenetic "cement".

This sample has undergone slight apparent compaction.

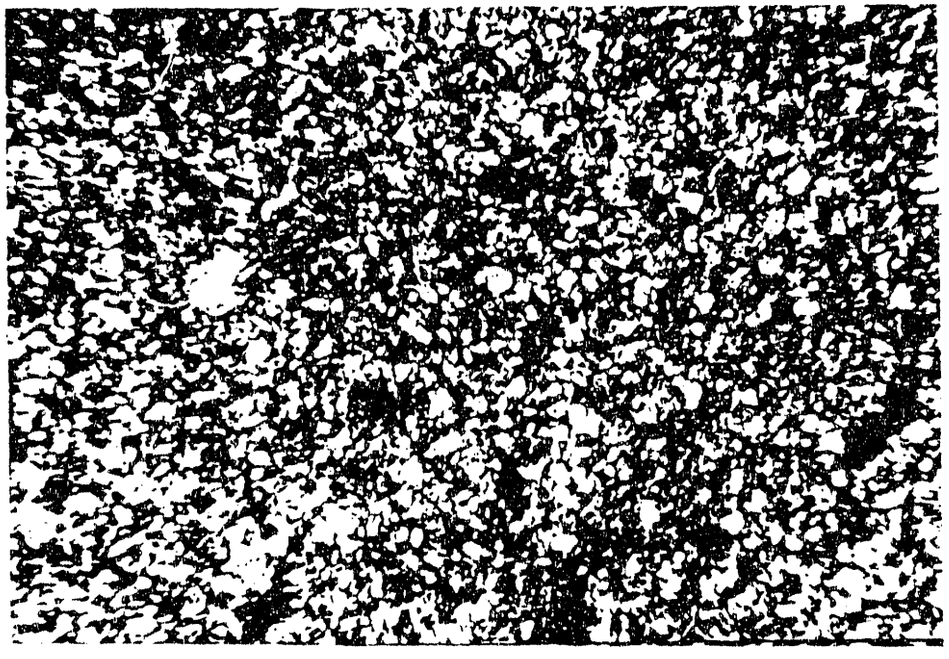

Figure 2.23: West Sak SWPT #1, 3812' (50 x PL)

F. West Sak SWPT #1, 3804' (West Sak Zone).

Description:

Lithic Wacke. Framework grains (70%): predominantly very fine sand-sized, with subordinate amounts of fine sand-sized materials, poorly-moderately sorted, angular/subangular/subrounded, consisting of quartz (38%), feldspars (5%; plagioclase and potassium feldspars), lithic fragments (54%), and other minor-trace constitutents, including micas, chlorite, glauconite, and organic materials.

Detrital matrix (19%) as patches richer in silt and clays. Fair sedimentary layering. Moderately burrowed.

Visible porosity (shown in blue) estimated as 11%, principally as semi-pervasive intergranular; moderately effective. Somewhat patchy-discontinuous.

Moderate microporosity, associated with clays. Cement not apparent, some clay might represent diagenetic "cement". Some speculative amount of the carbonate minerals present might represent intergranular cement (?).

This sample has undergone slight apparent compaction.

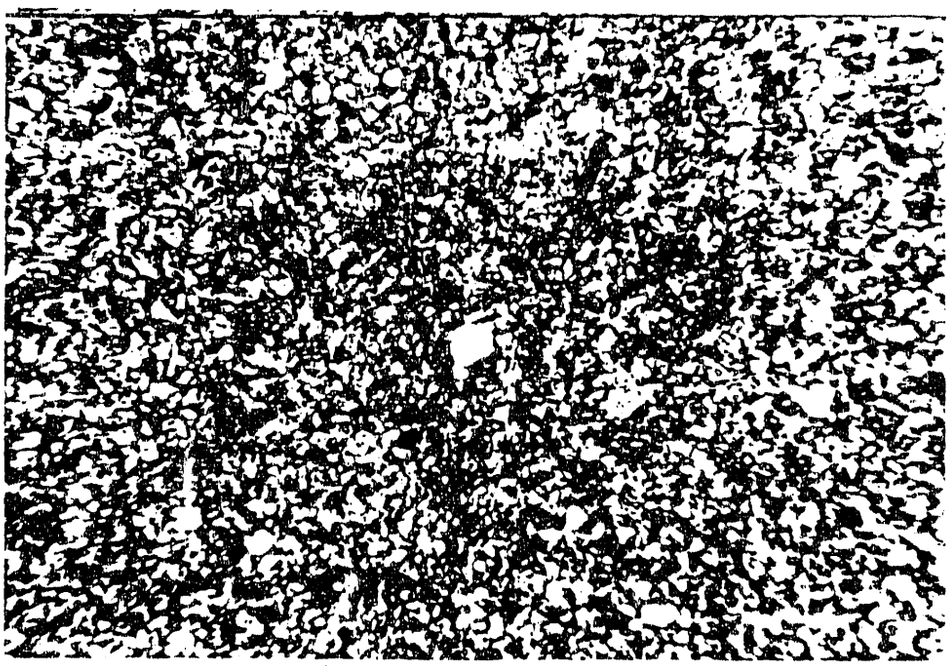

Figure 2.24: West Sak SWPT #1, 3804' (50 x PL)

G. West Sak SWPT #1, 3780' (West Sak Zone).

Description:

Litharenite. Framework grains (68%): predominantly fine sand-sized, with subordinate amounts of very fine sand-sized materials, moderately-well sorted, angular/subangular/subrounded, consisting of quartz (42%), feldspars (3%; plagioclase and potassium feldspars), lithic fragments (52%), and other minor-trace constitutents, including micas, chlorite, opaque iron-oxide minerals, glauconite, and organic materials (some recognizable plant fragments.

Detrital matrix (10%) evenly disseminated, silt-clay. Faint indication of sedimentary layering.

Visible porosity (shown in blue) estimated as 13%, principally as intergranular, pervasive; moderately-highly effective.

Trace of microporosity, associated with clays. Cement not apparent, although at least some of the "matrix" clays might well represent diagenetic clay "cement". Some irregular patches of iron-oxide minerals may be replacive of precursorial pyrite.

This sample has undergone slight apparent compaction.

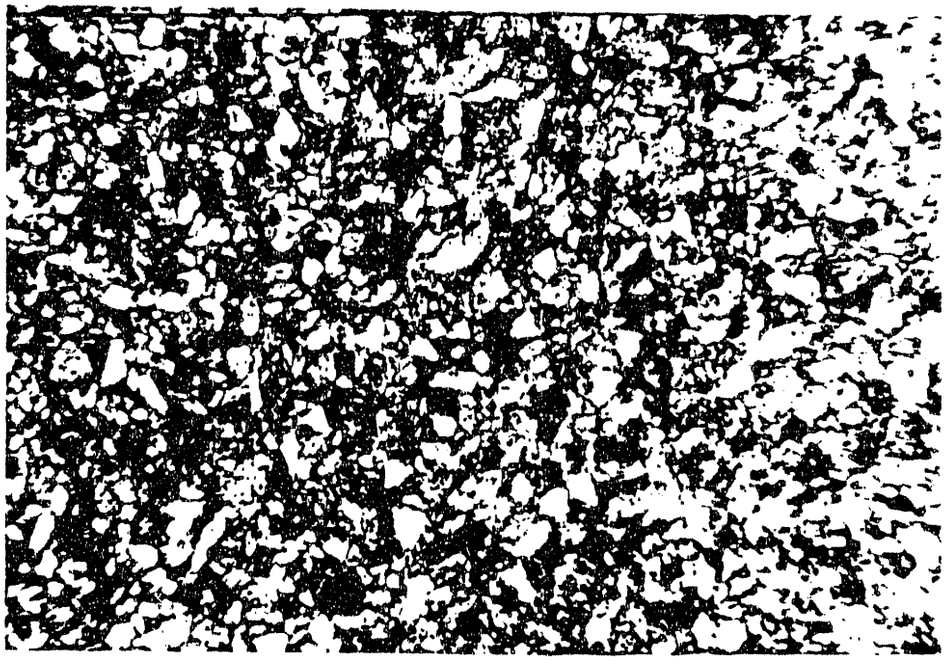

Figure 2.25: West Sak SWPT #1, 3780' (50 x PL)

H. West Sak SWPT #1, 3769' (West Sak Zone).

Description:

Siltstone. Sand-size grains (21%): predominantly very fine sand-sized, with trace amounts of fine and medium sand-sized materials, poorly-very poorly sorted, angular/subangular/subrounded, consisting of quartz (69%), feldspars (9%; plagioclase and potassium feldspars), lithic fragments (20%), and other minor-trace constitutents, including micas, chlorite, and organic materials.

Detrital matrix (76%) semi-pervasive; fair sedimentary layering. Somewhat burrowed.

Visible porosity (shown in blue) estimated as <3%, principally as intergranular, discontinuous, associated with burrow fillings; poorly effective.

Some microporosity, associated with clays.

Cement not apparent, although some of the clays might represent diagenetic "cement". Pyrite (<3%) as extremely fine-grained (framboids?) some with euhedral faces on margins. Some (<3%) iron-oxide minerals (red- and black-colored), up to 0.5 mm in size, side-by-side with pyrite particles.

This sample has undergone slight apparent compaction.

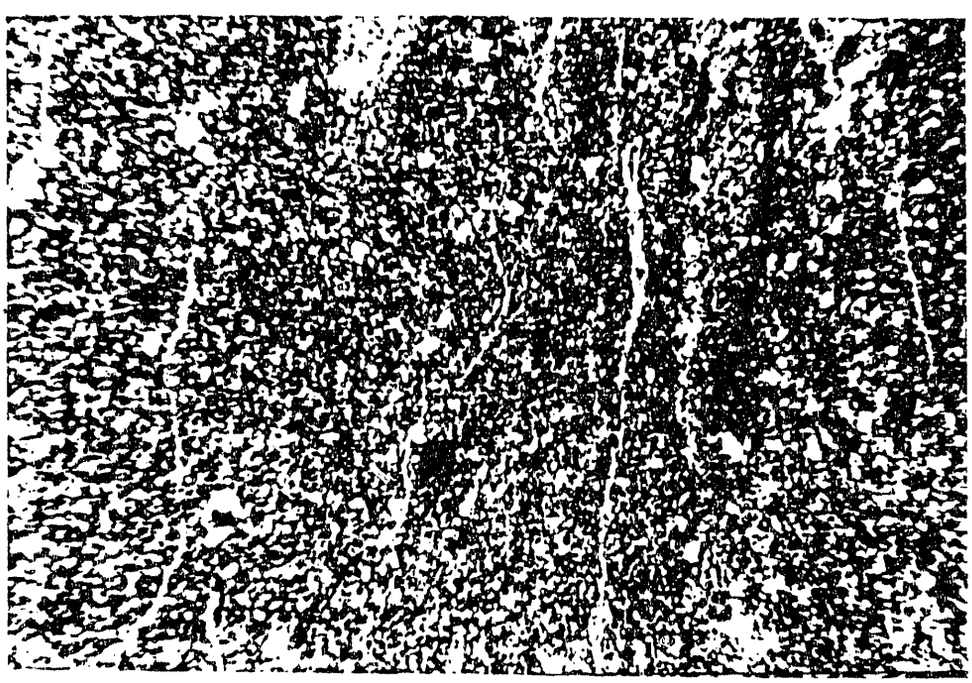

Figure 2.26: West Sak SWPT #1, 3769' (50 x PL)

I. West Sak SWPT #1, 3761' (West Sak Zone).

Description:

Siltstone. Sand-size grains (25%): predominantly very fine sand-sized, with trace amounts of fine sand-sized materials, poorly sorted, angular/subangular/subrounded, consisting of quartz (44%), feldspars (8%; plagioclase and potassium feldspars), lithic fragments (40%), and other minor-trace constitutents, including organic materials (5%), micas, chlorite, and glauconite (?).

Detrital matrix (69%) semi-pervasive; fair sedimentary layering, somewhat streaky-patchy. Somewhat burrowed.

Visible porosity (shown in blue) estimated as 2%, principally as intergranular to burrow-filling grains; poorly effective.

Some microporosity, associated with clays. Cement not apparent, Pyrite (4%) as irregular patches up to 1.0 mm in size; also as framboids (?) with euhedral faces projecting from margins; some with red-colored margins (hematite/geothite?).

This sample has undergone slight apparent compaction.

Figure 2.27: West Sak SWPT #1, 3761' (50 x PL)

J. West Sak SWPT #1, 3723' (West Sak Zone).

Description:

Litharenite. Framework grains (66%): predominantly fine sand-sized materials, well-very well sorted, angular/subangular/subrounded/rounded, consisting of quartz (44%), feldspars (5%; plagioclase and potassium feldspars), lithic fragments (49%), and other trace constitutents, including organic materials and glauconite.

Detrital matrix essentially nil.

Visible porosity (shown in blue) estimated as essentially nil.

Cement (34% of sample) consists of intergranular carbonate (calcite?) mineral(s).

This sample has undergone slight apparent compaction.

Figure 2.28: West Sak SWPT #1, 3723' A (50 X PL) B (50 X xsPL)

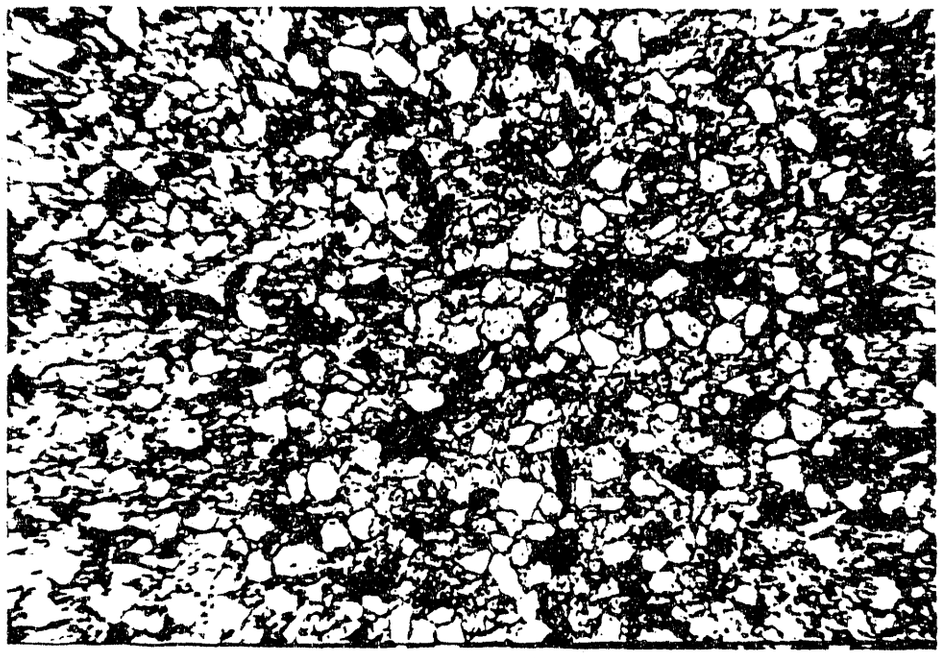

A (50 X PL)

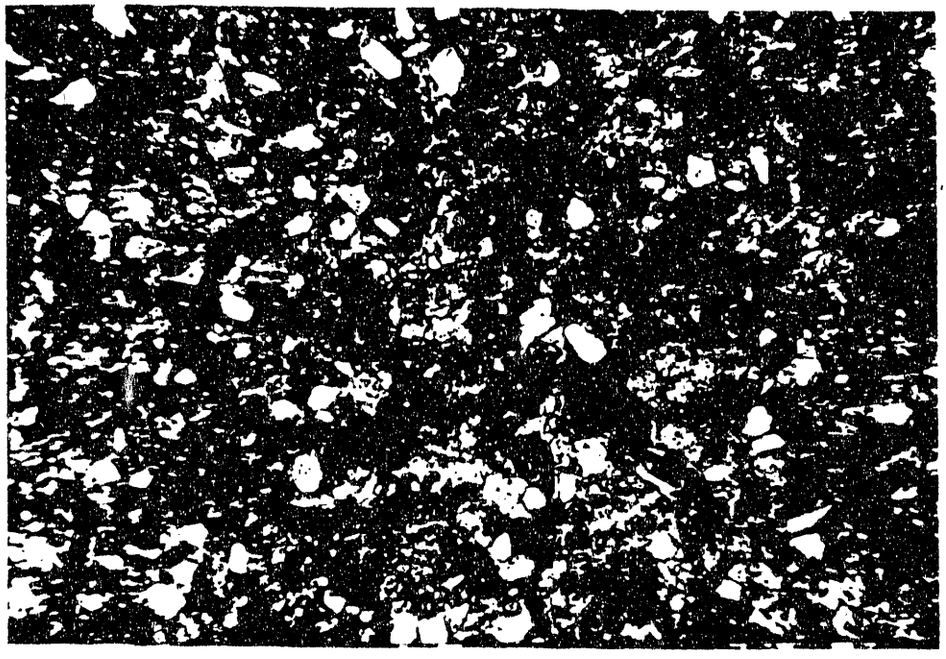

B (50 X xsPL)

K. West Sak SWPT #1, 3715' (above West Sak Zone).

Description:

Siltstone. Sand-size grains (40%): predominantly fine and very fine sand-sized materials, poorly-very poorly sorted; angular/subangular/subrounded, consisting of quartz (34%), feldspars (9%; plagioclase and potassium feldspars), lithic fragments (49%), and other minor-trace constitutents, including micas, chlorite, glauconite, and organic materials (5%).

Detrital matrix (55%) patchy-streaky/semi-pervasive; fair sedimentary layering, somewhat burrowed.

Visible porosity (shown in blue) estimated as 4%, principally as discontinuous patches of intergranular, associated with burrow-filling grains. Poorly effective.

Some microporosity, associated with clays. Cement not apparent, Pyrite (2%) as irregular patches up to 0.6 mm in size; some with euhedral faces on margins, representing authigenic/diagenetic materials.

This sample has undergone slight apparent compaction.

Figure 2.29: West Sak SWPT #1, 3715' (50 x PL)

CHAPTER 3.0

MODELING OF ASPHALTENE EQUILIBRIA: A POLYDISPERSED MOLECULAR THERMODYNAMIC MODEL

3.1 INTRODUCTION

It is well known that, the flocculation of asphaltenes in petroleum reservoirs, casing and production tubing of the wells and surface separation and upgrading facilities pose technical problems and increase the cost of production and processing of crude oils. There have been many instances in both field and laboratory studies that have reported asphaltene deposition during recovery of asphaltic crudes by immiscible or miscible gas flooding. Other field conditions conducive to asphaltene precipitation include: natural depletion, gas-lift operations, caustic flooding and acidization. Such cases were reported in the Princess Field, Greece (Adialalis, 1982), the Mata-Acema Field, Venezuela (Lichaa, 1977), the Hassi-Messahoud Field, Algeria (Haskett and Tartera, 1965), the Ventura Field, California (Tuttle, 1983), the Midale Unit, Saskatchewan, Canada (Novasad and Costain, 1990), the Ula reservoir, North Sea (Chung, et al, 1991), the Little Greek Field, Mississippi (Hansen, 1977) and the San Andres Unit, Seminole, Texas (Chung, et al, 1991). Recently, a good overview of field experiences with asphaltene deposition, modeling of asphaltene precipitation and equilibria, and different ways of dealing with it were provided by Leontaritis and Mansoori (1988), and Leontaritis (1989). Industry is looking for ways to control organic deposition and economic ways to remedy the problem. The development of a predictive technique which is crucial to the solution of this problem is the objective of this work.

In miscible flooding, enriched hydrocarbon gases, LPG's or CO_2 (termed solvents) are injected into the reservoir to reduce oil viscosity, and interfacial tension, to provide drive mechanism and to achieve (dynamic or direct contact) miscibility with the reservoir oil thus resulting into very high displacement efficiency and ultimate oil recovery. In such processes, however, the miscible solvents can cause precipitation and aggregation of asphaltenes by altering the ratio of "heavy" to "light" components and "polar" to "non-polar" components (or resin to asphaltene ratio) in the crude. The asphaltene deposition problem is particularly very important in miscible flooding since it can alter rock wettability, reduce absolute permeability, affect well injectivities and productivities and in some cases even cause plugging of

producing wells (Danesh, et al., 1988; Stalkup, 1983). The amount of asphaltene precipitation depends upon the oil composition (the original asphaltene and resin content of the crude), the solvent composition, the pressure and temperature conditions and the phase behavior of solvent-oil mixtures. Asphaltene deposition in the reservoir is an even more complex phenomenon since several processes such as solvent mixing due to diffusion and dispersion, fingering, mass transfer of hydrocarbon components between oil and solvent in a multi-contact process, adsorption of asphaltenes on preferential rock sites occur simultaneously. Detailed investigations into asphaltene precipitation have been impeded by a shortage of reliable experimental data and techniques needed to quantify the degree of asphaltene precipitation.

The State of Alaska is the largest oil producing state in the nation and currently contributes nearly 25% of the nation's oil production. Alaska currently has nearly 20% of the total U.S. proven reserves and there is further potential to add to these reserves if the exploration in the Arctic National Wildlife Refuge begins. The key to sustaining the long-term oil production in Alaska is to improve recovery efficiencies from the giant fields such as Prudhoe Bay, Kuparuk River, Endicott and to develop marginally economic fields such as West Sak heavy oil reservoir. The need to study asphaltene deposition problem is particularly important to Alaska due to type of enhanced oil recovery projects planned or currently underway. For example, part of the Prudhoe Bay field is produced by enriched gas miscible flood project where asphaltene deposition has been observed. Similar floods are also planned for Kuparuk River and Endicott fields. Miscible flooding is also considered as one of the candidates for recovery of heavy oil from super-giant West Sak reservoir.

In our previous report, we presented the experimental data on the amount of asphaltene precipitation during addition of solvents to West Sak oil (Sharma, 1990). The first set of tests were conducted for two types of West Sak Stock tank oils. Solvents used include: ethane, carbon dioxide, propane, n-butane, n-pentane, n-heptane, Prudhoe Bay natural gas (PBG) and natural gas liquids (NGL). Effect of solvent to oil ratio on the amount of precipitation was studied. Alteration of crude oil composition due to asphaltene precipitation was measured using gas-liquid chromatography. A second set of experimental tests was conducted to measure asphaltene precipitation due to addition of CO_2 to live West Sak crude. Effects of pressure and CO_2 composition in CO_2-oil mixture on the amount of asphaltene

precipitation were determined. These data form basis for fitting parameters to the predictive models. We also presented a thermodynamic model based on the Flory-Huggins polymer solution theory coupled with Equation of State (EOS) model and Peng Robinson departure function to predict the amount of asphaltene precipitation. This model treated asphaltenes as a single (homogeneous) component represented by an average molecular weight and other average properties. The model parameters were derived by fitting the asphaltene precipitation test data for West Sak tank oils. We also presented several problems with such modeling technique and it's inadequacy in representing asphaltene phase equilibria. Thus, to improve the thermodynamic equilibria predictions, in this work we have considered the asphaltenes to exist in crude oil in the broad range of sizes and molecular weights.

3.2 NATURE OF ASPHALTENES AND RESINS

Asphaltenes were originally described by Boussingault (1837) as alcohol insoluble but turpentine soluble solids, obtained from distillation residue of asphalt. Then later, several investigators determined asphaltenes as the low molecular weight n-paraffin insoluble and benzene soluble fraction of crude oil [Long (1981); McKay, et al., (1978); Speight (1981); Chillinger and Yen (1978); Yen (1982)]. In general, asphaltenes can be classified as polar, aromatic-based, high molecular weight hydrocarbons of amorphous structure and they exist in crude oils in the form of colloidally dispersed fine particles and partly as dissolved compounds. Corbett and Petrossi (1978), showed that asphaltenes must be classified by the particular precipitating solvent since different solvent cause different amounts of precipitation of asphaltenes of different molecular weight. Although, the exact chemical structure of asphaltenes will be function of the type of crude, their chemical structure consists of aromatic ring structures with oxygen nitrogen and sulphur present in heterocyclic side chains and oxygen, in alkyl side chains. Speight and Moschopedis (1981) showed that the, elemental compositions of asphaltene fractions precipitated by different solvents from various crudes are different. According to Long (1981), asphaltenes exist in a broad range of size distributions, polarities and molecular weights.

For practical purposes, the asphaltene fraction of an oil is defined as that part precipitated by the addition of n-heptane using IP-143 test. This is the definition

used in this study. The asphaltene fraction generally consists of condensed aromatic and naphthenic molecules of molecular weights in the range of 1,000 to 500,000. They contain larger carbon to hydrogen ratios than are prevalent in crude oils. Thus, addition of low molecular weight n-paraffinic solvents which have lower carbon to hydrogen ratio than crude oils, cause precipitation of the asphaltene colloids. This is accompanied by the removal (dissolution and desorption) of maltenes which are n-heptane soluble fraction of oil. Apart from n-paraffins, CO_2, water and acids also cause precipitation of asphaltenes. CO_2 in addition to reducing the solubility of asphaltenes in oil, causes rigid asphaltene film to form on the interfaces due to its effect on the pH value of the water present. Measurement of the surface tension indicates that there exists a critical micelle concentration (CMC) for dilute solution of asphaltenes in toluene (Rogacheva, et al, 1980). Below CMC, asphaltenes in the solution are in a molecular state, but above CMC, they tend to associate and agglomerate.

Resins are also polycyclic aromatic-based compounds, with somewhat lower molecular weight (250-1000) than asphaltenes. They are nonpolar compared to polar asphaltenes. Resins are the easily adsorbed in common adsorbents like clay or silica gel. Resins are defined as the fraction of crude oil insoluble in ethyl acetate but soluble in n-heptane. According to Margusson (1931), there is a close relationship between asphaltenes and resins which may exist in a crude. Resins are primary cause of keeping asphaltene particles from coagulation and agglemoration. The heavy polycyclic aromatic compounds upon oxidation form neutral resins, while asphaltenes form as a result of further oxidation of resins. The term asphalt is used as a general term to designate the mixture that flocculates out of oil and contains asphaltene particles surrounded by resins, oil, and other liquid entities in oil that are trapped in the flocculated mass.

Asphaltene deposition as a result of flocculation of finer asphaltene particles is a complex phenomenon. Some of the recent studies (Leontaritis and Mansoori, 1987; Hirshberg, et al., 1984) provide more comprehensive description of the causes of asphaltene deposition.

Asphaltenes are lyophobic with respect to low molecular weight paraffinic hydrocarbons and lyophillic with respect to aromatics and resins. That is why resin molecules are adsorbed on the surface of asphaltene particles or micelle (onion skin

model). As a result, when asphaltene particles are completely surrounded by resin molecules, they remain in fine colloidal suspension and do not agglomerate or precipitate. This process is called as "peptization". The degree of dispersion of asphaltenes in crude oils depends upon the chemical composition of crude. In heavy, highly, aromatic crudes, the asphaltenes are well dispersed; but in the presence of paraffinic hydrocarbons, they flocculate and precipitate. Also, in crudes with high resin contents the degree of asphaltene precipitation is less.

Makey, et al. (1978) suggested that the ratios of "polar to non-polar" and "heavy to light" molecules in a crude are particularly important in keeping mutual solubility of the compounds in the crude. By the addition of a solvent to the crude, this ratio is altered. The heavy and polar (asphaltene) molecules separate from the mixture, either in the form of another liquid phase or to a solid precipitate. Hydrogen bonding and the sulfur (and/or the nitrogen) containing segments of the separated (asphaltene) molecules start to aggregate (or polymerize) and as a result produce the asphaltene deposits which are insoluble in solvents.

In general, any action of chemical, mechanical and electrical nature which depeptizes the asphaltene micelle can lead to precipitation of the asphaltenes from the crude oil-asphaltene suspension. The amount of resins adsorbed on the surface of the asphaltenes is essentially a function of the concentration of the resin in the liquid phase of the oil. Processes which deplete or dilute the resin concentration in the oil may lead to asphaltene precipitation. For example, when miscible solvents (CO_2 or lighter hydrocarbons) are added to asphaltene containing crudes, the resin concentration may be so depleted that the entire surfaces of the asphaltene micelles cannot be covered. The result is flocculation of the asphaltenes and sludging or precipitation.

Problems of asphaltene deposition during natural depletion (primary recovery) have been encountered in the well tubing of the Hassi-Messahoud field in Algeria (Haskett and Tartera, 1965) and in the Ventura Field in California (Tuttle, 1983). In both fields the crude was strongly undersaturated with respect to gas. At Hassi-Messahoud, heavy asphaltene precipitation took place in a 450m region of the tubing located just below the level at which bubble point was reached. Furthermore, upon gas injection, a reduced injectivity (factor of two) was experienced due to asphaltene deposition. In the Ventura Field, severe asphaltene

plugging was experienced in the first period of field development until 1970. However, once the reservoir pressure reached the bubble point, the wells produced without trouble of asphaltene deposition.

Reduction in well injectivity or productivity by a factor of two to three during several CO_2 flood field projects (Stalkup, 1978) and water alternating gas drives (Dyes et al, 1972; Harvey et al, 1977) due to asphaltene deposition has been reported. The asphaltene deposition problems have also been reported for the Little Creek CO_2 injection EOR pilot in Mississippi (Tuttle, 1983).

Asphaltenes have an electrical charge and thus their precipitation is possible by the application of electric field. Stream potential experiments conducted by Preckshot (1943) demonstrated that crude oil flowing through sand produces a potential and this appears to be responsible for the formation of precipitated asphaltenes in the flow of crude oil through porous reservoir rock. The same phenomena is thought to be responsible for asphaltene deposition in the slotted liners of low gravity wells in California.

Asphaltene deposition also occurs during release of low molecular weight hydrocarbons from the crude below its bubble point. There appears to be controversy over the issue whether asphaltene precipitation is reversible or irreversible mechanism, especially due to lack of sufficient experimental evidence. Hirshberg, et al. (1984) provides some proof as to reversibility in asphaltene deposition.

Use of hydrochloric acid as a well stimulation fluid can cause severe damage in wells containing asphaltenic crude. In such cases, a rigid asphaltene film gets deposited in the porous media around the wellbore.

3.3 ASPHALTENE PRECIPITATION MODELING: REVIEW

In formulating asphaltene thermodynamic model, two distinct approaches have recently emerged. One is the "Molecular-Thermodynamic" approach and the other is the "Thermodynamic Colloidal" approach. A good overview of past studies, modeling efforts and of current understanding of asphaltene behavior is provided by Leontaritis (1989). It is clear that the physical structure of asphaltenes in crude oils

and the mechanism of their precipitation remains to be resolved. This is partly due to system complexity, and partly also due to the fact that the techniques of studying asphaltene equilibria are not of in-situ type; in fact, they mostly destroy or alter asphaltene in-situ structure. The basic principles of each of the asphaltene modeling approaches are discussed next.

3.3.1. Molecular-Thermodynamic Approach

One of the first molecular-thermodynamic modeling efforts of predicting asphaltene phase behavior, was published by Fussel (1979). She attempted to describe the phase behavior of asphaltic systems by using the equation of state approach. Her model, which was based on the Redlich-Kwong EOS, used a simultaneous calculation of vapor-liquid and liquid-liquid equilibria to predict phase behavior of asphaltic crudes. Fussel considered the flocculating asphaltenes as a separate "heavy liquid" phase in thermodynamic equilibrium with the light liquid and vapor phases.

Hirschberg, et al. (1984), Burke, et al. (1988), Chung, et al. (1991) and our previous work (Sharma, 1990) followed a similar approach as that of Fussel (1979), except that the Flory-Huggins theory (Flory, 1953; Huggins, 1941) was utilized to perform the liquid-liquid equilibrium calculation between the oil and asphaltene phases. Such modeling approach considered the asphaltene entities as mono dispersed polymeric molecules. Thus, asphaltenes were considered to be single pseudocomponent and the properties of asphaltenes were derived from their average molecular weight. The treatment of asphaltenes as a single component liquid which is non-associating liquid is the inherent limitation of such modeling approach.

An apparent improvement to Hirschberg, et al's approach was proposed by Kawanaka and Mansoori (1988). They considered the asphaltenes to exist in the crude oil in large range of sizes and molecular weights represented by continuous gamma distribution function. The polydisperse polymer theory of Scott and Magat (1945) was used in place of the Flory-Huggins theory to calculate the asphaltene-oil solid-liquid equilibria. In this modeling approach, the equilibrium solid phase is considered to contain only asphaltene fractions and the equilibrium liquid phase is considered to contain both asphaltene (dissolved) fractions and asphaltene free

fractions. Another inherent assumption of this model is that the process of asphaltene precipitation is considered to be a reversible process.

3.3.2 Thermodynamic - Colloidal Approach

The basic concept embodied in this type of modeling approach is that asphaltenes exist in the oil in colloidal suspension, stabilized by resins adsorbed on their surface. The transfer of peptizing agents (i.e. resins) from the asphaltene phase to the oil phase and vice versa is responsible for the aggregation of asphaltene micelles, and their flocculation into larger entities which cause them to drop out of suspension. The highly polar centers (kernels) of the asphaltene micelles have a natural tendency to attract each other (i.e., aggregate), grow in size (i.e., flocculate) and as a result, drop out of solution on suspension (i.e., precipitate). Leontaritis (1988), and Leontaritis and Mansoori (1987) first described a thermodynamic-colloidal model. The model uses conventional macroscopic thermodynamics and the EOS approach to perform VLE equilibrium calculations for establishing the liquid phase from which the asphaltenes may flocculate. The model uses the equilibrium of resins between asphaltene and oil phases. The chemical potential of the resin in the oil phase is obtained by considering resins as large polymeric molecules represented by the Flory-Huggins statistical thermodynamic polymer theory.

3.4 DESCRIPTION OF A GENERALIZED POLYDISPERSED MOLECULAR THERMODYNAMIC MODEL FOR ASPHALTENE EQUILIBRIA PREDICTIONS

In this section, we present a generalized molecular thermodynamic model for prediction of asphaltene equilibria and the amount of asphaltene precipitation for a reservoir oil under the influence of a miscible solvent. As stated earlier, the model considers that asphaltenes exist in crude oil in a range of molecular weights and sizes, as a heterogeneous mixture of various asphaltene fractions. This model is similar to the Kawanaka et al. (1988) polydispersed model which uses the Scott and Magat theory to represent the solid-liquid equilibria for various asphaltene fractions. The proposed model however differs from the Kawanaka et al. model in two respects. Firstly, this model uses a discretized normal distribution function to represent the various asphaltene fractions (or pseudocomponents having different average molecular weights) in the crude oil. Secondly, this model calculates the solubility parameters and other properties for each asphaltene components using

the average molecular weights of each asphaltene pseudocomponent from critical property correlation proposed by Twu (1984) and Kistyakowsky's equation (Gambill, 1957).

Figure 3.1 shows a schematic representation of various phases and fractions of the oil and oil-solvent mixtures for three scenarios:

a. asphaltenes in reservoir oil
b. asphaltenes precipitated from addition of solvents to tank oil, and
c. asphaltenes precipitated by addition of solvents to live oil.

In scenario (a), the live oil (LO) is considered to be a mixture of N_T components of which N_F are asphaltene free components and N_A are asphaltene pseudo-components. Thus, we have:

$$N_T = N_A + N_F \tag{3.1}$$

The live oil is considered to be made up of solution gas which is dissolved and contains lighter components *(SG)* and tank oil *(TO)* which is further divided into asphaltene free oil (B) and dissolved asphaltene fractions (A_i). In scenario (b), upon addition of certain proportion of solvent *(SOL)* to the tank oil *(TO)* an overall oil-solvent mixture (TO_{mix}) is formed which splits into vapor *(G)* and liquid (L_{Mix}) phase according to VLE calculations. The L_{mix} phase simultaneously splits into equilibrium solid(S) phase which contains only precipitated asphaltene fractions and equilibrium liquid (L) phase according to solid-liquid equilibrium calculations. Finally, the L phase consists of asphaltene free liquid *(B)* and dissolved asphaltene fractions (A_i). The scenario (c) is similar to (b) except solvents are added to live oil *(LO)* rather than tank oil *(TO)*.

A. Asphaltenes in Live Reservoir Oil

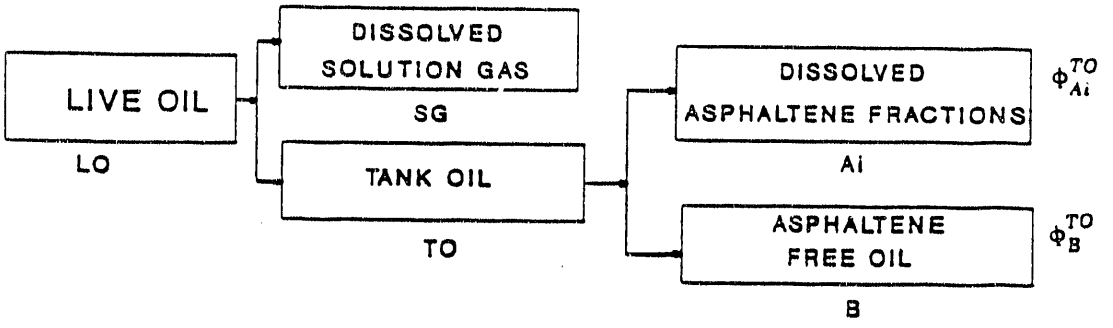

B. Asphaltene Precipitation from Addition of Solvents to Tank Oil

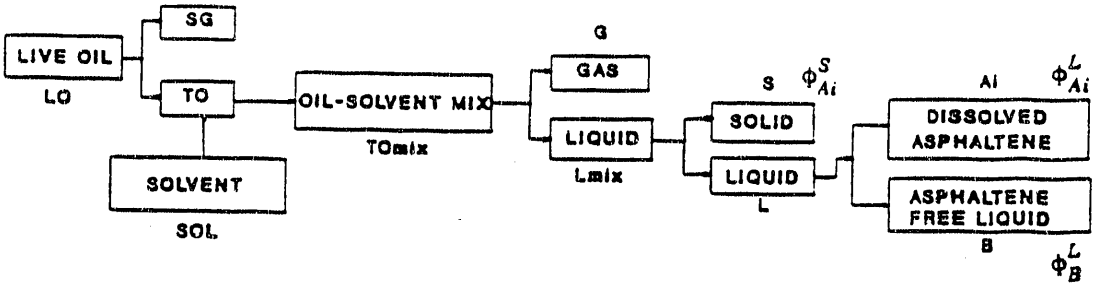

C.. Asphaltene Precipitation from Addition of Solvents to Live Oil

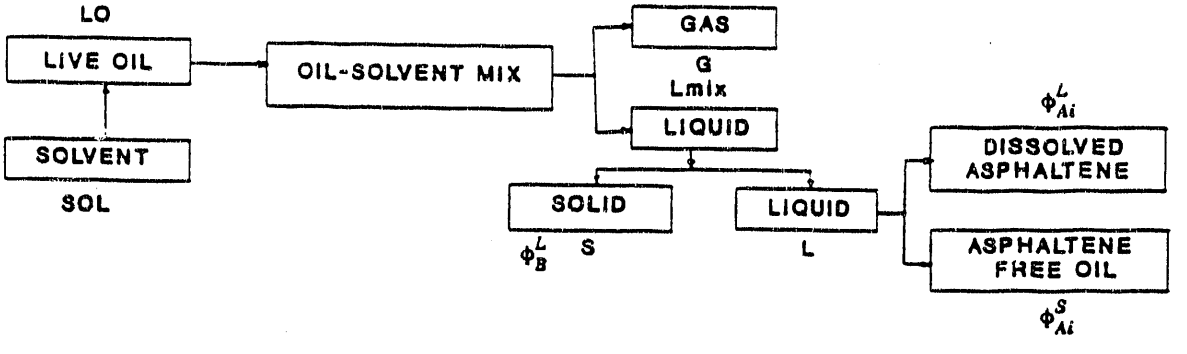

Figure 3.1: Schematic Representation of Various Fractions and Phases of Oil and Oil-Solvent Mixtures

3.4.1 Discretization of the Normal Distribution Function

Consider a continuous normal distribution function, $F(M_A)$, of the asphaltene molecular weights given by:

$$F(M_A) = \frac{1}{\sigma\sqrt{2\pi}} exp(-\xi^2/2) \tag{3.2}$$

$$where\ \xi = \frac{M_A - \overline{M_A}}{\sigma} \tag{3.3}$$

Here, M_A is the molecular weight of any asphaltene fraction, $\bar{M}_A$ is the average molecular weight of all asphaltene fractions, and σ is standard deviation of the normal distribution function. Now:

$$\int_{-\infty}^{\infty} F(M_A)\, dM_A = 1 \tag{3.4}$$

and

$$F(\overline{M}_A) = \frac{1}{\sigma\sqrt{2\pi}} \tag{3.5}$$

Now consider that the continuous normal distribution function is discretized such that the area under two curves in Figure 3.2 are same and the discretized distribution is characterized by N_A equal intervals of ΔM_A and initial value of M_{A_o} and final value of M_{A_F}. Theoretically, M_{A_O} tends to $-\infty$ and M_{A_F} tends to $+\infty$. But for practical purposes, it is sufficient to approximate the span of molecular weights equal to 6σ since it causes only 0.26% error in calculations. Therefore:

$$M_{A_F} - M_{A_O} = 6\sigma \tag{3.6}$$

Also:

$$M_{A_O} = \overline{M_A} - 3\sigma \tag{3.7}$$

$$M_{A_F} = \overline{M_A} + 3\sigma \tag{3.8}$$

$$\int_{-\infty}^{\infty} F(M_A)\, dM_A = \sum_{i=1}^{N_A} F(M_{Ai})\ \Delta M_A = 0.9974 \simeq 1 \tag{3.9}$$

It can also be shown that:

$$\frac{F(M_{A_O})}{F(\overline{M}_A)} = \frac{F(M_{A_F})}{F(\overline{M}_A)} = 0.01111 \tag{3.10}$$

and:

$$\Delta M_A = \frac{6\sigma}{N_A} \tag{3.11}$$

Thus, the molecular weight of ith fraction of asphaltenes, M_{A_i} is given by:

$$M_{A_i} = M_{A_o} + \frac{3}{N_A}\,[2i - 1] \quad i = 1, N_A \tag{3.12}$$

Also:

$$\xi_i = \frac{3}{N_A}\,[2i - 1 - N_A] \quad i = 1, N_A \tag{3.13}$$

If X_{AT} is the total mole fraction of asphaltenes in the liquid phase, then:

$$X_{AT} = \sum_{i=1}^{N_A} X_{Ai} \tag{3.14}$$

and:

$$X_{AT}\,\overline{M_A} = \sum_{i=1}^{N_A} X_{Ai}\,M_{Ai} \tag{3.15}$$

The mole fraction of each asphaltene fraction (or pseudo-component) is then obtained by:

$$X_{Ai} = \frac{3\sqrt{2}}{\sqrt{\pi}}\,\frac{X_{AT}}{N_A}\,exp\,(-0.5\,\xi_i^2) \quad i = 1, N_A \tag{3.16}$$

3.4.2 Asphaltene Pseudocomponent Property Estimation

Critical properties and accentric factors of the pseudocomponents are needed in the phase behavior calculations. Numerous correlations have appeared in the literature for generating critical properties from other measurable properties such as boiling point (T_b) or specific gravity (SG). In this work, the critical property correlation proposed Twu (1984) is used. The correlation uses the molecular weight as the primary variable. This method consists of two parts. The first part is called the reference part where the critical properties are correlated as a function of normal boiling point. The normal boiling point is obtained from the molecular weight of each asphaltene component. The second part (perturbation part) is correlated as a function of normal boiling (T_b) and the specific gravity differences (ΔSG) between the real system and the reference system. The specific gravities of the pseudocomponents are determined using the method proposed by Whitson (1989). This method assumes that the pseudocomponents in a given system have a common

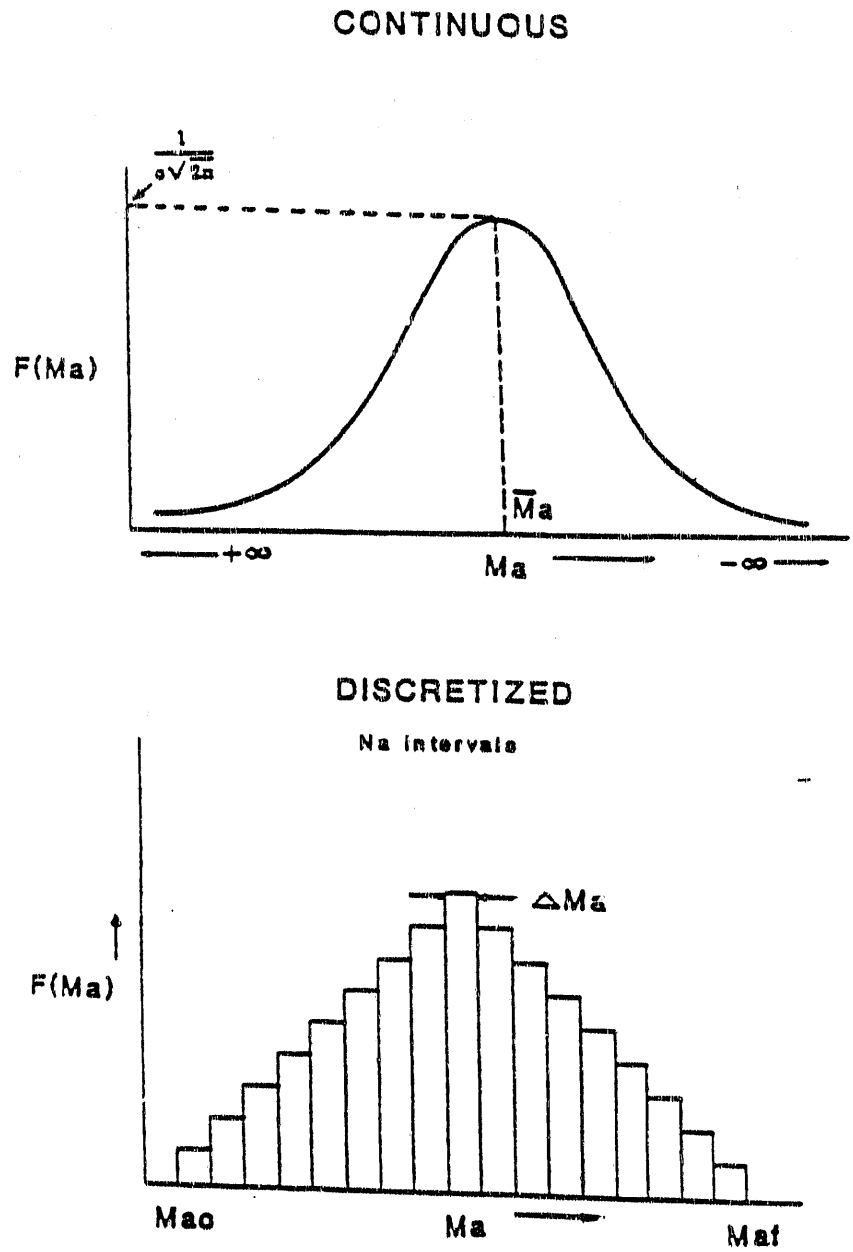

Figure 3.2: Discretization of a Continuous Normal Distribution Function of Asphaltene Fractions

characterization factor (v), where v is obtained from the average plus fraction specific gravity (SG_+) together with pseudocomponent mole fractions and molecular weight. The specific equations used for asphaltene pseudocomponent property estimation are described later.

3.4.3 Solid-Liquid Equilibria Calculations

Kawanaka and Mansoori (1988) first proposed the use of Scott and Magat theory to represent the solid-liquid equilibria for the asphaltene fractions. Considering that the asphaltenes behave as a heterogeneous mixture of polymers, the Scott and Magat theory can be used to calculate the chemical potential, M_{Ai} of the ith pseudocomponent of asphaltene in a mixture of asphaltene and a solvent. That is:

$$\left(\frac{\mu_{Ai} - \mu^{o}_{Ai}}{RT}\right) = ln\,(\phi_{Ai}) + 1 - \left(\frac{m_{Ai}}{m_A}\right)(1 - \phi_B) - m_{Ai}\phi_B + f m_{Ai}\phi_B^2 \tag{3.17}$$

Subscripts A_i and B refer to the ith fraction of asphaltene and the asphaltene free liquid phase respectively and superscript ^{o} refers to a standard reference state. The term ϕ_{Ai} is the volume fraction of ith fraction of asphaltenes, ϕ_B is the volume fraction of fraction B. Thus:

$$\sum_{i=1}^{N_A} \phi_{Ai} + \phi_B = 1 \tag{3.18}$$

m_{Ai} is the segment number of ith fraction of asphaltenes defined as:

$$m_{Ai} = \left(\frac{V_{Ai}}{V_B}\right) \tag{3.19}$$

$\bar{m}_A$ is the average segment number of asphaltenes defines as:

$$\overline{m_A} = \sum_{i=1}^{N_A} \left(\frac{X_{Ai}}{X_{AT}} \right) m_{Ai} \tag{3.20}$$

The parameter f in Equation (3.17) is defined as:

$$f = \frac{1}{r} + \Delta h_B^E / (RT\Phi_A^2) \tag{3.21}$$

According to Scott and Magat theory, the parameter f consists of two parts: A term $(1/r)$ resulting from entropy of mixing and a term $[\Delta h_B{}^E/(RT\ \phi_A{}^2)]$ resulting from the heat of mixing. Considering a binary system made up of average asphaltene fraction A and average asphaltene fraction B, the partial molar excess enthalpy change of mixing is given by:

$$\Delta h_B^E = V_B \Phi_A^2 \left[(\delta_A - \delta_B)^2 + 2K_{AB}\, \delta_A \delta_B \right] \tag{3.22}$$

where δ_A and δ_B are the solubility parameters for fractions A and B respectively, and K_{AB} is the interaction parameter between asphaltenes A and asphaltene-free fraction B; r is the coordination number between two successive segments in asphaltene molecules and has a value between 3 and 4 (Kawanaka and Mansoori, 1988). Equating the chemical potentials of each asphaltene fraction in the equilibrium liquid and solid phases, we can write:

$$\mu_{Ai}^S = \mu_{Ai}^L \qquad i = 1, N_A \tag{3.23}$$

Substituting $\mu_{Ai}{}^{S}$ and $\mu_{Ai}{}^{L}$ in Equation (3.23) from Equation (3.17) and considering $V_{Ai}{}^{S} = V_{Ai}{}^{L} = V_{Ai}$, $V_B{}^{S} = V_B{}^{L} = V_B$, $m_{Ai}{}^{S} = m_{Ai}{}^{L} = m_{Ai}$ and $\phi_B{}^{S} = O$, we get:

$$ln\left(\frac{\Phi_{Ai}^{L}}{\Phi_{Ai}^{S}}\right) = \left(\frac{1}{\bar{m}_A^L} - \frac{1}{\bar{m}_A^S}\right) + \left(1 - \frac{1}{\bar{m}_A^L}\right)\Phi_B^L - f^L(\Phi_B^L)^2 \tag{3.24}$$

Equation (3.24) can be used for calculation of the total volume fraction of asphaltene in a liquid mixture in equilibrium with a solid phase.

3.4.4 Estimation of Molar Volume and Solubility Parameter for the Oil or Oil-Solvent Mixture

In order to determine the solubility parameter (δ_{Lmix}) and molar volume (V_{Lmix}) for oil-solvent mixtures at a given pressure and temperature conditions, vapor-liquid equilibria calculations are performed using the Peng-Robinson Equation of State to determine the composition of the L_{mix} phase.
A separate Peng-Robinson EOS departure function program is written to determine the parameters δ_{Lmix} and V_{Lmix}.

The cubic form of the Peng-Robinson EOS is solved to determine the compressibility factor for the liquid phase, Z_{Lmix}:

$$Z^3 - (1 - B)\,Z^2 + (A - 3B^2 - 2B)Z - (AB - B^2 - B^3) = 0 \tag{3.25}$$

where:

$$A = \frac{a_{Lmix}P}{(RT)^2} \tag{3.26}$$

and:

$$B = \frac{b_{Lmix}P}{RT} \tag{3.27}$$

The molar volume V_{Lmix} is then obtained using:

$$V_{Lmix} = \frac{Z_{Lmix} RT}{P} \tag{3.28}$$

The internal energy function ΔU^V_{Lmix} is obtained from:

$$\Delta U^V_{Lmix} = \left(\frac{a_{Lmix}}{2\sqrt{2}\, b_{Lmix}} - \frac{T}{2\sqrt{2}\, b_{Lmix}} \frac{da_{Lmix}}{dT} \right) ln \left(\frac{V_{Lmix} + 2.414 b_{Lmix}}{V_{Lmix} - 0.414 b_{Lmix}} \right) \tag{3.29}$$

The solubility parameter is then obtained from:

$$\delta_{Lmix} = \left(\frac{\Delta U^V_{Lmix}}{V_{Lmix}} \right)^{0.5} \tag{3.30}$$

3.4.5. Stepwise Procedure for Prediction of Asphaltene Precipitation Upon Addition of a Solvent to Oil

Step 1) The PVT data for the oil is initially used to tune the Equation of State parameters. The Peng-Robinson Equation of State is used in this model.

Step 2) Using the overall composition of the live reservoir oil, pressure and temperature as the input data, the vapor-liquid equilibria calculations are performed to determine the composition of the equilibrium liquid phase. In case of prediction of precipitation of asphaltenes due to addition of solvents to the tank oil, the stock tank oil composition is determined from vapor-liquid equilibria calculations.

Step 3) For a given solvent/oil ratio, the overall composition of the solvent/oil mixture is then determined.

Step 4) The solvent-oil mixture is then flashed at given P and T to determine the composition of liquid phase (L_{mix}).

Step 5) The molar volume (V_{Lmix}) and solubility parameter (δ_{Lmix}) are then determined for the L_{mix} phase using the Peng-Robinson departure function model (Equations 3.25-3.30).

Step 6) The mole fractions and molecular weights of each asphaltene fraction in the tank oil (or live oil) and the oil-solvent mixture (L_{mix}) are obtained as follows:

The plus fraction is split to generate one asphaltene free pseudocomponent and N_A asphaltene pseudocomponents. Note that the original oil contains (N_F-1) asphaltene free real components and one plus fraction. By splitting the plus fraction, we generate total ($N_F + N_A$) or N_T components of which (N_F-1) are the asphaltene free ($i=1, N_F$-1) real components, one asphaltene free pseudo component ($i = N_F$) and N_A asphaltene pseudocomponents ($i = N_F+1$ to N_T).

In order to split the plus fraction, the average molecular weight of asphaltenes ($\bar{M}_A$), the standard deviation of the asphaltene molecular weight distribution (σ), mole fraction of plus fraction and the ratio of total mole fraction of asphaltenes to the mole fraction of plus fraction (β) must be known. $\bar{M}_A$, β, and σ are the model parameters which are obtained by fitting experimental asphaltene precipitation data. For tank oil:

$$X_{AT}^{TO} = \beta X_{+}^{TO} \tag{3.31}$$

where X_{AT}^{TO} is the total mole fraction of asphaltenes in the tank oil. The mole fraction of asphaltene free pseudo fraction is then:

$$X_{NF}^{TO} = X_{+}^{TO} - X_{AT}^{TO} \tag{3.32}$$

The mole fraction of each asphaltene fraction is then computed as:

$$X_{i+NF}^{TO} = X_{Ai}^{TO} = \frac{3\sqrt{2}}{\sqrt{\pi}} \frac{X_{AT}^{TO}}{N_A} exp(-0.5\,\xi_i^2) \qquad i = 1, N_A \tag{3.33}$$

where ξ_i is obtained from Equation (3.13).

The molecular weights of each asphaltene fraction are computed as:

$$M_{i+NF}^{TO} = M_{Ai}^{TO} = \overline{M}_A^{TO} + \sigma\,\xi_i \qquad i = 1, N_A \tag{3.34}$$

The molecular weight of $N_F th$ fraction (asphaltene free pseudo fraction) is obtained from:

$$M_{NF}^{TO} = \frac{\overline{M}_+ - \overline{M}_A^{TO} X_{AT}^{TO}}{X_{NF}^{TO}} \tag{3.35}$$

For the $Lmix$ phase, a similar approach (Equations 3.31 through 3.35) is used to determine X_{AT}^{Lmix}, X_{NF}^{Lmix}, X_{Ai}^{Lmix}, M_{Ai}^{Lmix} and M_{NF}^{Lmix}.

Step 7) The properties of each asphaltene fraction $(i = 1, N_A)$ are computed as follows:

The molar volume of each asphaltene fraction is given by:

$$V_{Ai} = V_{Ai}^{Lmix} = V_{Ai}^{L} = V_{Ai}^{S} = \frac{M_{Ai}^{Lmix}}{\bar{\rho}_A} \tag{3.36}$$

where $\bar{\rho}_A$ is the average density of asphaltenes.

The average molecular weight of asphaltene free fractions in the L_{mix} phase is given by:

$$\overline{M}_B^{Lmix} = \sum_{j=1}^{N_F} M_j^{Lmix} x_j^{Lmix} \tag{3.37}$$

The interaction parameter K_{AB} is treated as a linear function of the molecular weight:

$$K_{AB} = a' + b' \overline{M}_B^{Lmix} \tag{3.38}$$

where a' and b' are two parameters obtained by fitting experimental asphaltene precipitation data.

The normal boiling point of each asphaltene fraction T_{bi} (^oR) is obtained from Equations (3.39) and (3.40).

$$\beta_i' = ln\,(M_{Ai}^{Lmix}) \qquad i = 1, N_A \tag{3.39}$$

$$T_{bi} = exp\left[5.71419 + 2.71579\,\beta_i' - 0.286590\,\beta_i'^2 - \frac{39.8544}{\beta_i'} - \frac{0.122488}{\beta_i'^2}\right]$$

$$- 24.7522\,\beta_i' + 35.3155\,\beta_i'^2 \tag{3.40}$$

The reference critical temperature, Tc_i^o (^oR) is given by:

$$Tc_i^o = T_{bi} \Big/ \left[0.533272 + 0.191017 \times 10^{-3}\,T_{bi} + 0.779681 \times 10^{-7}\,T_{bi}^2\right.$$

$$\left. -0.284376 \times 10^{-10}\,T_{bi}3 + 0.959468 \times 10^{28} / T_{bi}^{13}\right] \tag{3.41}$$

The reference specific gravity SG_i^o is obtained from Equations (3.42) and (3.43) as follows:

$$\alpha_i = 1 - \frac{T_{bi}}{T_{ci}^o} \tag{3.42}$$

$$SG_i^o = 0.843593 - 0.128624\,\alpha_i - 13.36159\,\alpha_i^3 - 13749.5\,\alpha_i^{12} \tag{3.43}$$

The critical temperature T_{ci} (^oR) is obtained from Equations (3.44) through (3.51).

$$T_{ci} = T_{ci}^o \left[\left(\frac{1 + 2f_T^i}{1 - 2f_T^i} \right) \right]^2 \tag{3.44}$$

where:

$$f_T^i = \Delta SG_T^i \left[\frac{-0.362456}{\sqrt{T_{bi}}} + \Delta SG_T^i \left(0.0398285 - \frac{0.948125}{\sqrt{T_{bi}}} \right) \right] \tag{3.45}$$

$$\Delta SG_T^i = exp \left[5\,(SG_i^o - SG_i) \right] - 1 \tag{3.46}$$

$$SG_i = 6.0108\, M_{Ai}^{0.13541}\, V^{-1.18241} \tag{3.47}$$

$$V = \left[\frac{0.16637 SG_+ S_o}{(Z_+ M_+)} \right]^{-0.84573} \tag{3.48}$$

$$Z_+ = \sum_{i=1}^{N_A} X_{Ai}^{Lmix} \tag{3.49}$$

$$S_o = \sum_{i=1}^{N_A} X_{Ai}^{Lmix} M_{Ai}^{0.86459} \tag{3.50}$$

$$SG_+ = \frac{\rho_+}{62.4} \tag{3.51}$$

where ρ_+ is the average density of the plus fraction prior to splitting. The heat of vaporization (Btu/lb mole) is then obtained for each asphaltene fraction.

$$(\Delta H_i)_{T_B} = 1.014 \left[T_{bi} ((8.75 + 4571 \log_{10} (T_{bi})) \right] \tag{3.52}$$

$$(\Delta H_i)_T = (\Delta H_i)_{T_B} \left[\frac{Tc_i - T}{Tc_i - T_{bi}} \right]^{0.38} \tag{3.53}$$

The solubility parameter for each asphaltene fraction is given by:

$$\delta_{Ai} = \left(\frac{(\Delta H_i)_T - RT}{V_{Ai}^{Lmix}} \right)^{0.5} \tag{3.54}$$

The volume fraction of each asphaltene component in the L_{mix} phase are then obtained:

$$\phi_{Ai}^{Lmix} = \frac{X_{Ai}^{Lmix} V_{Ai}^{Lmix}}{V_{Lmix}} \tag{3.55}$$

and

$$\phi_B = \phi_B^{Lmix} = 1 - \sum_{i=1}^{N_A} \phi_{Ai}^{Lmix} \tag{3.56}$$

The average solubility parameter for asphaltenes (δ_A) and asphaltene free liquid (δ_B) are then obtained.

$$\delta_A = \left(\frac{\sum_{i=1}^{N_A} \phi_{Ai}^{Lmix} \delta_{Ai}}{(1 - \phi_B)} \right) \tag{3.57}$$

$$\delta_B = \left(\frac{\delta_{Lmix} - \delta_A (1 - \phi_B)}{\phi_B} \right) \tag{3.58}$$

The molar volume of asphaltene free liquid (V_B) and asphaltenes (V_A) is then obtained:

$$V_B = \left(\frac{V_{Lmix} - \sum_{i=1}^{N_A} V_{Ai}^{Lmix} X_{Ai}^{Lmix}}{(1 - X_{AT}^{Lmix})} \right) \tag{3.59}$$

$$V_A = \frac{\sum_{i=1}^{N_A} V_{Ai}^{Lmix} X_{Ai}^{Lmix}}{X_{AT}^{Lmix}} \tag{3.60}$$

For each asphaltene fraction, the ratio of ϕ^s_{Ai} to ϕ^L_{Ai} are then obtained from:

$$ln \left| \frac{\Phi_{Ai}^S}{\Phi_{Ai}^L} \right| = \left(\frac{V_{Ai}}{V_A} - \frac{V_{Ai}}{V_B} \right) \Phi_B + f \frac{V_{Ai}}{V_B} \Phi_B^2 \tag{3.61}$$

The parameter f is obtained from Equation (3.21) and (3.22).

Step 8) An iterative procedure is then used to calculate the molar distribution (mole fractions of each asphaltene fraction) in the equilibrium solid and liquid phases.

We assume:

$$V_A^{Lmix} = V_A^L = V_A \tag{3.62}$$

and

$$V_B^{Lmix} = V_B^L = V_B \tag{3.63}$$

As an initial guess, we consider:

$$X_{AT}^L \ (assumed) = X_{AT}^{Lmix} \tag{3.64}$$

Then:

$$V_L = V_A X^L_{AT} + V_B (1 - X^L_{AT}) \tag{3.65}$$

and the equilibrium constants for each asphaltene fraction, K_{Ai} are then computed as:

$$K_{Ai} = \frac{X^S_{Ai}}{X^L_{Ai}} = \frac{\phi^S_{Ai}}{\phi^L_{Ai}} \frac{V_A}{V_L} \tag{3.66}$$

By considering the material balance for each asphaltene fraction between $Lmix, L\ and\ S$ phases we can obtain an expression to calculate the mole fractions of asphaltenes in L phase using:

$$X^L_{Ai} = \frac{X^{Lmix}_{Ai}}{\left[\left(\frac{V_{Lmix} - V_A}{V_L - V_A}\right) + \left(\frac{V_L - V_{Lmix}}{V_L - V_A}\right) K_{Ai}\right]} \tag{3.67}$$

$$X^L_{AT}\ (calc) = \sum_{i=1}^{N_A} X^L_{Ai} \tag{3.68}$$

At this point, the calculated value of $X^L{}_{AT}$ from Equation (3.68) and the assumed value of $X^L{}_{AT}$ from Equation (3.64) are compared for convergence. If convergence has not occurred, the calculations are repeated. Then:

$$X^S_{Ai} = K_{Ai}\ X^L_{Ai} \tag{3.69}$$

Step 9) The weight fraction of asphaltenes precipitated (gm of asphaltene precipitated/gm of tank oil or live oil) is then calculated.

$$\phi_{Ai}^{L} = X_{Ai}^{L} \frac{V_{Ai}}{V_L} \tag{3.70}$$

$$\phi_{A}^{L} = \sum_{i=1}^{N_A} \phi_{Ai}^{L} \tag{3.71}$$

$$\phi_{Ai}^{S} = \phi_{Ai}^{L} \; K_{Ai} \; V_L/V_A \tag{3.72}$$

$$W_{AD}(calc) = \left(\frac{V_L - V_{Lmix}}{V_L - V_A} \right) \frac{\overline{M}_s}{\overline{M}_{Lmix}} \left(\frac{X_{AT}^{TO}}{X_{AT}^{Lmix}} \right) \Bigg| \frac{1}{\overline{M}_{TO}} \tag{3.73}$$

where $W_{AD}(calc)$ is the weight fraction asphaltene deposited,
$\bar{M}_{TO}$ is the average molecular weight of tank oil,
$\bar{M}_{LMIX}$ is the average molecular weight of $Lmix$, and
$\bar{M}_S$ is the average molecular weight of solid phase.

3.4.6. Future Work

A computer program has been developed based on the above model to predict asphaltene equilibria. The model has five parameters namely, $\alpha, \bar{M}_A$, β, a' and b'. A regression technique has been developed to obtain these parameters by fitting the experimental data on asphaltene precipitation due to addition of solvents to tank oil or live oil. The performance of this model will be tested in our future work. Experimental data on West Sak oil gathered previously will be used for this purpose.

3.5 NOMENCLATURE

A	Peng Robinson EOS constant defined in Equation (3.26)
a	Peng Robinson EOS constant defined in Equation (3.26)
a '	Model Parameter in Equation (3.38)
B	Peng Robinson EOS constant defined in Equation (3.27)
b	Peng Robinson EOS constant defined in Equation (3.27)
b '	Model Parameter in Equation (3.38)
f	Parameter defined in Equation (3.21)
$F(M_A)$	Normal Distribution Function
i	component i
j	component j
K_{AB}	Interaction parameter between asphaltenes and asphaltene free liquid
K_{Ai}	Solid-liquid equilibrium constant for ith fraction of asphaltene
M	Molecular weight
$\bar{M}$	Average molecular weight
M_{Ao}	Lowest value of asphaltene molecular weight in the distribution function
M_{AF}	Highest value of asphaltene molecular weight in the distribution function
M_{Ai}	Segment number of ith fraction of asphaltenes
$\bar{M}_A$	Average segment number of asphaltenes
N_A	Number of asphaltene components
N_F	Number of asphaltene free components
N_T	Total number of components
P	Pressure
R	Universal gas constant
S_o	Oil Saturation
SG	Specific gravity
T	Temperature
T_{bi}	Boiling point of ith fraction
T_{ci}	Critical point of ith fraction
T_{ci}^{o}	Reference critical point of ith fraction
U^v	Internal energy function
V	Molar volume
X	Mole fraction
Z	Overall mole fraction in crude oil

Subscripts

A	asphaltene
A_i	ith fraction of asphaltene
B	asphaltene free liquid phase
i	ith fraction or component
j	jth fraction or component
L	L phase
$Lmix$	Lmix phase
NF	N_Fth fraction
s	solid phase
$+$	plus fraction

Superscripts

B	asphaltene free liquid phase
o	reference state
L	L phase
TO	Tank oil
$Lmix$	Lmix phase
S	Solid phase

Greek Symbols

α_i	Variable defined in Equation (3.42)
β	Ratio of total mole fraction of asphaltenes to mole fraction of the plus fraction
B_i'	Variable defined in Equation (3.39)
δ	Solubility parameter
$(\Delta H_i)_{TB}$	Heat of vaporization at boiling point for ith fraction
$(\Delta H_i)_T$	Heat of vaporization at temperature T for ith fraction
$(\Delta h_B{}^E)$	Excess heat of mixing
μ	chemical potential
μ^o	Reference chemical potential
ϕ	Volume fraction
ν	Parameter defined in Equation (3.48)
ρ	Density
$\bar{\rho}_A$	Average density of asphaltenes
σ	Standard deviation of normal distribution function
ξ	Variable defined in Equation (3.13)

3.6 REFERENCES

Adialalis, S.: *"Investigation of Physical and Chemical Criteria as Related to the Prevention of Asphalt Deposition in Oil Well Tubings,"* M.Sc. Thesis Petroleum Eng. Dept., Imperial College, University of London, London (Sept. 1982).

Boussingault, M.: Memoire sur la Composition des Bitumes. Annales de Clinic Ser. 2, vol. 64 (1837), p. 141.

Burke, N.D., Hobbs, R.D. and Kashou, S.F.: *"Measurement and Modelling of Asphaltene Precipitation from Live Reservoir Systems,"* SPE Paper #18273, proceedings of 63rd Annual Technical Conference and Exhibition of SPE held in Houston, TX, Reservoir Eng. vol., (Oct. 2-5, 1988), pp. 113-126.

Chillinger, G.V. and Yen, T.F., Bitumens, Asphalts and Tar Sands, Elsevier Scientific Pub. Co., Amsterdam (1978).

Chung, F., P. Sarathi, R. Jones: *"Modeling of Asphaltene and Wax Precipitation"*, U.S. DOE Report NIPER-498, 1991.

Coats, K.H.: *"Equation of State PVT Program: User's Manual,"* Scientific Software Intercomp, Denver, Colorado (Nov. 1984).

Corbett, L.W. and Petrossi, U.: *"Differences in Distillation and Solvent Separated Asphalt Residue,"* Ind. Eng. Chem. Prod. Res. Dev., vol. 17 (1978).

Danesh, A., Krinis, D., Henderson, G.D. and Peden, J.M.: *"Asphaltene Deposition in Miscible Gas Flooding of Oil Reservoirs,"* Ind. Chem. Eng. Prod. Res. Dev., vol. 66, No. 7 (1988), pp. 339-344.

Dyes, A.B. et al.: *"Alternate Injection of HPG and Water - A Two Well Pilot,"* SPE Paper #4082, proceedings of 1972 SPE Annual Meeting held in San Antonio, TX (Oct. 8-11, 1972).

Flory, P.J.: *"Principles of Polymer Chemistry"*, Cornell Univ. Press, Ithaca, NY, 1953.

Fussel, L.T.: "A Technique for Calculating Multiphase Equilibria", SPE J., August 1979, pp 203-208.9

Gambill, W. R.: *"Determine Heat of Vaporization"*, Chem. Eng., V. 64, No. 12, Dec. 1957, pp 261-266.

Hansen, P.W, "A CO_2 Tertiary Recovery Pilot-Little Creek Field, Mississippi", pres. at the SPE Annual Fall Tech. Conf. and Exhibition, Denver, CO, Oct. 9-12, 1977, SPE Paper 6747.

Harvey, M.T., Jr., Shelton, L.J. and Kelm, C.H.: *"Field Injectivity Experiences with Miscible Recovery Projects Using Alternate Rich Gas and Water Injection,"* J. Pet. Tech. (Sept. 1977), pp. 1051-55.

Haskett, C.E. and Tartera, M.: *"A Practical Solution to the Problem of Asphaltene Deposits - Hassi Messahoud Field, Algeria,"* J. Pet. Tech. (April 1965), pp. 387-391.

Hirshberg, A., deJong, L.N.J., Schipper, B.A. and Meijer, J.G.: *"Influence of Temperature and Pressure on Asphaltene Flucculation,"* SPEJ No. 6 (1984), pp. 283-293.

Huggins, M.L.: J. Phys. Chem., Vol. 9, 1944, pp 440.

Kawanaka, S., Park, S.J. and Mansoori, G.A.: *"The Role of Asphaltene Deposition in EOR Gas Flooding: A Predictive Technique,"* SPE/DOE Paper #17376, SPE/DOE Enhanced Oil Recovery Symposium held in Tulsa, OK (April 17-20, 1988), pp. 617-625.

Leontaritis, K.J.: *"Asphaltene Deposition: A comprehensive Description of Problem Manifestations and Modelling Approaches"*, SPE Paper No. 18892, presented at the SPE Production Operations Symposium held in Oklahoma City, Oklahoma, March 13-14, 1989.

Leontaritis, K.J.: *"Asphaltene Deposition: A Thermodynamic-Colloidal Model"*, Ph.D. Dissertation, U. of Illinois at Chicago, 1988.

Leontaritis, K.J. and Mansoori, G.A.: *"Asphaltene Flocculation During Oil Recovery and Processing: A Thermodynamic Colloidal Model,"* SPE Paper #16258, proceedings of 1987 SPE Symposium on Oil Field Chemistry (1987).
Lichaa, P.M.: *Asphaltene Deposition Problem in Venezuela Crudes - Usage of Asphaltene in Emulsion Stability Oil Sands,"* SPEJ (1977), pp. 609-624.

Long, R.B. *"The Concept of Asphaltene,"* The Advances in Chemistry Series No. 195 (1981), p. 17.

McKay, J.F., Amend, P.J., Cogswell, T.E., Harnsberger, P.M., Erickson, R.B. and Latham, D.R.: *"Analytical Chemistry of Liquid Fuel Sources,"* Adv. in Chem. Series 170 Chapt. 9 (1978), pp. 128-142.

Novosa Z. and Costain, T.G.: *"Experimental and Modelling Studies of Asphaltene Equilibria For a Reservoir Under CO_2 Injection,"* SPE Paper No. 20530, presented at the 65th Annual Technical Conference and Exhibition of the Society of Petroleum Engineers held in New Orleans, LA, Sept. 23-26, 1990.

Prekshot, G.W. et al.: *"Asphaltene Substances in Crude Oils,"* Trans AIME No. 151 (1943), pp. 188-194.

Rogacheva, O.V., Rimaev, R.N., Gubaidullin, V.A. and Khakinov, D.K.: *"Investigation of the Surface Activity of the Asphaltene of Petroleum Residues,"* Colloid J. vol. 42 (1980), p. 490.

Sharma, 1990 Characterization of Oil and Gas Reservoir Heterogeneity, PDL Annual Report for the Period Nov. 1, 1989 - Oct. 31, 1990, submitted to U.S. DOE (Idaho Operations Office). Grant #DE-FG-07-90 ID12839.

Speight, J.G.: *On the Molecular Nature of Petroleum Asphaltenes,"* Adv. in Chemistry Series No. 195 (1981), p. 1.

Speight, J.G. and Moschopedis, S.C.: *"On the Molecular Nature of Petroleum Asphaltenes,"* proceedings of American Chemical Society Meeting, Chemistry of Asphaltenes Symposium, Washington, D.C. (1981), PP. 1-15

Stalkup, F.I.: *"Carbon Dioxide Miscible Flooding, Past, Present, and Outlook for the Future,"* J.P.T. (Aug. 1978), pp. 1102-12.

Stalkup, F.I.: Miscible Displacement, SPE Monograph (June 1983).
Tuttle, R.N.: *High Pour Point and Asphaltic Crude Oils and Condensates,"* J.P.T. (June 1983), p. 1192.

Twu, C.H.: *"An Internally Consistent Correlation for Predicting Critical Properties and Molecular Weight of Petroleum and Coal-Tar Liquids."* Fluid phase Equilk, Vol. 6, 1984, pp. 137-150.

Yen, T.F.: *"The Nature of Asphaltenes in Heavy Oils,"* Pan Pac. Synfuels Conf. 2 (1982), p. 547.

CHAPTER 4.0

MILNE POINT UNIT

4.1 INTRODUCTION

Milne Point Unit is located adjacent to West Sak Field and lies 6 to 10 miles east-northeast of Kuparuk Field (Figure 4.1). Reserves are estimated at 100 million barrels of oil (Oil and Gas Journal, 1985). The field is operated by Conoco, Inc., and produces from the Cretaceous Kuparuk River Formation at about 6950 to 7000 feet subsea.

PDL maintains approximately 40 digital well log tapes from the approximately 50 wells drilled at Milne Point. We have undertaken well log analysis of 10 of these wells (listed in Table 4.1 and highlighted in Figure 4.2), and plan to continue analysis of a sufficient number of wells to adequately characterize the reservoir. Faulting as determined from this initial analysis is also shown. Upon completion of analysis, contour maps, 3-D plots, and cross sections will be generated and included in the reservoir description.

Drilling and evaluation by Conoco shows the Kuparuk Formation at Milne Point to be composed of two high-quality, consolidated, oil-bearing sandstone members, occurring within the Middle and Lower Kuparuk. Two high-quality sand lobes (the MK-1 and MK-2) occur at the top of the Middle Kuparuk, and two additional high-quality sand lobes (the LK-1 and LK-2) are found at the top of the Lower Kuparuk. A plot of well log traces taken from a typical well at Milne Point (the B-3) is presented in Figure 4.2.

The formation nomenclature selected at Milne Point by Conoco differs from that used at the larger Kuparuk Field, not withstanding the fact that the Kuparuk Formation consists of two main sand members at both locations. In contrast to Milne Point, the producing zones at Kuparuk Field are defined as occurring within the Upper and Lower Kuparuk members, rather than within the Middle and Lower members. As at Milne Point, these zones are divided into units, being labeled A through D. Units A and C are further subdivided into units A-1 through A-6 and C-1 through C-4, respectively (Masterson and Paris, 1987).

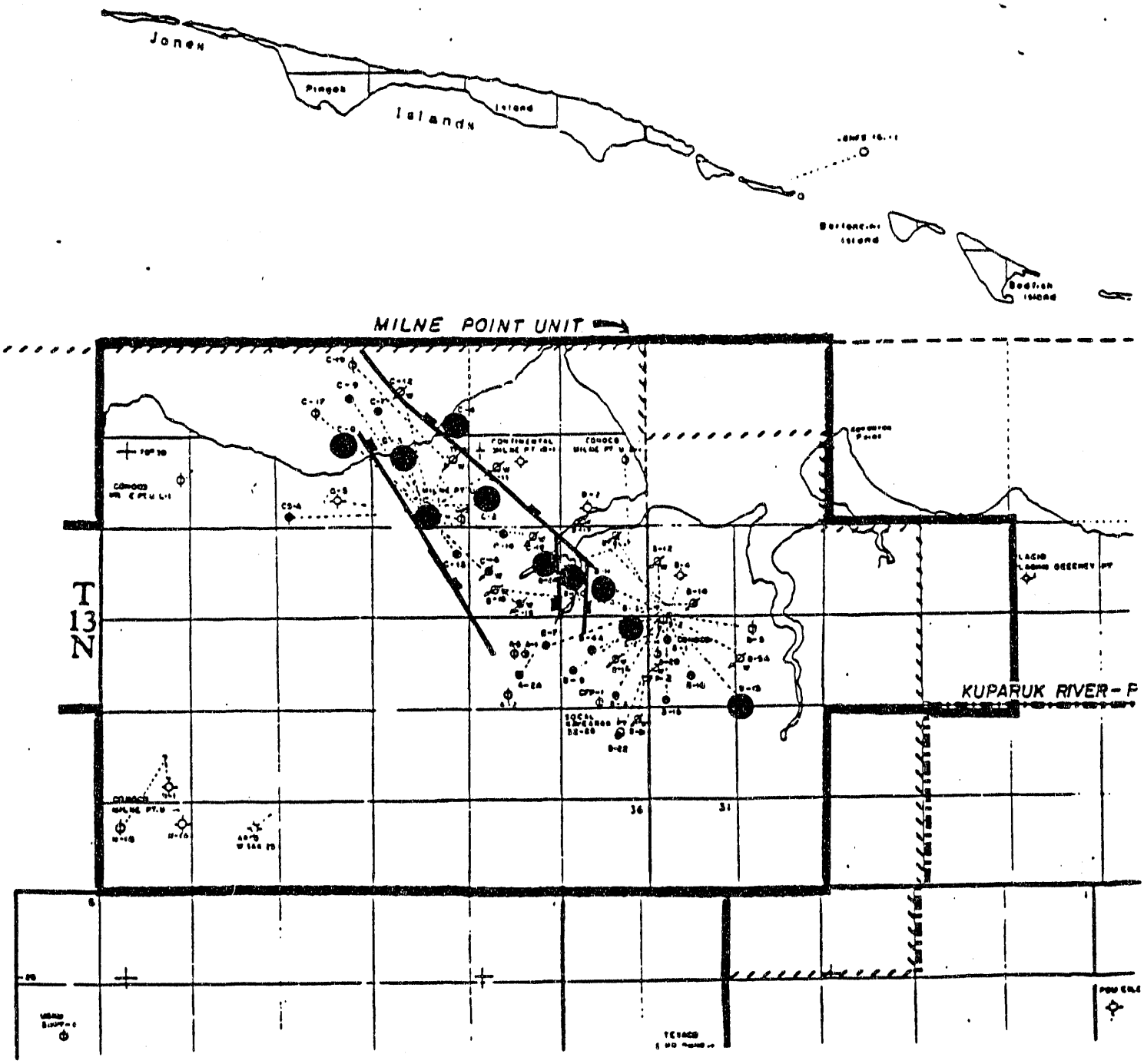

Figure 4.1: Base Map of Milne Point Wells with Analyzed Wells Indicated by Larger Circles.

Table 4.1
Milne Point Wells Utilized in Well Log Analysis to Date

Full Well Name	Abbreviated Well Name
1. Milne Point Unit B-3	B-3
2. Milne Point Unit B-10	B-10
3. Milne Point Unit B-11	B-11
4. Milne Point Unit B-13	B-13
5. Milne Point Unit C-1	C-1
6. Milne Point Unit C-2	C-2
7. Milne Point Unit C-3	C-3
8. Milne Point Unit C-4	C-4
9. Milne Point Unit C-8	C-8
10. Milne Point Unit D-24	D-24

After petrophysical analysis at Milne Point has reached a satisfactory point of completion, in addition to subsequent reservoir description, a comparison will be made between the Kuparuk River Formation at Milne Point Field and at Kuparuk Field to determine existing petrophysical differences. Environments of deposition will be evaluated and results will be included with the reservoir description. Core data will be integrated into the project in an effort to better delineate the productive horizons in the Milne Point Unit.

4.2 RESULTS TO DATE

Tables 4.2 and 4.3 list subsea tops, gross thicknesses, and net pay corresponding to the wells analyzed to date. Porosities and water saturations as measured in the Middle Kuparuk pay zones are also included. Figure 4.3 presents these porosities and water saturations in a bar graph in order as they occur in the field from northwest-to-southeast. Lower Kuparuk porosities and water saturations in the ten wells selected for analysis to date are being calculated at this time. Porosities in the Middle Kuparuk pay zones range from a low of 16% in the B-13 to a high of 29% in the C-1, while water saturations range between 33% in well B-11 to 98% in well C-3.

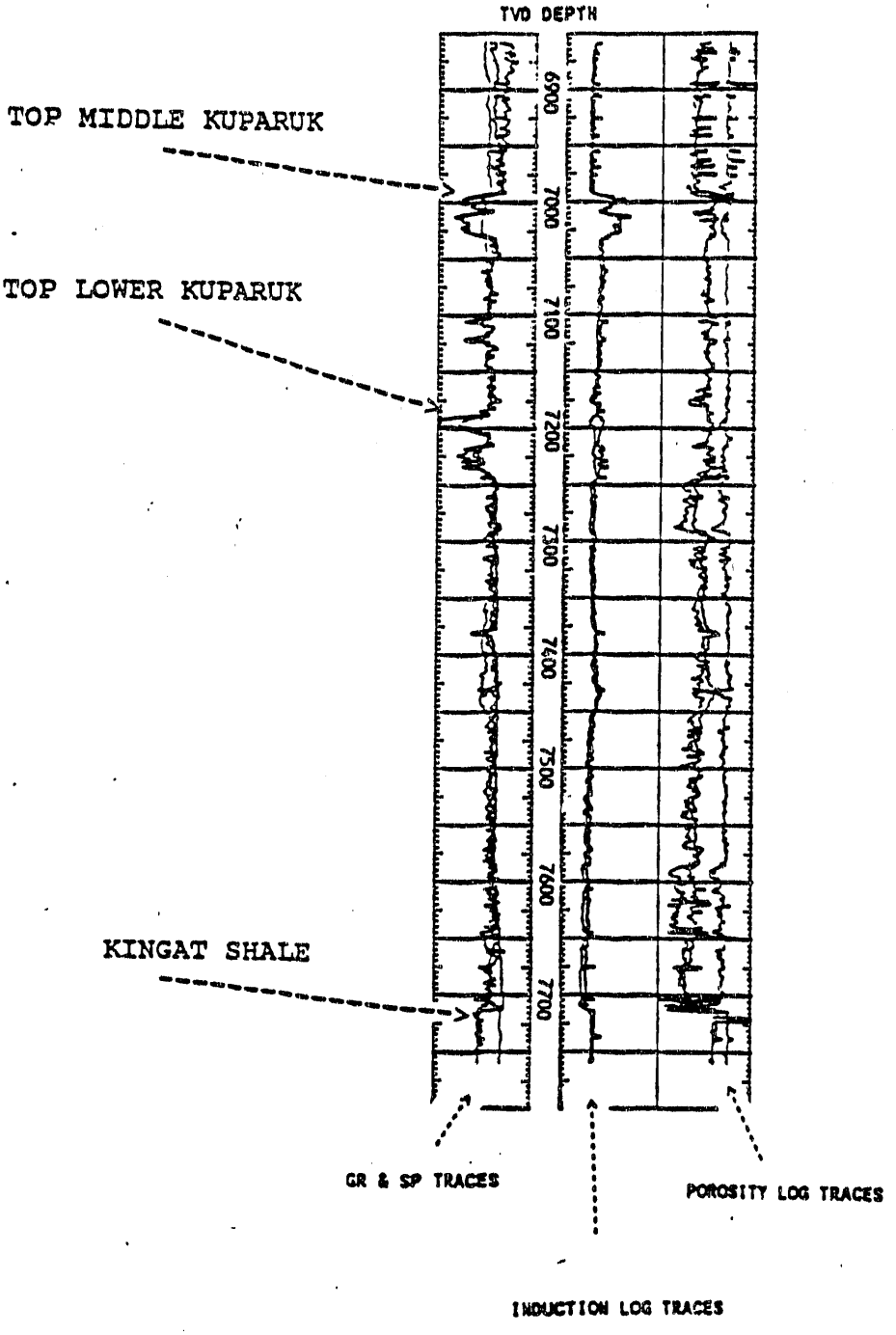

Figure 4.2: TVD Log Plot of Milne Point Well B-3.

As additional wells are analyzed, a more complete picture of the distribution of petrophysical properties in the Milne Point Unit will be available.

Table 4.2

Petrophysical Properties of the Middle Kuparuk, Milne Point Unit, as Determined to Date

Well	Subsea Depth to Middle Kuparuk (ft)	Gross Thickness (ft)	Net Pay (ft)	Avg. Ø (%)	Avg. Sw (%)
B-3	-6886	202	30	27	41
B-10	-6871	215	29	24	42
B-11	-6922	200	24	24	33
B-13	-6975	235	19	16	43
C-1	-6899	163	9	29	58
C-2	-6917	175	15	29	55
C-3	-6892	146	71	20	98
C-4	-7186	156	17	21	79
C-8	-6741	139	31	24	62
D-2A	-6923	201	30	21	52

4.3 PRELIMINARY GEOLOGICAL ANALYSIS

The analysis completed to date provides strong evidence of faulting at Milne Point Unit, especially between wells C-8 and C-3. A preliminary cross section (to be finalized and presented in the final report) strongly suggests that well C-3 is downthrown approximately 150 feet with respect to well C-8. In addition, the completion report for well C-8 indicates that a fault cuts this well approximately 45 feet above the top of the Middle Kuparuk. This fault is, in all probability, the fault across which the Kuparuk Formation is downthrown in well C-3.

Table 4.3

Petrophysical Properties of the Lower Kuparuk, Milne Point Unit

Well	Subsea Depth to Lower Kuparuk (ft)	Gross Thickness (ft)	Net Pay (ft)
B-3	-7088	554	0
B-10	-7086	NDE	6
B-11	-7122	NDE	0
B-13	-7210	NDE	0
C-1	-7062	456	38
C-2	-7092	NDE	80
C-3	-7038	520	16
C-4	-7342	NDE	0
C-8	-6879	NDE	33
D-2A	-7123	NDE	0

Additional faulting is undoubtedly present at Milne Point, as the literature reports the existence of a great number of normal faults in the Kuparuk Field (Masterson and Paris, 1987). The top of the Middle Kuparuk in well C-4 is considerably lower than in well C-3, and is probably due to faulting. Normal faults appear to exist on either side of well B-10, as the top of the Middle Kuparuk occurs approximately 40 feet shallower in this well than in the surrounding D-2A and B-3 wells. This suggests that well B-10 lies within a small graben.

Stratigraphically, the combined MK-1 and MK-2 sand package generally thickens toward the southeast, with this thickening first becoming noticeable in well D-2A. The MK-2 sand may not be present north of this well, as the "double-lobed" nature

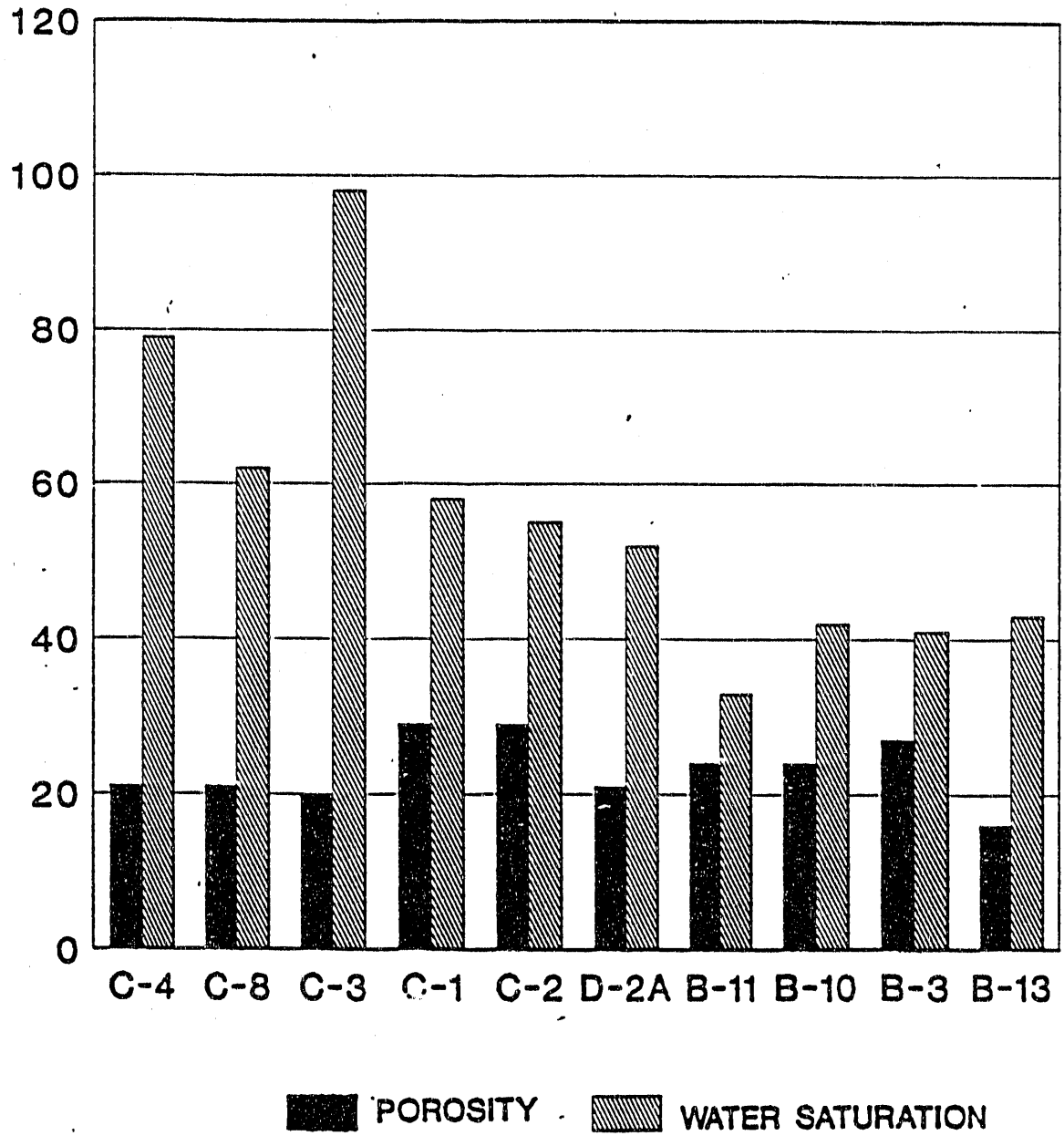

Figure 4.3: Middle Kuparuk Porosity & Sw, Milne Point Unit.

of the Middle Kuparuk is not readily apparent north of well D-2A. As such, the MK-2 appears to be the thickening within the Middle Kuparuk southward.

The Lower Kuparuk, in contrast, shows no general thickening toward the south. Both the LK-1 and LK-2 sands are relatively well developed in all the analyzed wells. Although both MK and LK member sand lobes were deposited on a marine shelf (as is the case for the Kuparuk sand lobes at the Kuparuk Field), the absence of the LK2 in the northern part of the field reflects a differing depositional environment in this area during MK-2 time, barring erosion. Were sands transported elsewhere during this time or was there a paucity of sand available for deposition for a relatively short geological time interval? These are questions which will be pursued as the analysis progresses.

Kuparuk Formation dip is generally toward the south, although it is slight (less than 1 degree). Faulting increases the difficulty in evaluating the amount of dip existing at Milne Point. Analysis of additional wells will provide a clearer picture of the fault pattern and aid in determining dip direction.

4.4 FUTURE PLANS

As previously indicated, petrophysical well log analysis will be performed on additional wells as required in order to provide a complete and accurate reservoir description of this field. Reservoir characterization will also provide the necessary data for PDL reservoir simulation modeling. Of interest to PDL is determination of reservoir differences that may exist at Milne Point as compared to Kuparuk Field. Resolving differences in fault patterns, stratigraphy, and environments of deposition, as well as petrophysical attributes will aid in evaluation of Milne Point future production potential.

4.5 REFERENCES

1. Oil and Gas Journal, 1985, Milne Point Unit–Small but Welcome: v. 83, no. 25, p. 55-58.

2. Masterson, W. D., and Paris, Chester E., 1987, Depositional History and Reservoir Description of the Kuparuk River Formation, North Slope, Alaska, *in* Alaskan North Slope Geology, v. 1, p. 95.

APPENDIX

Published AAPG Abstract from Mowatt et al.

The American Association of Petroleum Geologists Bulletin
V. 75, No. 3 (March 1991), P. 515-700

Association Round Table

1991 ANNUAL CONVENTION
WITH DPA/EMD DIVISIONS AND SEPM, AN ASSOCIATED SOCIETY
April 7-10, 1991, Dallas, Texas

MOWATT, THOMAS C., U.S. Bureau of Land Management, Anchorage, AK, and D. O. OGBE, V. A. KAMATH, and G. D. SHARMA, University of Alaska, Fairbanks, AK

Petrologic-Petrophysical Relationships, West Sak and Ugnu (Brookian), Northern Alaska

Petrographic-mineralogic analyses have been combined with petrophysical information derived from wireline logs, as part of an investigation of geological and engineering characteristics of the West Sak and Ugnu (Brookian) stratigraphic intervals in several wells in the central portion of the Alaskan Northslope.

The strata are semi- to unconsolidated clastics—sand, silt, clay in size—"cemented" by viscous (API gravity 8° to 22°) hydrocarbon material. This presents serious problems in terms of sample integrity during borehole recovery and subsequent storage, transportation, and sample preparation. Pressure changes from subsurface to surface conditions pose particular difficulties.

Textural relationships in thin section are often problematic with respect to original relationships in the undisturbed subsurface. In-situ analyses—e.g., wireline logs—represent the potentially most useful means of elucidating petrophysical-engineering properties of concern to drilling, completion, and production. Petrographic-mineralogic analysis of sample materials, as feasible, is essential for rigorous application of such in-situ techniques.

The present work confirms the heterogeneous nature of the West Sak and Ugnu intervals, with frequent, often substantial proportions of silt-clay size materials associated intimately within, and/or interbedded with, coarser grained reservoir intervals. Major intervals with moderate-good reservoir properties are recognized, as well as significant intervals ranging from relatively poor reservoir quality to good seal quality materials.

Hydrocarbon production will undoubtedly require enhanced recovery techniques, hence thorough, detailed reservoir/nonreservoir characterization will be imperative to achieve viable efficiency.

END

DATE
FILMED
8/31/92